

# Porphyrin Adsorption and Reactivity on Oxide Surfaces

## Adsorption und Reaktivität von Porphyrinen auf Oxidoberflächen

Der Naturwissenschaftlichen Fakultät der Friedrich-Alexander-Universität  
Erlangen-Nürnberg  
zur Erlangung des Doktorgrades Dr. rer. nat.

vorgelegt von  
**Daniel Wechsler**  
aus Neuendettelsau

Als Dissertation genehmigt  
von der Naturwissenschaftlichen Fakultät  
der Friedrich-Alexander-Universität Erlangen-Nürnberg

Tag der mündlichen Prüfung: 18.09.2020

Vorsitzender des Prüfungsorgans: Prof. Dr. Georg Kreimer

Gutachter/in: Prof. Dr. Hans-Peter Steinrück  
Prof. Dr. Federico José Williams

## Contents

1.	Introduction .....	1
1.1.	Porphyrins on Oxide Surfaces.....	3
1.2.	Porphyrins at the Solid/Liquid Interface .....	4
2.	Experimental Methods .....	7
2.1.	X-ray Photoelectron Spectroscopy (XPS).....	7
2.1.1.	Chemical Shift.....	8
2.1.2.	Coverage Calculation.....	9
2.1.3.	Measuring on Non-conductive Samples .....	11
2.2.	Near-edge X-ray Absorption Fine Structure (NEXAFS) .....	12
2.2.1.	General Concept.....	13
2.2.2.	Photon Flux Measurements.....	14
2.2.3.	Auger-yield NEXAFS and Photoelectron Features .....	14
2.2.4.	Adsorption Angle Determination .....	16
3.	Experimental Details .....	19
3.1.	Preparation of Cobalt Oxide Thin Films .....	19
3.2.	Preparation of Rutile TiO <sub>2</sub> (110) Crystals.....	20
3.2.1.	Preparation for UHV Experiments.....	20
3.2.2.	Preparation for Wet-chemical Experiments .....	22
3.3.	Deposition of Molecules .....	23
3.3.1.	Evaporation in UHV .....	23
3.3.2.	Deposition from Solution under Argon Atmosphere .....	24
3.3.3.	Deposition from Solution under Ambient Conditions .....	25
4.	Results .....	27
4.1.	Porphyrin Reactions at Oxide Surfaces.....	27
4.1.1.	Influence of Surface Structure [P1].....	28
4.1.2.	Influence of Anchoring Groups [P2, P3] .....	32
4.2.	Porphyrins at Solid/Liquid Interfaces .....	38
4.2.1.	Reactions of Porphyrin Layers in Solution [P2] .....	38
4.2.2.	Deposition of Porphyrin Layers from Solution [Unpublished].....	41
4.2.3.	Full Ambient-condition Preparation of Porphyrin Monolayers [P4] .....	43
4.3.	Removing Photoemission Features from Auger-yield NEXAFS Spectra [P5].....	50
5.	Conclusion and Outlook.....	57
6.	Zusammenfassung .....	59
7.	Acknowledgement.....	61
8.	References .....	63
9.	Appendix: Articles P1 – P6.....	71



# 1. Introduction

The first surface science studies about porphyrins were published in the 1970s<sup>1-6</sup> and since then the topic has found increasing interest. To understand the fascination for such large organic molecules on surfaces we must have a closer look at some of the most important processes in nature. Figure 1 shows four biologically important porphyrin derivatives. The central framework is in all cases remarkably similar: four pyrrole rings form a macrocycle with all four nitrogen atoms pointing to the middle.<sup>7, 8</sup> In the shown examples this central cavity is filled by different metal ions which are coordinated by the four nitrogen atoms. What is different are the different side groups and the metal center; both influence the colors of the molecules and their functionality.

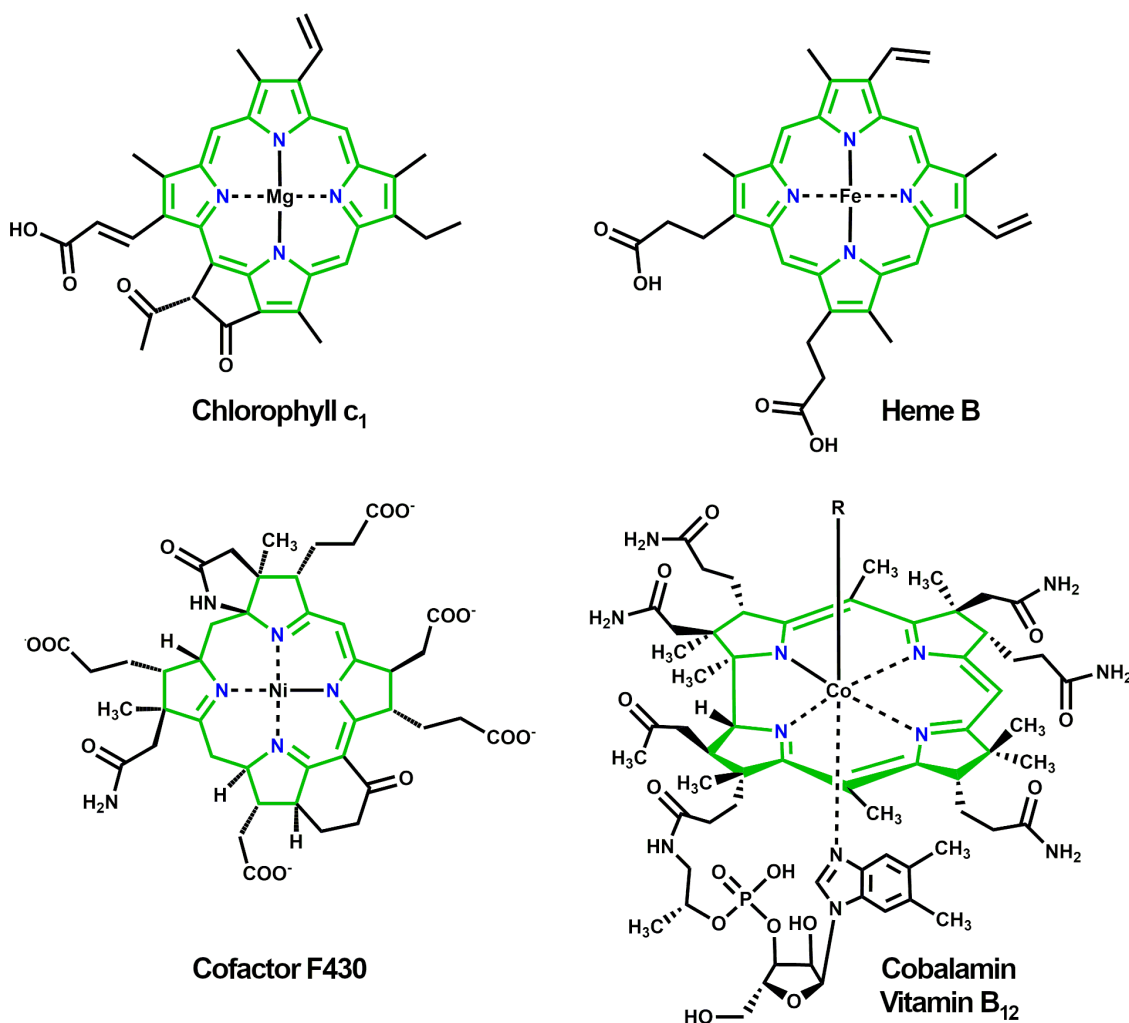


**Figure 1:** Four biologically important porphyrin derivatives: Chlorophyll c<sub>1</sub>, Heme B, Cofactor F430 and Vitamin B<sub>12</sub>.

Chlorophylls, like the depicted chlorophyll c<sub>1</sub>, are Mg(II) porphyrin derivatives that absorb blue and red light.<sup>9</sup> They are not only the reason why plants appear green, but they also take a central role in photosynthesis, one of the most important processes for every living being on earth. Structurally very similar, but with Fe(II) instead of Mg(II), is the group of heme molecules.<sup>10</sup> As

part of Hemoglobin and Myoglobin, the porphyrin Heme B transports and stores oxygen in mammalian cells. The porphyrin-derivate Cofactor F430 has Ni(I) in its central cavity and is part of an enzyme for methane production in prokaryotic archaea.<sup>11</sup> The last example, cobalamin, is also the most complex one of the four. Also known as Vitamin B<sub>12</sub>, cobalamin plays an important role in the production of red blood cells and for the function of the nervous system.<sup>12</sup> Its metal center is Co(I).

Over the years, the list of porphyrin molecules has been enlarged by synthetic chemists with many different combinations of side groups and metal centers. Today, porphyrins exist with most metals of the periodic table as metal centers and numerous different chemical and physical properties.<sup>13-18</sup> This variety makes them interesting for various applications and it was shown that porphyrins can be used in catalysis for example to reduce nitric oxides<sup>19</sup> or to synthesize cyclic carbonates from CO<sub>2</sub><sup>20</sup> or in medical applications for photodynamic therapies<sup>21,22</sup>. Besides that, they can also be used to build chemical sensors<sup>23,24</sup> and cheap dye-sensitized solar-cells on titania surfaces<sup>25,26</sup>. In many of these cases, porphyrins will be adsorbed onto a solid support and this is where surface science studies come into play. The adsorption of porphyrins and their reaction behavior on different surfaces was investigated with a variety of microscopic and spectroscopic techniques.<sup>27-36</sup> Most of those works were performed on single-crystalline metal surfaces, because they offer an easy to prepare and controllable system. However, for a proper description of processes in real-world applications this is not suitable, because the important interface is in most cases not an organic/metal interface but an organic/oxide interface.

When I started on my Ph.D. in 2016, there was an increased interest in oxide surfaces and organic molecules adsorbed on them. The research unit “Functional Molecular Structures on Complex Oxide Surfaces” (funCOS, FOR 1878) which started in 2014 played an important role on that. We shifted our focus away from metal surfaces to mainly three different oxide surfaces: magnesium-, cobalt-, and titanium oxide. First results have shown that some concepts that are known from studies on metal single crystals, are also applicable for porphyrin-on-oxide studies. The coordination of metals from the surface to form metalloporphyrins is one of them<sup>37-39</sup>, even though the mechanism behind is completely different. Other findings like the formation of a covalent bond between functionalized porphyrins and oxide surfaces<sup>36,40</sup>, were not known from metal surfaces and opened new possibilities. Also, outside of funCOS the interest in oxide surfaces and how to functionalize them with organic molecules raised.<sup>40-44</sup>

The aim of this thesis is twofold: the first part is to deepen the knowledge on the adsorption and reaction behavior of porphyrin molecules on oxide surfaces, namely cobalt oxide and titanium dioxide. In the second part, the concept of funCOS is pushed even further. Instead of working on oxide crystals in UHV, the preparation is stepwise brought into solution. This comes even closer to real applications and should give important insights how ambient conditions influence the

adsorption and reactivity of porphyrins. The appendix P6 contains an article about the adsorption geometry of CoTPP on Ag(100) which I also published during my Ph.D. studies. Besides XPS and NEXAFS, LEED and the X-ray Standing Wave technique were applied to gain insights into this system. However, the focus of this thesis is on oxide surfaces and thus the data will not be discussed in detail. The porphyrins that were used during most of the work are free-base porphyrins with phenyl groups attached, namely 2-H-tetraphenylporphyrin (2HTPP) and 5-(monocarboxyphenyl)-10,15,20-triphenylporphyrin (MCTPP).

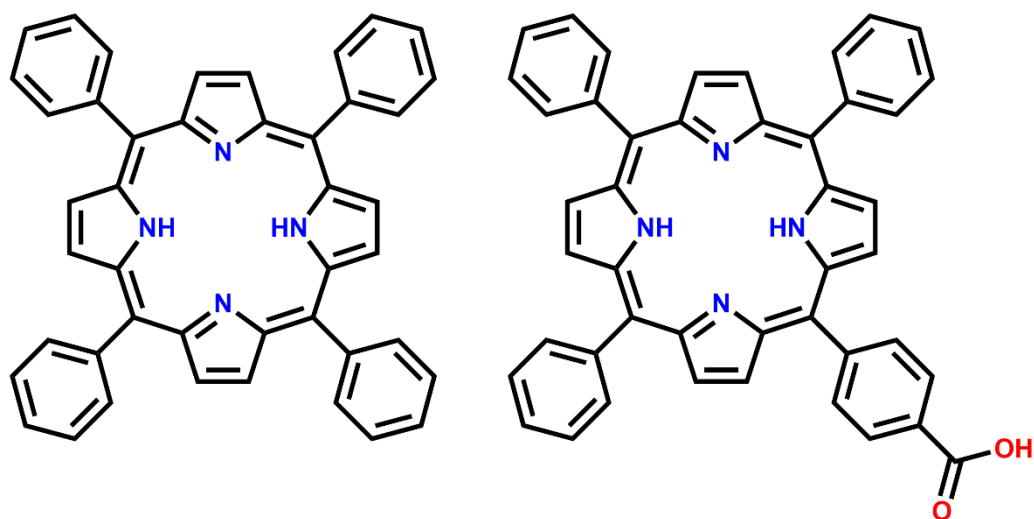


**Figure 2:** 2H-Tetraphenylporphyrin (left) and 5-(Monocarboxyphenyl)-10,15,20-Triphenylporphyrin (right)

The following pages give a brief introduction to the work already done on porphyrins on surfaces (Chapter 1.1 and 1.2). The focus is on concepts relevant for this thesis. A detailed summary is found in the excellent review article written by J. Michael Gottfried.<sup>45</sup> This is followed by an overview of the basic concepts of X-ray photoelectron spectroscopy and near-edge X-ray absorption fine structure measurements (Chapter 2), the preparative details (Chapter 3) and a summary of the achieved results (Chapter 4).

### 1.1. Porphyrins on Oxide Surfaces

From different studies on metal surfaces, it is known that tetraphenylporphyrins adsorb usually with the macrocycle parallel to the surface.<sup>46-51</sup> Due to steric hindrance induced by the phenyl rings the macrocycle deforms upon adsorption. This saddle-shape deformation, where two opposing pyrrole rings point to the surface and the other two away from it, is well known and is found on different metal surfaces, like Cu(111)<sup>49, 52</sup>, Ag(111)<sup>52</sup> and Au(111)<sup>53</sup>; recently, an inverted porphyrin structure was found for 2HTPP on Cu(111).<sup>50</sup> It is believed that these distorted conformations lead to higher interactions with the substrate and play therefore an important role in the self-metalation process. In this reaction, the porphyrin coordinates a metal atom from the metal surface with its four nitrogen atoms and incorporates it into the central cavity to form a

metalloporphyrin.<sup>30, 54, 55</sup> This is done by a redox reaction where the metal gets oxidized into +2-state and the two protons on the aminic nitrogen atoms get reduced to atomic hydrogen.<sup>56</sup> On the metal substrate, they can combine and desorb as H<sub>2</sub>. This was used by our group<sup>35, 57</sup> and others<sup>58</sup> to follow the metalation reaction with temperature-programmed desorption measurements. Self-metalation but also the reaction with codeposited metals are well-studied concepts and are known for many different types of porphyrins and metals.<sup>30, 56, 59, 60</sup>

Fewer studies exist for porphyrins adsorbed on metal oxides. It is known that 2HTPP adsorbs with the macrocycle parallel to the surface on TiO<sub>2</sub>(110)<sup>61</sup> and on MgO<sup>62</sup>. By functionalizing porphyrins with linker groups, like –COOH, the molecules can be covalently attached to oxide surfaces. This is a known concept for small carboxylic acids<sup>63-65</sup> and was proven to work with porphyrins as well<sup>32, 40</sup>. Infrared spectroscopy studies on Co<sub>3</sub>O<sub>4</sub>(111) have shown that MCTPP adsorbs parallel to the surface at low coverages, but with increasing coverage the molecules start to stand up.<sup>32</sup> Similar results were found for MCTPP metalated with zinc on TiO<sub>2</sub>(110): AFM measurements show that there exist also molecules with low and high tilt angles. CuTCPP, the copper-tetraphenylporphyrin that has a carboxylic acid group on each phenyl ring does not adsorb in a tilted geometry on NiO(001). It was also shown that self-metalation happens on oxide surfaces as well. 2HTPP was found to metalate at elevated temperatures on TiO<sub>2</sub>(110)<sup>37, 39</sup>. Whereas on MgO(100) the same porphyrin partially metalates already at room temperature<sup>38</sup>. The reaction mechanism has to be different than on metal surfaces. Instead of a redox reaction an ion-exchange mechanism is proposed where the metal ion is complexated by the four nitrogen atoms and the two protons take its former place on the surface and form hydroxyl groups.<sup>38</sup> Except that porphyrins metalate on both oxides, there are very few similarities between the behavior of 2HTPP on both surfaces. Besides the higher temperatures needed for metalation on TiO<sub>2</sub>(110) there is also another species besides the free-base porphyrin present at room temperature<sup>37, 66</sup>: a protonated porphyrin species that we believe is formed by interaction of the nitrogen atoms of the porphyrin with hydroxyl groups on the surface. The protonated species is even more resilient to metalation and needs even higher temperatures to metalate. The first part of this thesis is about characterizing the metalation of porphyrins on oxide surfaces. Therefore, we studied two different cobalt oxide surfaces and compared them to data measured previously in our group on MgO(100) and TiO<sub>2</sub>(110). Afterwards, the covalent linking of MCTPP on TiO<sub>2</sub>(110) is discussed. The focus was on finding out if a similar coverage-dependent adsorption geometry change like observed on Co<sub>3</sub>O<sub>4</sub>(111) takes place and if this would influence the self-metalation reaction.

## 1.2. Porphyrins at the Solid/Liquid Interface

In the second part of this thesis the influence of solution and air on the adsorption and reactivity of porphyrins on TiO<sub>2</sub>(110) is discussed. Many studies exist about the behavior of dissolved porphyrins, about how they metalate in solution<sup>67, 68</sup>, exchange their metal centers<sup>69-71</sup> or

demetalate again<sup>69, 72</sup>, but only very few studies tackle the question about how adsorbed porphyrins behave when exposed to solutions. Franke et al. have shown in 2015 that 2HTPP evaporated on Au(111) and exposed to Zn(OAc)<sub>2</sub> solution forms ZnTPP.<sup>73</sup> Furthermore, they have shown that an already metalated molecule can exchange its metal-center when exposed to a metal-ion containing solution.<sup>74</sup> Demetalation, another reaction known from solution chemistry where the metal atom from the central cavity is removed and a free-base porphyrin molecule is formed, was also attempted by Franke et al. and shown not to be possible for adsorbed molecules, even at pH 0. Fernández et al. studied the influence of the surface on the metalation of adsorbed porphyrins in solution.<sup>75</sup> They found that the metalation temperature is rising when they increase the distance between the surface and the porphyrin by introducing a self-assembled monolayer as spacer. In this thesis, the focus was on adsorbing porphyrins from solution and metalating them in solution.



## 2. Experimental Methods

X-ray photoelectron spectroscopy (XPS) is our technique of choice to study the adsorption and reactivity of organic molecules on oxide surfaces. We apply it to verify the cleanliness of our surfaces prior to each experiment, to ensure the intactness of the deposited molecules and to determine coverages of the organic overlayers. Besides that, XPS distinguishes between a free-base and a metalated porphyrin and this allows us to follow the metalation reaction.

Near-edge X-ray absorption fine structure spectroscopy (NEXAFS) is the technique we use to study the adsorption geometry of molecules. From the measured spectra we can determine if a molecule adsorbs flat or tilted.

On the next pages I will briefly introduce the two techniques. The focus is on aspects that are necessary to understand the following work. A detailed introduction to XPS is found in the books written by Watts/Wolstenholme<sup>76</sup> and Briggs/Seah<sup>77</sup>, and the standard literature about NEXAFS is “NEXAFS Spectroscopy” by Joachim Stöhr<sup>78</sup>.

### 2.1. X-ray Photoelectron Spectroscopy (XPS)

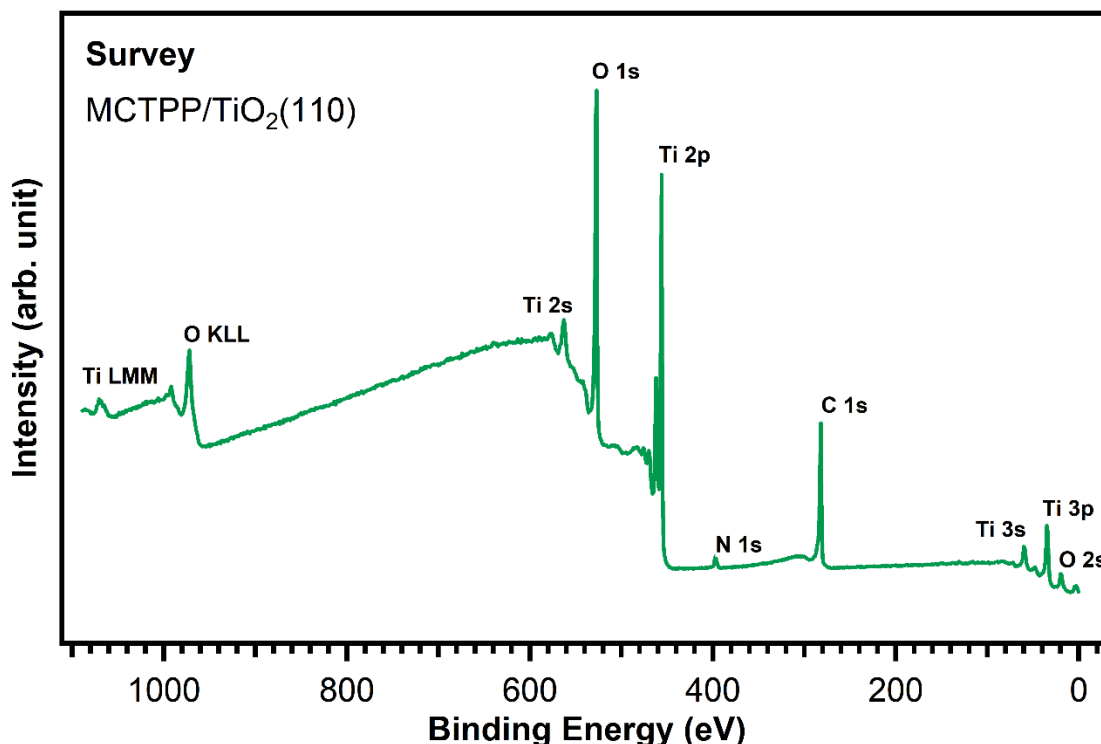


**Figure 3:** XP survey spectrum of the carboxylic acid functionalized porphyrin MCTPP adsorbed on TiO<sub>2</sub>(110).

In an XPS measurement, the element-specific binding energies of core-level electrons of a sample are detected. Figure 4 shows a typical XP spectrum of MCTPP, a carboxylic acid functionalized porphyrin, adsorbed on TiO<sub>2</sub>(110). Each peak represents electrons originating from a specific energy level and this allows one to identify the different elements a surface is made of. The

theoretical fundament for XPS is the photoelectric effect, which was described 1905 by Albert Einstein and earned him the Nobel Prize in 1921<sup>79</sup>: when a photon hits a surface, an electron can be excited. If the photon energy is high enough to overcome the binding energy of the electron, it is emitted from the atom and the remaining photon energy is converted to kinetic energy. In an XPS measurement, these ejected electrons, which are called photoelectrons, are separated by their kinetic energies and detected in an analyzer. With the measured kinetic energy and knowledge of the X-ray photon energy and the work function inside the analyzer, the binding energy is obtained:

$$E_B = h\nu - E_{\text{kin}} - \phi_{\text{analyzer}}$$

The work function is determined by measuring a reference sample, often a gold or silver foil, and comparing the obtained binding energies to literature values.

The high binding energy side of Figure 3 shows also peaks labeled with Ti LMM and O KLL. These peaks are caused by Auger electrons, not by photoelectrons. After the photoemission process the atom is left with an unstable core hole. This can be filled by an outer shell electron and the energy difference is either emitted as a fluorescence photon or another electron is ejected as an Auger electron.

### 2.1.1. Chemical Shift

Unlike the outer-lying electrons in the valence band, core-level electrons do not contribute to the chemical bond and are therefore mostly unaffected by the chemical environment. This is why the binding energies of core-level electrons are element specific. However, small shifts are observed as a function of the chemical environment. A more positive electronic charge localized on an atom leads to an increased attractive interaction between the electron and the core and therefore to a higher binding energy. Vice versa, a negative charge leads to lower binding energies. Figure 4 shows how this effect, called chemical shift, can be used to distinguish between a free-base and a metalated porphyrin. In the first case, the two different types of nitrogen lead to the two green peaks in the N 1s spectrum with the peak of the aminic ( $-\text{NH}-$ ) nitrogen atoms at around 2 eV higher binding energies than that of the iminic ( $-\text{N}=\text{}$ ) ones. In a metalated porphyrin all four nitrogen atoms bind to the metal center and have a similar electronic environment. This leads to only one peak which is usually located in-between the two free-base peaks.

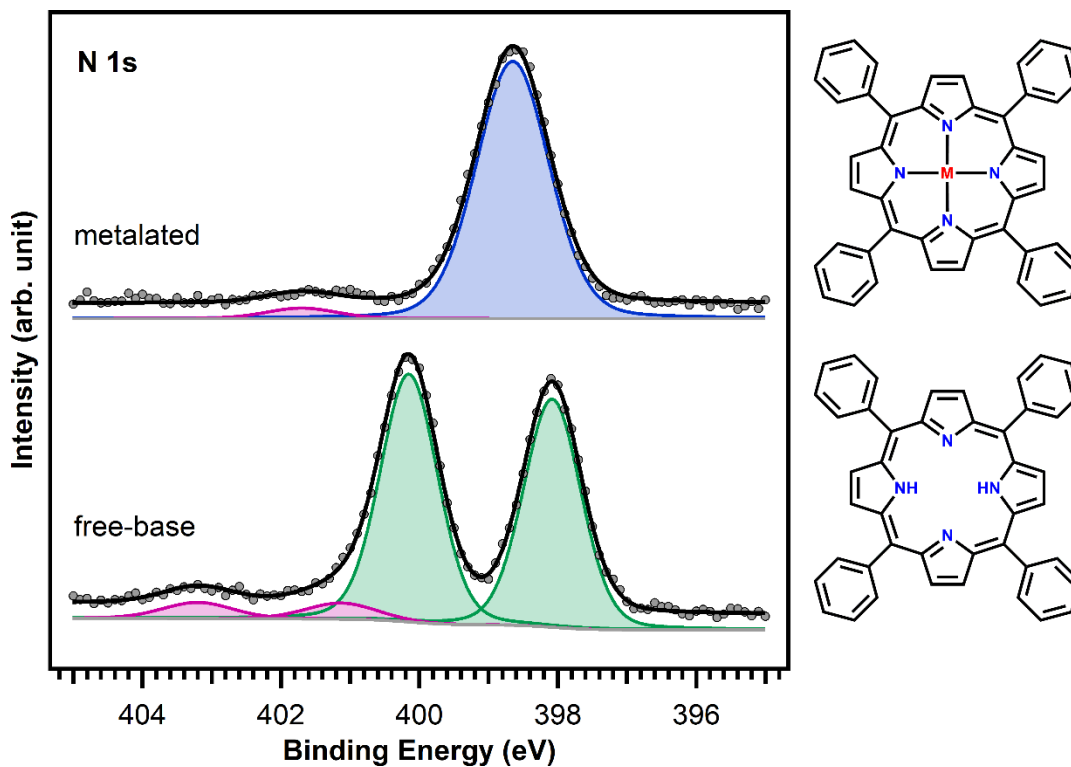


**Figure 4:** N 1s spectra of a metalated and a free-base porphyrin. Both can clearly be distinguished in XPS by the number of nitrogen peaks.

The barely visible violet peaks at higher binding energies are shake-up satellites and are caused by relaxation processes that occur during the photoemission process to compensate the increased positive charge. This relaxation can lead to different effects, like an excitation of an electron. The excitation energy is lost for the photoelectron and thus its kinetic energy is lower; it will appear at higher binding energies in the XP spectrum. If the valence electron is excited into a bound energy level, the process is called shake-up. The energy difference - and therefore also the energy loss of the photoelectron - is discrete and thus a peak is observable. If the transferred energy is high enough to eject the valence electron from the atom the process is called shake-off. Here, the energy difference is not discrete, and this leads generally not to a visible peak but to an increase of the background at higher binding energies. In porphyrin photoelectron spectra shake-up satellites are usually visible for multilayers in both the C 1s and the N 1s region and are often a hint whether the number of molecules is below or above a full first layer.

### 2.1.2. Coverage Calculation

XPS is not only a qualitative method but can also be used quantitatively because the core-levels are almost completely unaffected by the chemical state. This means the cross-sections for the elements are also unaffected and therefore independent of the chemical surrounding of the atom. When factors like the photon flux, the cross-section and the device-specific constants are known, one can calculate the absolute number of atoms. In many cases, including this work, it is not necessary to know absolute numbers. The more important questions we want to answer are what

the atomic composition of the molecules is, especially how many carbon atoms are detected per nitrogen atom to check the intactness of the porphyrins, and how many layers of molecules adsorb. The first is answered by comparing peak areas of the respective elements after correcting for the sensitivity factors.<sup>80,81</sup> In the second case, the Beer-Lambert law is used<sup>82</sup>: when X-rays penetrate a material, photoelectrons are created but only the ones that can leave the material without further inelastic interactions contribute to an XPS peak. Electrons of deeper layers have a higher probability of scattering and therefore contribute less to the peak intensity and more to the background. For a two-component system, like porphyrin molecules adsorbed on TiO<sub>2</sub>(110), the substrate signal intensity  $I_S$  is given by:

$$I_S = I_S^0 \cdot e^{-\frac{d}{\lambda \cos\theta}}$$

$I_S^0$  is the substrate signal without overlayer,  $d$  is the adsorbate thickness,  $\lambda$  the inelastic mean free path, and  $\theta$  the detection angle with respect to the surface normal. This and all following equations are only valid when the adsorbate forms uniformly thick layers. To be able to calculate coverages the inelastic mean free path has to be determined. This is done by measuring the substrate signal  $I_S$  of a sample with known adsorbate coverage and the same signal of the adsorbate free surface  $I_S^0$ . To create a reference sample with known coverage we utilize the property of porphyrins to form very stable fully closed first layers on many metal and oxide surfaces. By depositing multilayers and desorbing them, a reproducible number of molecules is left and this we define as 1 ML.<sup>27, 83</sup> With multilayer desorption we obtain similar inelastic mean free paths and therefore also similar amounts of molecules for 2HTPP adsorbed on different surfaces, like Co<sub>3</sub>O<sub>4</sub>(111), CoO(111), TiO<sub>2</sub>(110), Cu(111) and Ag(100). However, in the case of MCTPP adsorbed on TiO<sub>2</sub>(110), between 3.2 and 3.5 times more molecules are left on the surface and we think this is because they adsorb in a tilted adsorption geometry (see Chapter 4.1.2). Using the measured XPS intensity of a sample with the defined coverage of 1 ML in the equation, one can calculate  $\lambda$  and then every unknown coverage of any samples. With this we found that 1 ML of 2HTPP attenuates substrate signals by approximately 10% when using Al K $\alpha$  radiation and by 50% when using synchrotron radiation and choosing the photon energy such that the substrate photoelectrons have a kinetic energy of 100 eV. However, this method has some disadvantages: when the X-ray beam is not stable between the measurement on the clean surface and after adsorption or when the distance between sample and analyzer is not constant this method can introduce errors. To overcome these uncertainties, we combine the first equation with a second one:

$$I_A = I_A^0 \cdot \left(1 - e^{-\frac{d}{\lambda \cos\theta}}\right)$$

This equation gives the intensity of an adsorbate signal  $I_A$  with a thickness  $d$ .  $I_A^0$  is the signal of an - for XPS - infinitely thick overlayer. This is obtained by measuring multilayers that are so

thick that no substrate signal is detected anymore. By using the intensity ratios  $I_A/I_S$  instead of the absolute values, the mentioned problems are overcome:

$$d = -\lambda \ln \frac{I_A^0/I_S^0}{I_A/I_S + I_A^0/I_S^0}$$

This equation is only valid when the mean free path of electrons coming from substrate and adsorbate is the same; therefore, the kinetic energy has to be the same or very similar. For synchrotron radiation, the photon energy can be set so that this is fulfilled, and for laboratory-source XPS lines with a similar binding energy should be used.

In a similar way, an equation can be derived to describe three-component systems. The attenuation in the adsorbate A, the intermediate layer B and the substrate C can be described by the following equations:

$$I_A = I_A^0 \cdot \left(1 - e^{-\frac{d_A}{\lambda \cos\theta}}\right)$$

$$I_B = I_B^0 \cdot \left(1 - e^{-\frac{d_B}{\lambda \cos\theta}}\right) \cdot e^{-\frac{d_A}{\lambda \cos\theta}}$$

$$I_C = I_C^0 \cdot e^{-\frac{(d_A+d_B)}{\lambda \cos\theta}}$$

By forming relative intensities, the three equations can be combined to calculate the thicknesses of the adsorbate A and of the intermediate layer B:

$$d_A = \lambda \cos\theta \ln \left(1 + \frac{I_B^0 I_C^0 I_A}{I_A^0 I_C^0 I_B + I_A^0 I_B^0 I_C}\right)$$

$$d_B = -\lambda \cos\theta \left[ \ln \frac{I_A^0 I_C}{I_C^0 I_A} + \ln \left(1 - e^{-\frac{d_A}{\lambda \cos\theta}}\right) \right] - d_A$$

These equations were used to calculate coverages of 2HTPP adsorbed on thin films of cobalt oxide that were grown on Ir(100).

### 2.1.3. Measuring on Non-conductive Samples

During the XPS process photoelectrons are emitted, and if the sample is not grounded or is insulating, a positive charge will accumulate. This results in a higher attractive interaction between the surface and the photoelectron and therefore in a lower kinetic energy. This leads to a peak shifting to higher binding energies. In addition, if the charge accumulation is not uniform across the surface, different photoelectrons will be shifted by different amounts and this causes a broadening of the XPS peaks. When measuring on metal surfaces, this is usually not a problem, but many oxides are insulating, and suitable methods have to be used to compensate the accumulating charge. In this work, I present measurements performed on two different oxide

surfaces. The first is cobalt oxide and we performed our measurements on in situ grown thin films on Ir(100). The low oxide-film thickness allows for electrons of the metal support to compensate the charge on the oxide surface. The second surface is TiO<sub>2</sub>(110) and here we used bulk crystals. In the first set of experiments, we annealed the crystals in ultrahigh vacuum to bulk-reduce them and increase their conductivity to measure XPS. We also performed experiments with wet-chemically prepared TiO<sub>2</sub>(110) crystals in air. These crystals were not reduced; instead, a low energy electron flood gun was used to compensate the positive charge. This can lead to an accumulation of negative charge in the region surrounding the X-ray spot on the sample and this repels electrons from the flood gun resulting in a worse neutralization.<sup>84</sup> To account for that, we used an automated dual beam charge neutralization setup with an additional argon ion gun to reduce the negative potential. As seen in the comparison of a Ti 2p measurement of a bulk-reduced TiO<sub>2</sub>(110) crystal without neutralization with a non-reduced crystal measured with neutralization in Figure 5, the neutralization setup overcompensates the charge slightly and peaks are shifted to lower binding energies by around 3 eV. We corrected the measurements to match the binding energies of the reduced crystals.

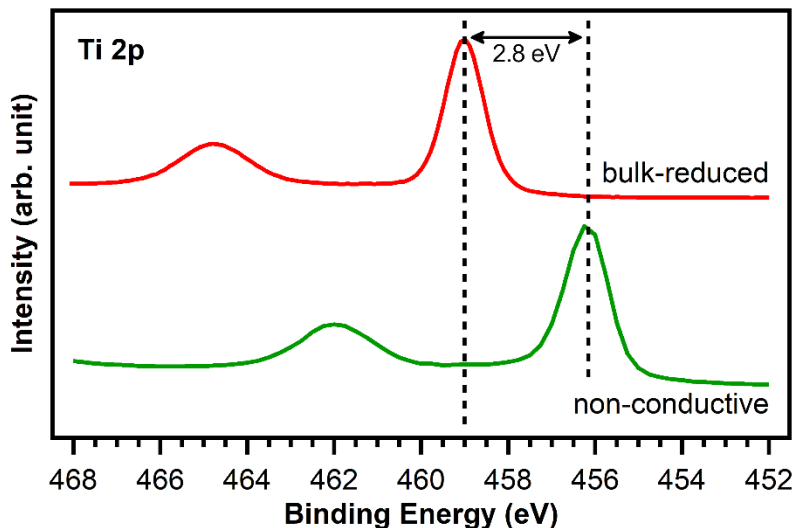


**Figure 5:** Ti 2p photoelectron spectra of a non-conductive TiO<sub>2</sub>(110) crystal measured with charge neutralization and of a reduced TiO<sub>2</sub>(110) crystal. The binding energy shift is 2.8 eV.

## 2.2. Near-edge X-ray Absorption Fine Structure (NEXAFS)

NEXAFS spectroscopy provides information about the electronic structure, especially of the unoccupied states, and about the adsorption geometry of molecules. In contrast to XPS the X-ray energy is swept, while the X-ray absorption is measured and, thus, synchrotron radiation is needed.

### 2.2.1. General Concept

In a NEXAFS measurement the X-ray absorption around an absorption edge is measured: if the photon energy is high enough to ionize an atom an increase in absorption intensity, the so-called edge jump, is detected. The left part of Figure 6 shows a schematic NEXAFS spectrum and the right part shows a typical C K-edge measurement of phthalic acid adsorbed on  $\text{Co}_3\text{O}_4(111)$ . NEXAFS spectra can be divided into two parts: the  $\pi^*$ -region below the edge jump and the  $\sigma^*$ -region above. Transitions into  $\pi^*$  orbitals result usually in narrow and intense peaks, whereas  $\sigma^*$  peaks have a larger linewidth.

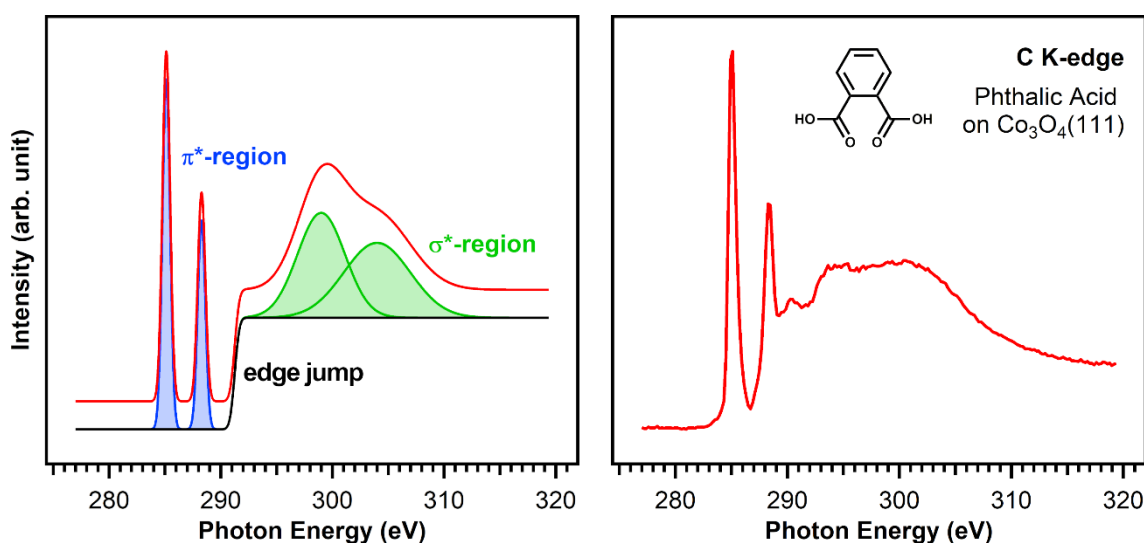


**Figure 6:** Left: Schematic NEXAFS spectrum showing the typical features. Right: C K-edge measurement of phthalic acid adsorbed on  $\text{Co}_3\text{O}_4(111)$ .

The typical way to measure X-ray absorption of thin organic adsorbates is to count secondary electrons. Depending on the energy window of the detected electrons one distinguished between total-, partial- and Auger-yield detection. In total-yield measurements all emitted electrons are detected. This results in a relative high signal intensity and the shortest measurement time of the three electron yield detection techniques. However, total-yield measurements are less surface sensitive than partial- and Auger-yield measurements because not only electrons from the top layers but also electrons from deeper layers are detected. To overcome this, in partial-yield detection mode a retarding voltage is applied to repel bulk electrons which have low kinetic energies due to inelastic scattering processes on their way to the surface. Auger-yield detection is even more surface sensitive. Here, only Auger electrons with a specific energy are detected. A disadvantage of Auger-yield detection is the weak signal intensity and the resulting longer measurement times. This leads to an increased risk of beam-induced degradation of the sample. In the NEXAFS measurements I present here, we used Auger-yield and total-yield detection.

### 2.2.2. Photon Flux Measurements

Independent of the chosen detection method the number of X-ray photons that hit the sample has to be recorded to determine the X-ray absorption. Organic contaminants on the beamline optics, caused by the adsorption of organic materials, lead to X-ray absorption at the absorption edges of the impurity elements and thus to a decrease in the X-ray intensity in this photon energy range. To overcome this, the photon flux can be measured with a gold mesh that is placed in the beam path just in front of the sample. However, just as the beamline optics, organic impurities can also adsorb onto the gold mesh. In our case, at the Material Science Beamline at the Elettra Sincrotrone in Trieste, Italy, the gold mesh detected a correct photon flux signal for photon energies around the N K-edge, see Figure 7, but carbon impurities on the gold mesh prevented us from measuring the photon flux in the C K-edge region. The resulting measured mesh current is a NEXAFS spectrum of the carbon impurities on the mesh (Figure 7, middle spectrum) and not the actual X-ray intensity as a function of photon energy.

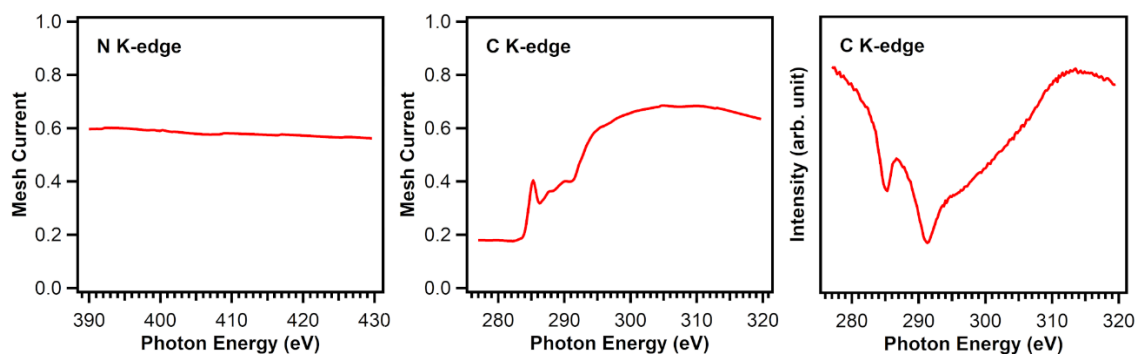


**Figure 7:** Photon flux recorded with a gold mesh for N K-edge (left) and C K-edge (middle). The signal in the carbon region is strongly influenced by carbon impurities on the mesh and does not resemble the photon flux on the sample. The right spectrum shows the photoelectron intensity of the Ti 3p peak for the photon energies used in a C K-edge measurement and is used as photon flux reference.

To account for that, the photoemission intensity of a XPS peak was measured as a function of photon energy and used as photon flux (Figure 7, right spectrum). On cobalt oxide, this was the Ir 4f peak (between 70 – 57 eV) and on TiO<sub>2</sub>(110) the Ti 3p peak was followed (32 – 45 eV). With this method we neglect variations of the cross-section when changing the photon energy and photoelectron diffraction effects, but the error in the resulting photon flux is still smaller than when measured with the gold mesh.

### 2.2.3. Auger-yield NEXAFS and Photoelectron Features

We measure Auger-yield NEXAFS spectra as two-dimensional images with the kinetic energy plotted against the photon energy. Figure 8 shows an example of the C K-edge region of phthalic acid adsorbed on Co<sub>3</sub>O<sub>4</sub>(111). The image contains several vertical lines from Auger electrons; the two sharp features between 285 and 290 eV are caused by transitions into  $\pi^*$  orbitals and the broader feature between 290 and 305 eV is caused by transitions into  $\sigma^*$  orbitals. Another feature,

but diagonal not vertical, is visible between 310 and 320 eV. Following this feature, the kinetic energy changes linearly with the photon energy: changing the photon energy by 10 eV from 310 to 320 eV, changes the kinetic energy by 10 eV as well. These diagonal features are caused by photoelectrons that are emitted and detected together with the Auger electrons. In a NEXAFS measurement these features are unwanted, and measures have to be taken to correct the measured spectrum to yield the true NEXAFS spectrum. We found photoemission features in all measurements we performed, including C and N K-edge measurements of different porphyrins and carboxylic acids on Ag(100), Ir(100), MgO(100), Co<sub>3</sub>O<sub>4</sub>(111) and TiO<sub>2</sub>(110) and we think this is a general problem in Auger-yield NEXAFS. The most common method to correct for those photoemission effects is to measure a reference NEXAFS spectrum of the clean surface and either subtract it from the measured data or divide by it. This method only achieves good results when the photoemission features do not change their binding energies or their shapes upon adsorbate adsorption and doesn't work at all when the photoemission features arise from the adsorbate itself. However, in many publications only little to no information about the applied corrections is given and from the one-dimensional spectrum it is not always clear if a correction method was successfully applied. This is why we record two-dimensional Auger-yield NEXAFS images and in addition, working with those two-dimensional NEXAFS images allowed us to develop a new method to remove photoemission features without the need of any additional reference measurements of the clean substrate. This method is presented in Chapter 4.3.

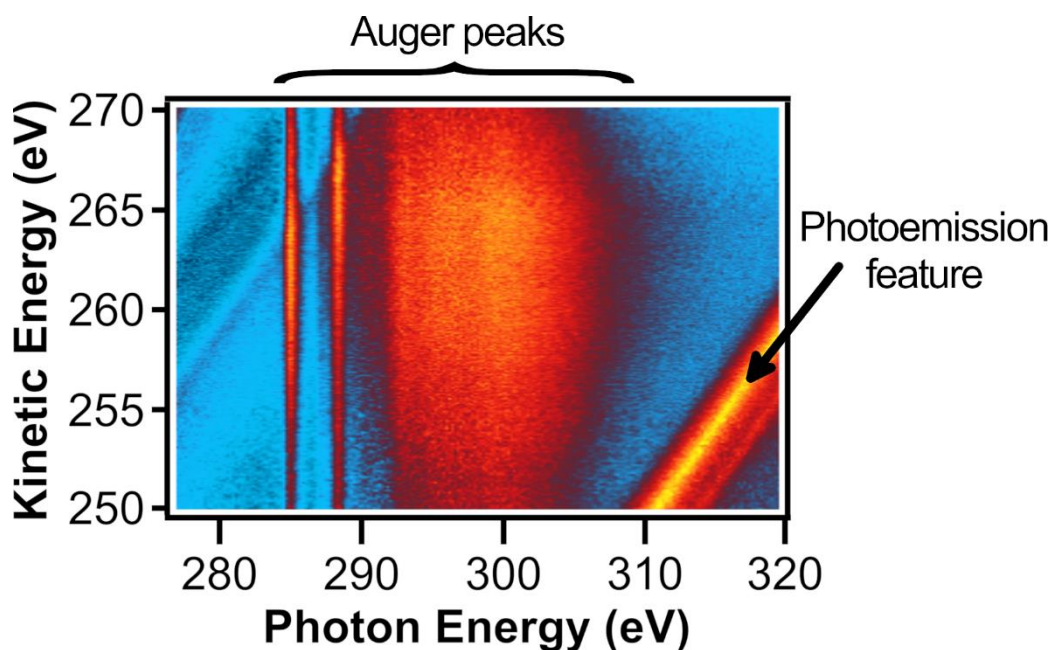


**Figure 8:** Two-dimensional NEXAFS image of phthalic acid on Co<sub>3</sub>O<sub>4</sub>(111). The vertical lines represent the wanted Auger signals. Diagonal lines (here especially in the lower right corner but also less intense in the upper left corner) come from XPS peaks that travel through the spectrum. These are unwanted and, if not removed, they will alter the one-dimensional NEXAFS spectrum.

### 2.2.4. Adsorption Angle Determination

The intensity of a NEXAFS signal, which is the electron transition from an initial state  $|\Psi_i\rangle$  to a final state  $|\Psi_f\rangle$  is, according to Fermi's Golden Rule, proportional to the transition dipole moment<sup>78</sup>:

$$I \propto |\langle \Psi_f | \mathbf{E} \mathbf{p} | \Psi_i \rangle|^2 = |\mathbf{E} \langle \Psi_f | \mathbf{p} | \Psi_i \rangle|^2$$

In the case of an 1s initial state the transition dipole moment points in the direction of the final state orbital vector  $\mathbf{O}$ :

$$I \propto (\mathbf{E}\mathbf{O})^2 = (E_x O_x + E_y O_y + E_z O_z)^2$$

Synchrotron radiation is usually elliptically polarized with the main component of the electric field parallel to the storage ring plane, and another one phase-shifted by  $\pi/2$  perpendicular to the ring plane.<sup>85, 86</sup> This allows for splitting up and describing the process as a sum of two linearly polarized beams:

$$I \propto (\mathbf{E}^{\parallel} \mathbf{O})^2 + (\mathbf{E}^{\perp} \mathbf{O})^2$$

The parallel  $\mathbf{E}^{\parallel}$  and the perpendicular electric field vector  $\mathbf{E}^{\perp}$  do not contribute equally intense to the NEXAFS signal. This is defined by the polarization factor P and is usually around 80%<sup>78</sup>:

$$I \propto P (\mathbf{E}^{\parallel} \mathbf{O})^2 + (1 - P)(\mathbf{E}^{\perp} \mathbf{O})^2$$

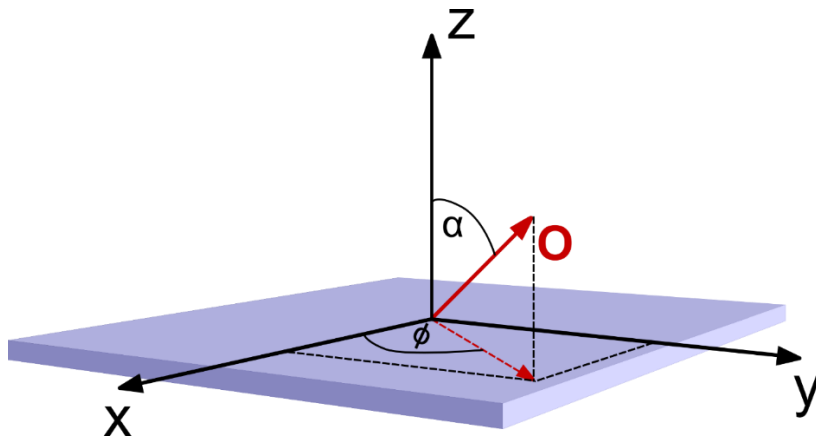


**Figure 9:** Schematic drawing of a crystal surface and a molecular orbital vector  $\mathbf{O}$ . The vector coordinates are defined by the polar angle  $\alpha$  and the azimuthal angle  $\phi$ .

In three-dimensional space a vector is defined by two angles, a polar angle which is relative to the z-axis and an azimuthal angle between the x-axis and the vector's orthogonal projection onto the xy plane. In our case, the z-axis is parallel to the surface normal and the surface lies in the xy plane. Furthermore, the x-axis is parallel to the principal symmetry axis of the surface. For our measurements, the sample was rotated around the y axis. The molecular vector  $\mathbf{O}$  with the polar angle  $\alpha$  and the azimuthal angle  $\phi$  has the coordinates:

$$\mathbf{O} = \begin{pmatrix} \sin \alpha \cos \phi \\ \sin \alpha \sin \phi \\ \cos \alpha \end{pmatrix}$$

And the main component of the electric field is described by the polar angle  $\theta$  and the azimuthal angle  $\eta$ :

$$\mathbf{E}^{\parallel} = \begin{pmatrix} \sin \theta \cos \eta \\ \sin \theta \sin \eta \\ \cos \theta \end{pmatrix}$$

The  $\mathbf{E}^{\perp}$  contribution lies in the xy plane and thus the polar angle is  $90^\circ$  and the azimuthal angle is orthogonal to the azimuthal angle of  $\mathbf{E}^{\parallel}$ .

$$\mathbf{E}^{\perp} = \begin{pmatrix} \sin(90^\circ) \cos(\eta + 90^\circ) \\ \sin(90^\circ) \sin(\eta + 90^\circ) \\ \cos(90^\circ) \end{pmatrix} = \begin{pmatrix} -\sin \eta \\ \cos \eta \\ 0 \end{pmatrix}$$

On surfaces with twofold symmetry, molecules can adsorb in a total of four mirror domains, differentiating by the sign of the polar or azimuthal angle. The total NEXAFS signal is then the average of all four single domains:

$$I_{\text{four domains}} \propto \frac{1}{4}I(\alpha, \phi) + \frac{1}{4}I(-\alpha, \phi) + \frac{1}{4}I(\alpha, -\phi) + \frac{1}{4}I(-\alpha, -\phi)$$

This simplifies the parallel and perpendicular contribution to:

$$I^{\parallel} \propto \sin^2 \alpha \cos^2 \phi \sin^2 \theta \cos^2 \eta + \sin^2 \alpha \sin^2 \phi \sin^2 \theta \sin^2 \eta + \cos^2 \alpha \cos^2 \theta$$

$$I^{\perp} \propto \sin^2 \alpha \cos^2 \phi \sin^2 \eta + \sin^2 \alpha \sin^2 \phi \cos^2 \eta$$

The equations presented here for twofold symmetric surfaces with 4 molecular domains were used to study the adsorption geometry of MCTPP on  $\text{TiO}_2(110)$  (P3).

In practical applications, the sample is usually rotated to measure at different polar incident angles. To measure at different azimuthal angles the sample has to be rotated around the surface normal. In many cases, including the beamlines where we measured at, this is not possible and the crystals have to be taken out of the ultrahigh vacuum, rotated, and remounted, and then inserted into the chamber again. In special cases, when the substrate symmetry is high enough, this can be avoided. On a hypothetical substrate with full rotational symmetry, the molecules can adsorb with all azimuthal angles and the equation can be simplified by integrating over all azimuthal adsorption angles  $\phi$ :

$$I^{\parallel} \propto \frac{1}{2} \sin^2 \alpha \sin^2 \theta + \cos^2 \alpha \cos^2 \theta$$

$$I^{\perp} \propto \frac{1}{2} \sin^2 \alpha$$

In practice, this equation can be used already for threefold symmetric surfaces and is also found in Joachim Stöhr's book "NEXAFS Spectroscopy"<sup>78</sup>. We used this equation to determine the adsorption angle for phthalic acid on the six-fold symmetric  $\text{Co}_3\text{O}_4(111)$  surface in Chapter 4.3.

### 3. Experimental Details

The results in this thesis are divided into two parts: the first part is a pure ultrahigh vacuum study to investigate the interactions of porphyrins with oxide surfaces. The second part is about porphyrin adsorption and reactions at the solid/liquid interface. In this Chapter the experimental details are discussed for both parts.

The first question we wanted to answer is if the surface structure of the oxide influences the reaction behavior of adsorbed molecules. Therefore we deposited 2HTPP on two different cobalt oxide surfaces,  $\text{Co}_3\text{O}_4(111)$  and  $\text{CoO}(111)$ . Bulk cobalt oxide is insulating and to be able to measure XPS, where usually a conductive sample is necessary, we grew thin films of cobalt oxide in situ onto a  $\text{Ir}(100)$  single-crystal. Besides the increased conductivity which allows us to measure XPS, the thin-film-approach also allows us to easily study porphyrin adsorption on two different cobalt oxide surfaces without the need of changing the crystal, because depending on the exact growth conditions, either  $\text{Co}_3\text{O}_4(111)$  or  $\text{CoO}(111)$  can be grown. The downside is that the preparation of a surface by growing it is more time consuming than sputter-cleaning. This is a major disadvantage especially during beamtimes at the synchrotron, when the measurement time is restricted.

The second system we wanted to study is MCTPP on rutile  $\text{TiO}_2(110)$ . A major part of these measurements is to investigate the interactions of adsorbed porphyrin molecules with solutions and therefore we immersed the crystals into different solutions. To avoid unwanted side-reactions with the substrate below, we decided not to work with  $\text{TiO}_2(110)$  thin films, which can be grown on metal substrates like  $\text{Ni}_{94}\text{Ti}_6(110)$ <sup>87</sup>,  $\text{Ni}(110)$ <sup>88</sup> or  $\text{Ge}(100)$ <sup>89</sup>, but to use bulk single crystals instead. To prevent charging effects during XPS, the  $\text{TiO}_2(110)$  crystals were reduced in ultrahigh vacuum for the first half of the measurements. The aim of the second half of the measurements on  $\text{TiO}_2(110)$  was to find a way to prepare porphyrin covered crystals outside of UHV with very basic means. This is why we did not reduce these crystals but used the charge neutralization setup described in Chapter 2.1.3 to measure XPS.

#### 3.1. Preparation of Cobalt Oxide Thin Films

For each experiment, a fresh layer of cobalt oxide was grown. Each grow step started with preparing the  $\text{Ir}(100)$  surface: impurities were cleaned off by accelerating argon ions at a pressure of  $2 \times 10^{-6}$  mbar onto the surface with an energy of 1 keV (sputtering). This removes the topmost layers from the surface and leaves a rough surface behind, which is cured by subsequent annealing to 1370 K for 3 minutes. Then, the crystal was annealed to 1270 K in oxygen atmosphere ( $10^{-7}$  mbar) for 5 minutes and annealed to 1370 K in UHV for another minute to yield a clean  $(5 \times 1)\text{-Ir}(100)$  surface. This was exposed to  $\text{O}_2$  ( $10^{-7}$  mbar) at 1270 K for 5 minutes and cooled down to 370 K in  $\text{O}_2$  to form a  $(2 \times 1)\text{-O}$  reconstructed surface. In the next step, cobalt was

evaporated in  $10^{-6}$  mbar  $O_2$  at 270 K.  $Co_3O_4(110)$  is obtained after annealing the surface to 520 K for 2 minutes in  $10^{-6}$  mbar  $O_2$  and subsequently in UHV to 670 K for 10 minutes. To prepare  $CoO(111)$ , the  $Co_3O_4(111)$  films were reduced by annealing in UHV to 830 K. Each step was followed by LEED. The thickness of the grown films was around 7 nm. This ensures that the conductivity of the sample is high enough to measure XPS, and at the same time the properties of the thin films resemble the ones from bulk cobalt oxide.

A more detailed description of the procedure to grow cobalt oxide thin films can be found elsewhere<sup>64, 90, 91</sup>

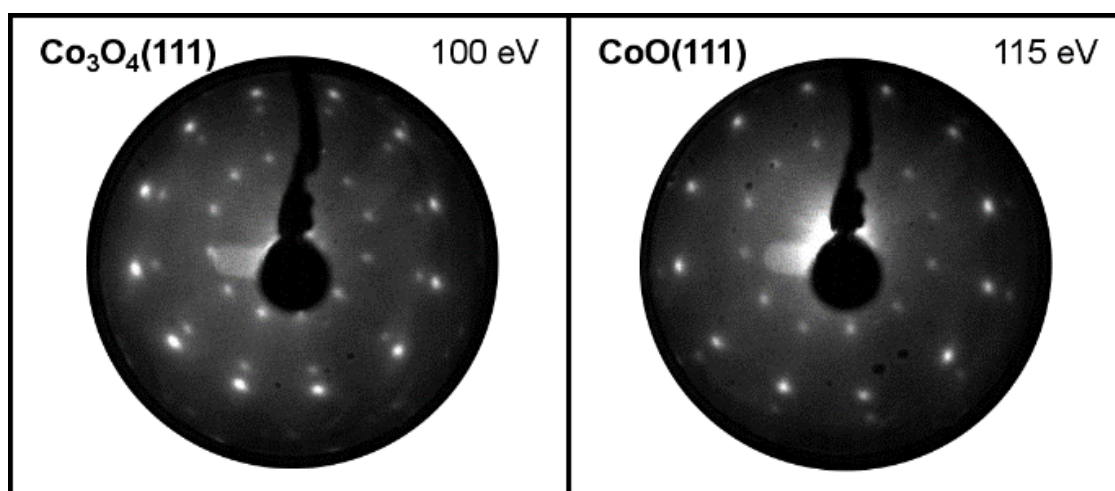


**Figure 10:** Typical LEED patterns of  $Co_3O_4(111)$  and  $CoO(111)$  thin films. Adapted in part from [P1] with permission from Chem. Eur. J.

## 3.2. Preparation of Rutile $TiO_2(110)$ Crystals

### 3.2.1. Preparation for UHV Experiments

In the measurements performed in Buenos Aires rutile  $TiO_2(110)$  crystals with an area of  $10 \times 10$  mm<sup>2</sup> were used. They were held by a 0.3 mm thin tantalum sheet, which was spot-welded onto the sample plate. Crystals with a thickness of 1 and 5 mm were used, and in both cases the tantalum sheets were never higher than the crystals to ensure that no tantalum is sputtered onto the crystal surface. This was also regularly controlled with XPS measurements. K-type thermocouples were in close distance to the crystal without touching it; because the thermal contact between the crystals and the tantalum sheet was low, the measured temperature of the sample holder was in all cases higher than of the crystal surface. After the measurements that are presented in this thesis, the sample mounting was changed. Now the crystals are glued with a magnesium oxide based ceramic glue (Kager Ceramabond 571) onto the sample holder and the thermocouples are glued directly onto the sides of the crystals, which gives an improved temperature reading. By comparing measurements done with both temperature readings, we

estimate the error of the non-glued crystals to be around 100 K at the highest temperatures of 1000 K.

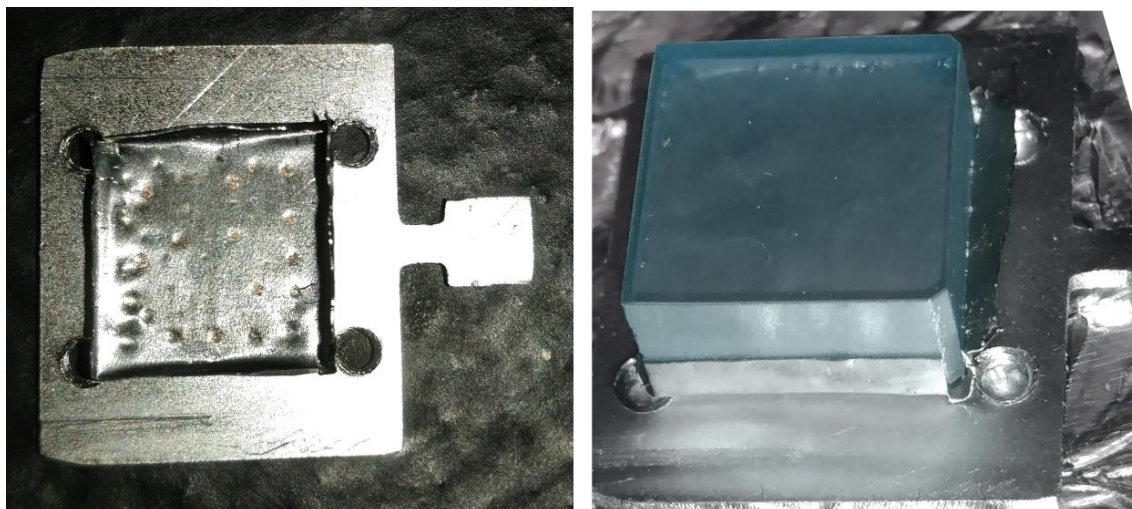


**Figure 11:** Tantalum sheets with bent sides were spot welded onto the sample plate and the  $\text{TiO}_2(110)$  crystals were held by these.  $\text{TiO}_2(110)$  crystals are usually non-conductive and to be able to measure XPS they were reduced by annealing them in ultrahigh vacuum. This changes the crystal color to blue.

$\text{TiO}_2(110)$  crystals are usually non-conductive; to be able to measure XPS, the crystal was reduced. This was done by annealing the crystals to 970 K in ultrahigh vacuum. The crystal color changes during this process from the usual white/yellowish color to light blue, see Figure 11 and Figure 12. Care has to be given that the temperature is not set too high, otherwise the crystal can be reduced too much, which results in dark blue to black crystals, see Figure 12.

The crystals were cleaned by consecutive cycles of sputtering with an ion energy of 1 kV at  $5 \times 10^{-6}$  mbar of argon pressure and subsequent annealing to 970 K.

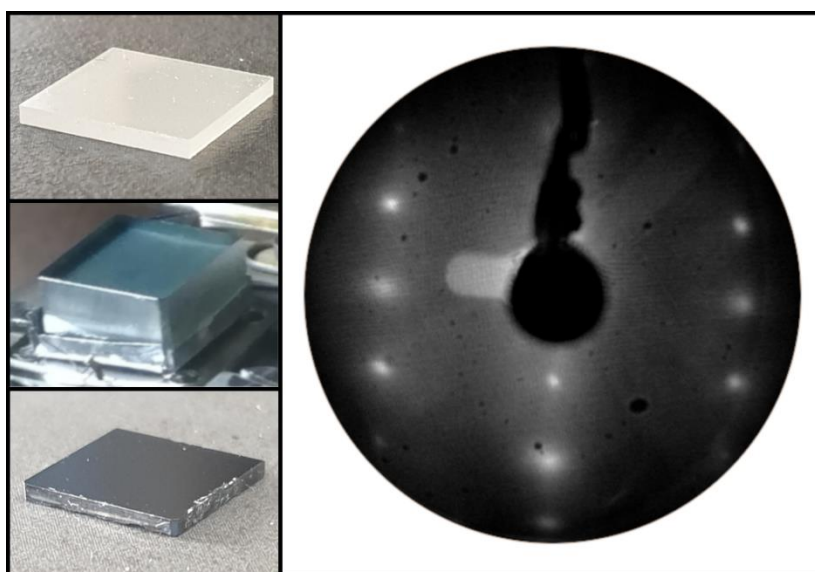


**Figure 12:**  $\text{TiO}_2(110)$  crystals untreated (top left), mildly reduced (middle left) and heavily reduced (bottom left). The right part shows a LEED pattern of the  $(1 \times 1)$  reconstructed surface.

### 3.2.2. Preparation for Wet-chemical Experiments

The aim of our wet-chemical experiments with TiO<sub>2</sub>(110) crystals was to completely leave ultrahigh vacuum and prepare the crystals fully in solution. XPS measurements, of course, were still performed in UHV. But in difference to the other experiments, the measurements of the wet-chemically prepared crystals in Chapter 4.2.3 (P4) were performed at an industrial XPS machine. We had the great opportunity to use the Phi Quantera II machine of the group of Prof. Karl Mayrhofer from the Helmholtz Institute Erlangen-Nürnberg for Renewable Energy. This device is equipped with a charge neutralization setup, and thus non-conductive unreduced TiO<sub>2</sub>(110) crystals can be measured without reducing them in vacuum. This greatly simplifies the sample preparation.

The liquid cleaning procedure as well as XPS and AFM measurements before and after cleaning are part of article P4 and will also be discussed in Chapter 4.2.3. However, to give the reader a better overview of the preparational steps, the details are described here.

All wet-chemical experiments were performed in standard-laboratory glass materials, such as beakers for the reactions itself, volumetric flasks to prepare solutions of reagents, Pasteur pipettes, petri dishes to cover beakers from dust and small glass vials to store crystals and solutions. To reduce the risk of contaminating crystals with metals and to prevent scratching the surface tweezers made of PMP were used instead of stainless-steel ones. Even small traces of metals can influence the measurements by reacting with the porphyrin molecules and forming metalloporphyrins.

Directly before usage, all glass materials were washed with ultrapure water that we thankfully got from the group of Prof. Jörg Libuda. Then an aqueous solution of 0.05 M KMnO<sub>4</sub>/0.005 M H<sub>2</sub>SO<sub>4</sub> was used to remove organic contaminants. To do so, all glass parts that will come in contact with either the TiO<sub>2</sub>(110) crystals or the reagent solutions - including the outside of pipettes or the outlets of beakers - were immersed in the cleaning solution for one hour. Afterwards, the acidic KMnO<sub>4</sub> solution is removed, and the glass materials were put in 10% H<sub>2</sub>O<sub>2</sub> solution for another hour. In the last step, after removing the peroxide solution, the glass ware was vigorously washed with ultrapure water. Even after cleaning new glass materials, especially Pasteur pipettes, often contaminate crystals and silicon is detectable in XPS. Therefore, all glass materials, also the disposable pipettes, were always reused and it was made sure to use them only for the same chemicals and processes.

The actual cleaning of the titania crystals is done by placing them in a beaker with 3% soap solution (Labwash premium extra) and sonicate them for 15 minutes to remove grease and particles. Afterwards they are sonicated in ultrapure water for another 15 minutes to remove remaining soap solution. The next step is the most important one and the actual cleaning step: the

crystals are heated to 65°C for 8 minutes in a three to one mixture of 25% NH<sub>3</sub> and 30% H<sub>2</sub>O<sub>2</sub>. To do so, the beaker is placed onto a heating plate and the temperature is measured in a second beaker with the same amount of solution that is also placed on the heating plate. This ensures that no impurities from the thermometer will come close to the crystals. Next, the crystals are thoroughly washed with ultrapure water and finally sonicated for another 15 minutes in water. Ideally, the crystals should be directly put in porphyrin solution afterwards to ensure that the amount of impurities picked up after cleaning is as low as possible. If this is not possible, storing them in closed glass vials filled with ultrapure water gave the best results.

The cleanliness of the TiO<sub>2</sub>(110) crystals is strongly dependent on the quality of the ultrapure water. Best results were obtained with Merck Milli-Q water and thus it was used in all steps.

The cleaning procedure described above also allowed us to clean crystals covered with porphyrins and thereby reuse the crystals. However, crystals that were used in metalation experiments and were placed in metal-ion containing solutions showed in some cases small XPS signals for those metals. Crystals that were placed in copper-solutions did not always get clean and, thus, were not reused.

We used double-sided UHV-compatible tape to glue the crystals onto the sample plate and this led to residues on the backsides of our crystals. In some cases, the cleaning procedure was not able to remove these residues completely on the first try and to account for that, we cleaned our crystals twice: the first time directly after the measurements and then they were stored in ultrapure water. Prior to each experiment we took the necessary number of crystals out of those already cleaned ones and cleaned them again. This resulted in reproducibly clean crystals.

Polished TiO<sub>2</sub>(110) crystals come with rough surfaces and to achieve a flat surface with large terraces, like UHV-annealed crystals usually have, we annealed our crystals in an oven to 950 °C for 22 hours in a pressurized air stream. AFM measurements before and after annealing are presented in Chapter 4.2.3.

### **3.3. Deposition of Molecules**

#### **3.3.1. Evaporation in UHV**

2HTPP was evaporated in a home-built Knudsen cell at 580 K, MCTPP at 473 K and phthalic acid at 380 K. For porphyrin samples, monolayers obtained by multilayer desorption (2HTPP: 525 K, MCTPP: 473 K) were used as coverage reference (more details in Chapter 2.1.2). When annealing porphyrin layers to multilayer desorption temperatures, they can undergo thermally induced changes: on Cu(111)<sup>35,92</sup> and on Ag(111)<sup>93</sup> a ring fusing reaction of the porphyrin phenyl rings to the macrocycle was observed for 2HTPP. This ring fusion should not change the number of porphyrins on the surface and we never observed changes in the XPS signal by annealing

porphyrin layers to multilayer desorption temperatures. Thus, it is valid to use those annealed monolayers as a coverage reference, but for actual measurements at the monolayer coverage, we directly evaporated the desired amount to avoid these structural changes.

### 3.3.2. Deposition from Solution under Argon Atmosphere

The porphyrin layers in Chapter 4.2.2 were deposited from solution onto a  $\text{TiO}_2(110)$  crystal that was cleaned in UHV. To reduce the risk of contaminating the crystals with impurities from air the deposition was done using an argon-filled liquid cell made of PTFE which is attached to a ultrahigh vacuum chamber in Prof. Federico J. Williams laboratory in Buenos Aires, Argentina. The same setup was used to expose titania crystals with evaporated porphyrins to metal-ion containing solutions (P2). Prior to each experiment, the reservoir that holds the solution was cleaned with acidic  $\text{KMnO}_4$  solution and  $\text{H}_2\text{O}_2$  (the same procedure as described above to clean glass materials). Ethanolic porphyrin solutions ( $c = 0.01 \text{ mM}$ ) were then poured into the liquid cell and the crystal was transferred out of UHV into the argon filled liquid cell. At no moment during transportation or exposure to the solution the crystal was in contact with air. To prevent contaminations from the sample holder or the surroundings it was made sure that only the crystal surface was touching the porphyrin solution.

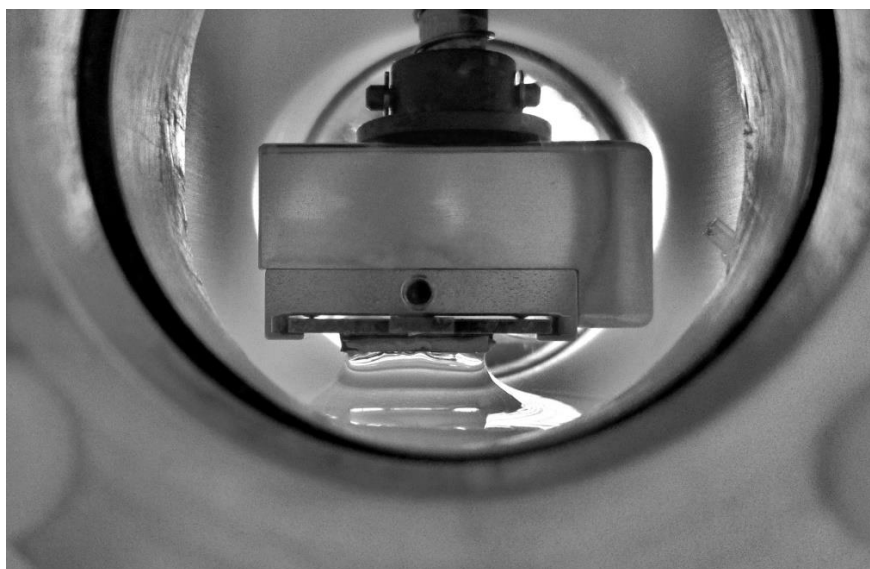


**Figure 13:**  $\text{TiO}_2(110)$  crystal touches solution in liquid cell.

After one minute, the crystal was retracted from the solution, rinsed either with ethanol or ultrapure water to wash away non-attached porphyrins and the remaining solvent droplet was blown off with an argon jet. Afterwards the crystal was transferred back to UHV.

This setup played an important role for the wet-chemical experiments in this thesis. It provided the necessary link between pure ultrahigh vacuum studies and measurements in ambient

conditions and helped us to gain first insights into the reaction behavior of adsorbed porphyrins with solutions.

### 3.3.3. Deposition from Solution under Ambient Conditions

In article P4 porphyrins were also deposited from solution but in air and not in a protective argon atmosphere. Ethanolic 0.01 mM porphyrin solutions were prepared and poured into a beaker. TiO<sub>2</sub>(110) crystals were placed in the solution and petri dishes were used to cover the beakers.

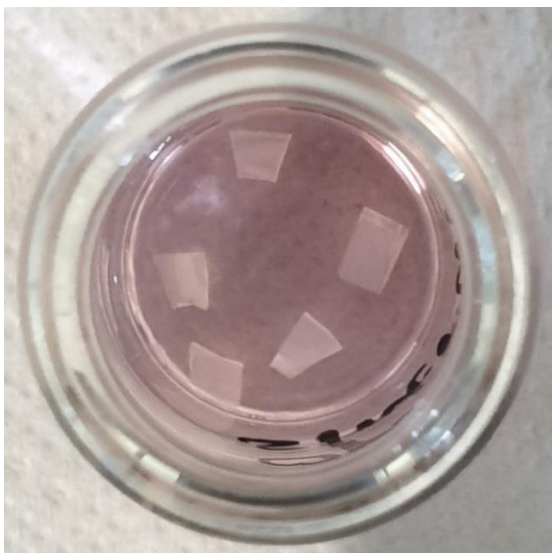


**Figure 14:** TiO<sub>2</sub>(110) crystals immersed in ethanolic 0.01 mM MCTPP solution in a beaker.

After 30 minutes, the crystals were rinsed with ethanol and either placed in the next solution (for example metal-ion-containing solutions to metalate the porphyrins) or prepared for XPS analysis. For the latter, the remaining ethanol on the crystal surface was blown off with nitrogen. After each preparation, the tweezers were cleaned with ethanol to avoid cross-contaminations during the rinsing process when crystals with different types of porphyrins were prepared. The dry crystals were glued with double-sided UHV-compatible copper tape onto the sample plate and transferred into the UHV chamber. To minimize the risk of picking up dust or other impurities from air, the time in air between the crystals being removed from solution and inserted into the vacuum chamber was kept as short as possible and was in all cases below 30 minutes. In addition, to prevent photodegradation the crystals were always kept in the dark.



## 4. Results

The results in this thesis are divided into three parts. Chapter 4.1 discusses the reactions of porphyrins adsorbed on oxide surfaces. In these ultra-high-vacuum studies, the influence of the surface structure was examined by comparing the reactions of 2H-tetraphenylporphyrin on two differently terminated cobalt oxide surfaces. Afterwards, the influence of the carboxylic acid anchoring group in functionalized tetraphenylporphyrins adsorbed on  $\text{TiO}_2(110)$  was investigated.

The second part describes a step-by-step approach to bring the preparation of porphyrin layers on rutile titania out of ultra-high vacuum and into solution. By studying the same system, MCTPP on  $\text{TiO}_2(110)$ , prepared with very different methods, the influence of solution-chemistry and of air was studied.

In the last part, a novel way to analyze 2D Auger-yield NEXAFS measurements is presented.

### 4.1. Porphyrin Reactions at Oxide Surfaces

In contrast to reactions of porphyrins on metal surfaces, only little was known about interactions with oxide surfaces when this work started. The adsorption of 2HTPP on  $\text{MgO}(100)$  done by Schneider et al.<sup>38</sup> was one of the first studies dealing with that topic. They have shown that the porphyrin molecules can pick up magnesium ions from the surface and incorporate them into the central porphyrin cavity forming the metalloporphyrin MgTPP. This reaction, also found on reactive metal surfaces, like copper<sup>30, 54, 92</sup>, iron<sup>60</sup> or nickel<sup>60</sup>, is known as self-metalation. The mechanism, however, is different on metal surfaces where a redox reaction takes place and the metal atom is oxidized while the central protons are reduced to  $\text{H}_2$ .<sup>56</sup> On oxide surfaces, we believe that the reaction happens through an ion-exchange mechanism where the metal ion is directly incorporated into the porphyrin pocket.<sup>38</sup> The protons are transferred to the surface and form hydroxyl groups at the location where the metal ion was sitting. In the case of  $\text{MgO}(100)$ , the magnesium ions are in oxidation state +2 and can easily be complexated by the porphyrins. Köbl et al.<sup>37</sup> and Lovat et al.<sup>39</sup> found that 2HTPP self-metalates on rutile  $\text{TiO}_2(110)$  as well.<sup>37, 39</sup> However, in contrast to  $\text{MgO}(110)$ , metalation does not happen at room temperature on  $\text{TiO}_2(110)$ , but needs elevated temperatures. We believe this is because the titanium ions are in oxidation state +4 and the formation of TiTPP is thus unlikely. Instead, a  $(\text{Ti}=\text{O})^{2+}$  unit is picked up and titanyl porphyrin is formed, which is a more complex reaction than the incorporation of a +2-metal ion.

Another difference between the two oxide surfaces, is the formation of a protonated porphyrin species on  $\text{TiO}_2(110)$ .<sup>37, 39, 66</sup> We believe that by an interaction with hydroxyl groups on the titanium surface the formerly non-protonated nitrogen atoms are protonated and an acidic porphyrin species is formed. Such a species is not observed on  $\text{MgO}(100)$ .

### 4.1.1. Influence of Surface Structure [P1]

These experiments were performed at the Material Science Beamline at the Elettra Sincrotrone Trieste in Italy.

Cobalt oxide thin films were grown in situ on Ir(100) (see Chapter 3.1). Depending on the preparation, the surface structure of cobalt oxide can easily be tuned<sup>64, 90, 91</sup>, and this allowed us to study the porphyrin reaction behavior on two different surfaces with only little additional preparational effort. The two structures that were chosen were reducible  $\text{Co}_3\text{O}_4(111)$  and non-reducible  $\text{CoO}(111)$ . The questions we wanted to answer were if self-metalation occurs on cobalt oxide surfaces as it does on  $\text{MgO}(100)$  and  $\text{TiO}_2(110)$ , but also if the different surface structures influence the metalation behavior, especially because the cobalt ions are very close to the surface in  $\text{Co}_3\text{O}_4(111)$  but more recessed in  $\text{CoO}(111)$  (Figure 15).

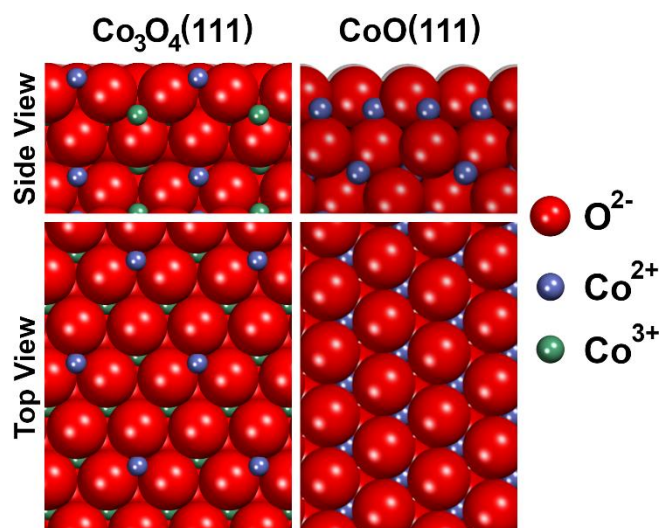


**Figure 15:** Model of  $\text{Co}_3\text{O}_4(111)$  (left) and  $\text{CoO}(111)$  (right). Adapted from [P1] with permission from Chem. Eur. J.

Figure 16 shows the N 1s XP spectra of an almost completed first layer of 2HTPP on both cobalt oxide surfaces at several temperatures. Already at 275 K, the spectra are a mixture of the typical two-peak-structure of a free-base porphyrin (green peaks) and the expected single-peak structure of the metalated molecule (blue peak). This means, that on both cobalt oxide surfaces, around 50% of the molecules self-metalate below room temperature and form – what we think is – CoTPP. On the first glance, this might be surprising: to be able to complexate the cobalt ion, it is necessary to break strong metal-oxygen bonds. However, as suggested by Schneider et al.<sup>38</sup>, we believe the reaction happens through an ion-exchange mechanism and the protons that were formerly attached to the nitrogen atoms form localized hydroxyl groups on the oxide surface. In addition, DFT calculations for 2HTPP on  $\text{MgO}$ <sup>38</sup> have shown that the energetics would favor a reaction at step-edges and corners and if this is also the case on cobalt oxide, this could not only

explain why CoTPP is formed already below room temperature, but also why the reaction is independent of the cobalt oxide terrace conformation.

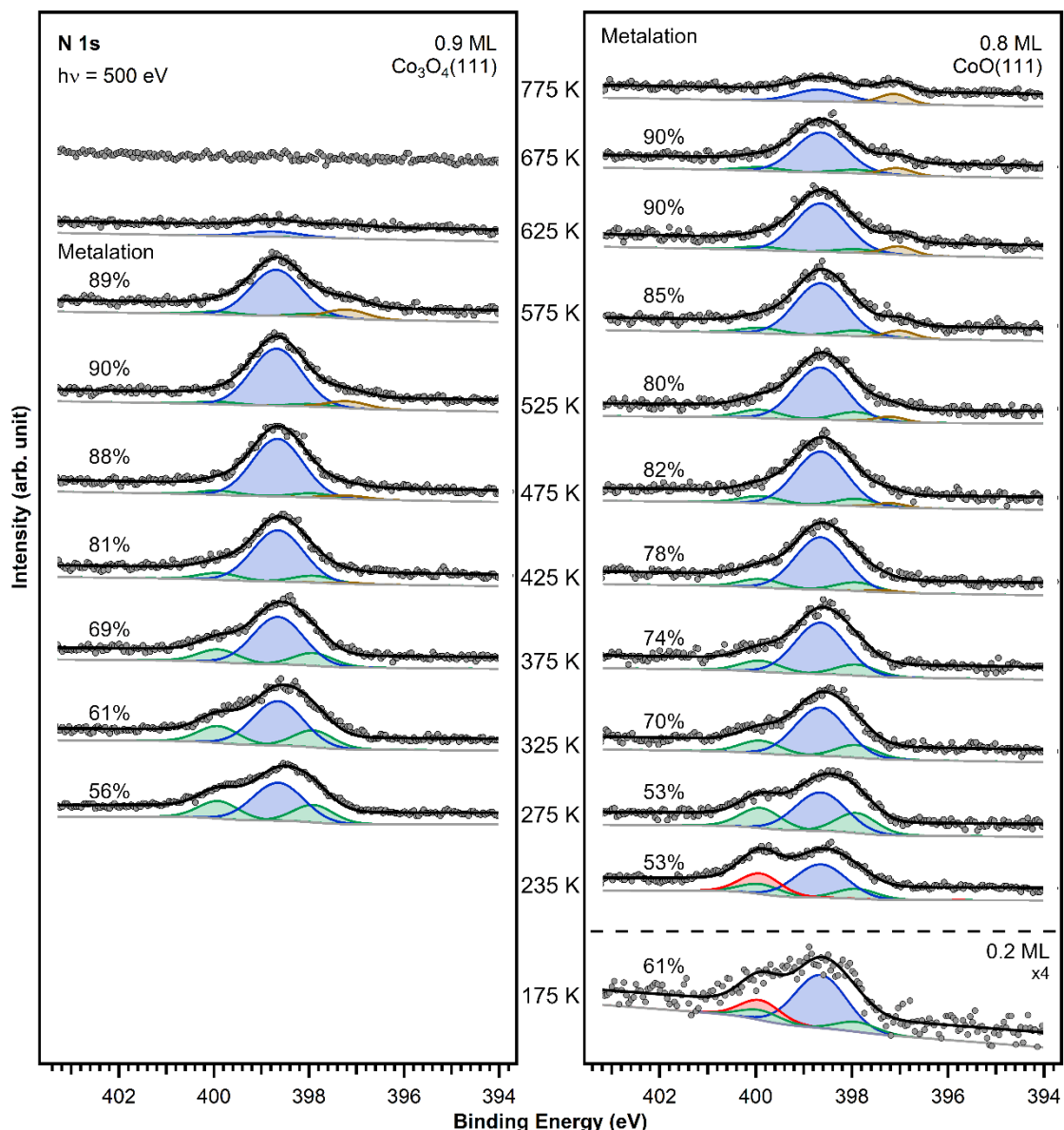


**Figure 16:** N 1s spectra of monolayer coverages of 2HTPP on  $\text{Co}_3\text{O}_4(111)$  (left) and  $\text{CoO}(111)$  (right) heated in 50 K steps, 10 minutes per step, to 775 K. Green peaks represent the free-base porphyrin molecules, protonated porphyrins give rise to the red peaks and the blue peaks are attributed to the metalloporphyrin species. Brown peaks are decomposition products at higher temperatures. Modified from [P1] with permission from Chem. Eur. J.

On  $\text{CoO}(111)$ , metalation was also detected at 175 K; notably an additional compound at the position of the high binding energy peak is present (red peak). This is very similar to the observation of protonated porphyrin species on  $\text{TiO}_2(110)$ .<sup>37, 39, 66</sup> There, the acidic porphyrin species is stable up to above 400 K and hinders the incorporation of metal ions during self-metalation. Furthermore, at low coverages, this species is the only visible one on  $\text{TiO}_2(110)$  and

no iminic nitrogen peak at lower binding energies is present, suggesting that not only one nitrogen atom per molecule but all two get protonated and a diacid porphyrin is formed. However, on cobalt oxide the species behaves different. It is only present at low temperatures and even at 0.2 ML a low binding energy species at around 398 eV is present. The ratio between the peak at around 400 and at 398 eV is always 3 to 1, and that could mean that – in difference to  $\text{TiO}_2(110)$  – not a mixture of diacid and free-base porphyrins is present but that all porphyrins are singly protonated and form a monoacid species. We assume that, because of the differences in the behavior and because hydroxyl groups on cobalt oxide should be stable up to much higher temperatures than 275 K<sup>94</sup>, a different reaction occurs in this case. Even in the low-pressure range, where the measurements were performed, there is still a substantial amount of water in the background pressure of the ultrahigh vacuum chamber and at low temperatures water adsorption is a common process. The desorption temperature of water on  $\text{CoO}(111)$  is known to be around 250 K<sup>95</sup> and lies therefore in between the two spectra where the protonated species vanishes. Therefore, we think that the interaction with intact adsorbed water and not with surficial hydroxyl groups forms the protonated species on cobalt oxide.

At temperatures above 575 K clear differences can be observed between the two cobalt oxide surfaces. Whereas  $\text{Co}_3\text{O}_4(111)$  shows almost no nitrogen at 625 K anymore and no organic compounds are detectable at 675 K,  $\text{CoO}(111)$  exhibits some nitrogen and also carbon (not shown) on the surface even at 775 K. We believe this is because porphyrin molecules are able to react with oxygen atoms in the reducible  $\text{Co}_3\text{O}_4$  thin film, thereby reducing  $\text{Co}_3\text{O}_4(111)$  to  $\text{CoO}(111)$ .  $\text{CoO}(111)$  is a non-reducible oxide and therefore no oxygen is evolving upon annealing. The porphyrins decompose (brown species) but cannot desorb. The signal decrease at 775 K could be caused by a segregation of the decomposition products into the bulk.

We have now shown that 2HTPP reacts on both cobalt oxide surfaces very similar. The behavior is very close to what was observed on  $\text{MgO}(100)$ <sup>38</sup>, but differs from the behavior on  $\text{TiO}_2(110)$ <sup>37, 39</sup> (see Figure 17). We believe this is because  $\text{MgO}(100)$ ,  $\text{CoO}(111)$  and  $\text{Co}_3\text{O}_4(111)$  all contain +2-metal ions which are easily inserted into the porphyrin pocket, whereas  $\text{TiO}_2(110)$  only contains  $\text{Ti}^{4+}$  ions, which can only be inserted into the porphyrin pocket as titanyl ( $\text{Ti}=\text{O}$ )<sup>2+</sup> units, a much more complicated reaction. We therefore, tentatively, suggest that room temperature metalation could be a common feature for +2-metal oxide surfaces, whereas elevated temperatures are required for surfaces without ions in oxidation state 2+.

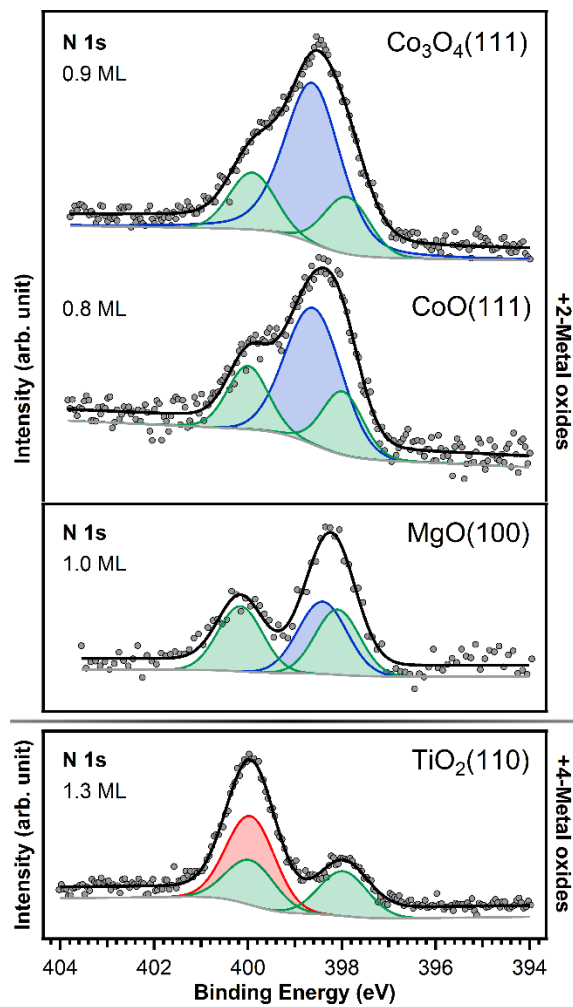


**Figure 17:** N 1s XP spectra after adsorption of 2HTPP on  $\text{Co}_3\text{O}_4(111)$  and on  $\text{CoO}(111)$  at 275 K and on  $\text{MgO}(100)$ <sup>38</sup> and  $\text{TiO}_2(110)$ <sup>37</sup> at room temperature. Modified from [P1] with permission from Chem. Eur. J.

#### 4.1.2. Influence of Anchoring Groups [P2, P3]

This data was measured in cooperation with the group of Prof. Federico J. Williams from the Universidad de Buenos Aires in Argentina.

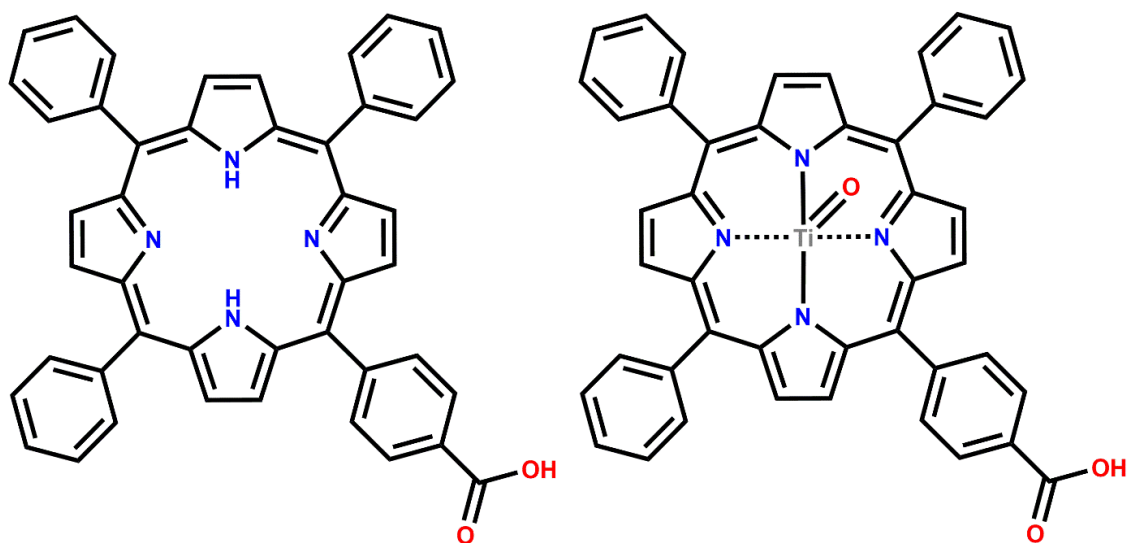


**Figure 18:** 5-(monocarboxyphenyl)-10,15,20-triphenylporphyrin (MCTPP) (left) and its metalated counterpart TiO-MCTPP (right). Adapted from [P2] with permission from J. Phys. Chem. C.

This part of the thesis addresses the influence of linker groups on the adsorption and reaction behavior of porphyrins on rutile  $\text{TiO}_2(110)$ . The studied molecule is 5-(monocarboxyphenyl)-10,15,20-triphenylporphyrin (MCTPP), which is structurally very similar to 2HTPP and has one additional carboxylic acid group in para-position on one of the phenyl rings (Figure 18). Comparing C 1s and O 1s spectra of mono- and multilayer preparations (not shown, see Figure 2 in article P2) shows that the acid group of the first layer, in direct contact with the  $\text{TiO}_2(110)$  surface, is deprotonated, which means that the molecules bind most likely covalently to the oxide surface. To prepare a reference sample for coverage calculation, multilayers of MCTPP were evaporated and annealed to 473 K. For many porphyrins on different metal and oxide surfaces this is a reproducible way to create one fully closed layer of molecules. In this case, the number of remaining molecules is also reproducible, but it is around three times higher than for 2HTPP on the same surface (Figure 19). This means either the first three layers of MCTPP are stabilized and do not desorb together with higher layers, or - what we assume - the remaining molecules after multilayer desorption adsorb in a tilted geometry. This was also observed for the same functionalized porphyrin on  $\text{Co}_3\text{O}_4(111)$ <sup>32</sup>: at low coverages, the molecules adsorb with the macrocycle parallel to the surface and with increasing coverage they start to tilt away from the surface. Coverage-dependent differences in reactivity, that are visible in the N 1s spectra in Figure 20 and will be discussed later, support the idea that there is a change in adsorption geometry.

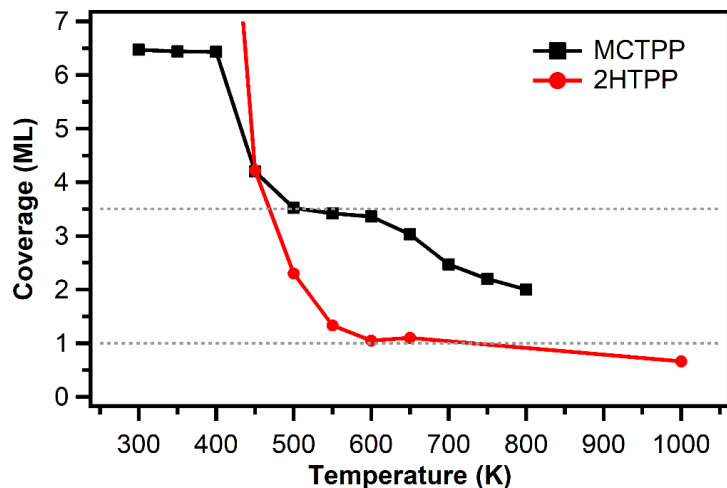


**Figure 19:** Comparison of the desorption of 2HTPP and MCTPP on  $\text{TiO}_2(110)$  (unpublished).

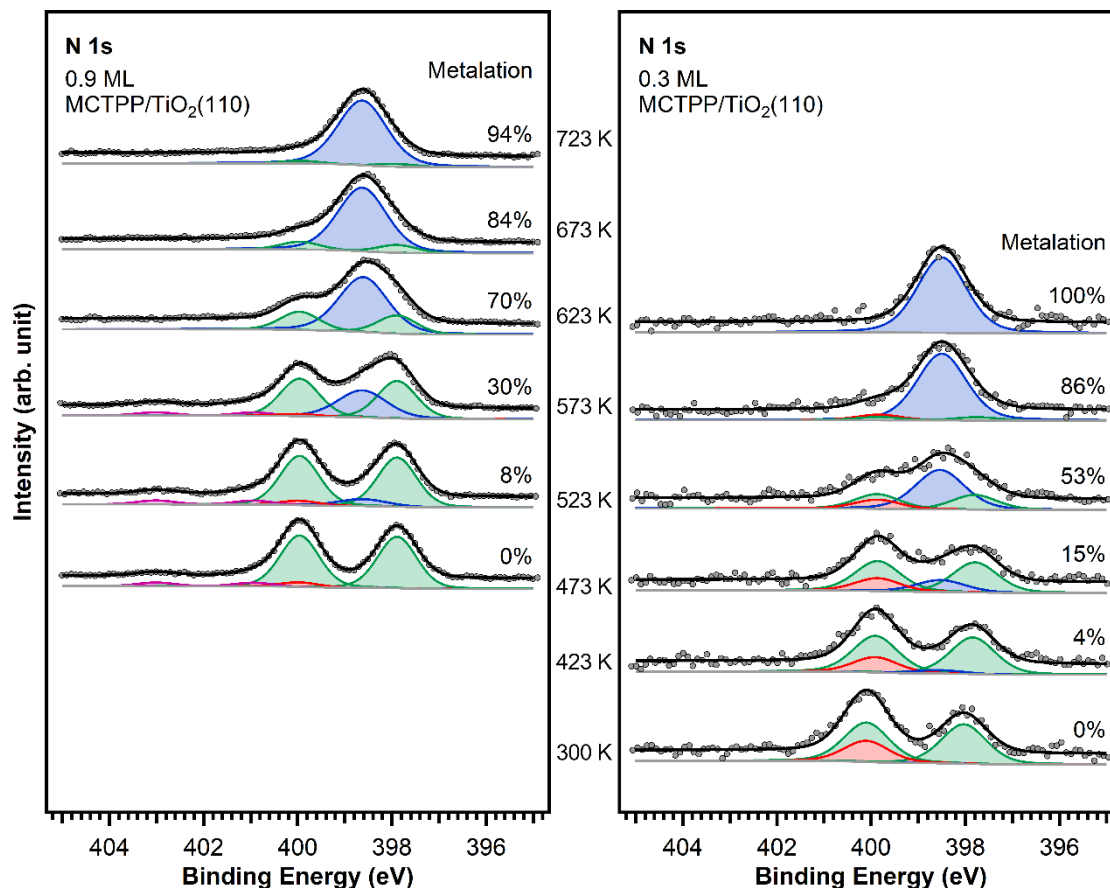


**Figure 20:** N 1s spectra of 0.9 and 0.3 ML MCTPP adsorbed on  $\text{TiO}_2(110)$  from 300 to 723 K. During annealing, the green peaks assigned to the free-base porphyrin are decreasing, while a new peak is rising. This feature is assigned to the self-metalation product, which we think is  $\text{TiO-MCTPP}$ . The 0.3 ML sample metalates at lower temperatures. We suggest this is due to a change in geometry, going from flat-lying to tilted adsorption structure with increasing coverage. Modified from [P2] with permission from J. Phys. Chem. C.

Figure 19 shows also that when annealing MCTPP to temperatures higher than 600 K there is a second desorption step. Based on carbon and oxygen XP spectra we suggested in article P2 that the desorbing species might be decomposed porphyrins that lost their linker group. But recent unpublished temperature-programmed desorption (TPD) measurements, done in our home laboratory in Erlangen, have shown that mainly intact MCTPP desorbs upon heating.

In the next step, the N 1s region of MCTPP on rutile  $\text{TiO}_2(110)$  as a function of temperature was studied. Especially, the differences between flat-lying, low coverage and tilted, high coverage preparations were investigated. Figure 20 shows N 1s spectra of 0.9 and 0.3 ML MCTPP (here 1 ML is the coverage of the upright-standing layer left after multilayer desorption; in comparison to flat-adsorbing 2HTPP the coverages would be 2.9 ML and 1.0 ML). Whereas the higher coverage preparation shows the expected one-to-one ratio between the peaks of the iminic ( $-\text{N}=\text{C}$ ) and aminic ( $-\text{NH}-$ ) nitrogen atoms, lower coverages show a clear deviation and a higher amount of the aminic nitrogen species. This additional amount is fitted with a separate, red-colored peak. This was already observed for 2HTPP<sup>37, 39, 66</sup> and we think this comes from an interaction of surface hydroxyl groups with the molecules and a formation of acidic porphyrins. If the high-coverage layers are really tilted away from the surface, the interaction would be weaker and therefore, it would not be surprising to see no (or only little) protonation on the left side of the Figure. In both cases, annealing leads to the formation of TiO-MCTPP (blue peak in Figure 20; see Figure 18 for molecular structure), but metalation occurs at significantly lower temperatures for lower coverages. We think this is also explained by the different adsorption geometry because the interaction between surface ions and the porphyrin nitrogen atoms is higher when they are closer. In all cases, metalation was never observed at room temperature or below, exactly as for 2HTPP on  $\text{TiO}_2(110)$  and in contrast to metalation on cobalt oxide surfaces as seen in the previous part.

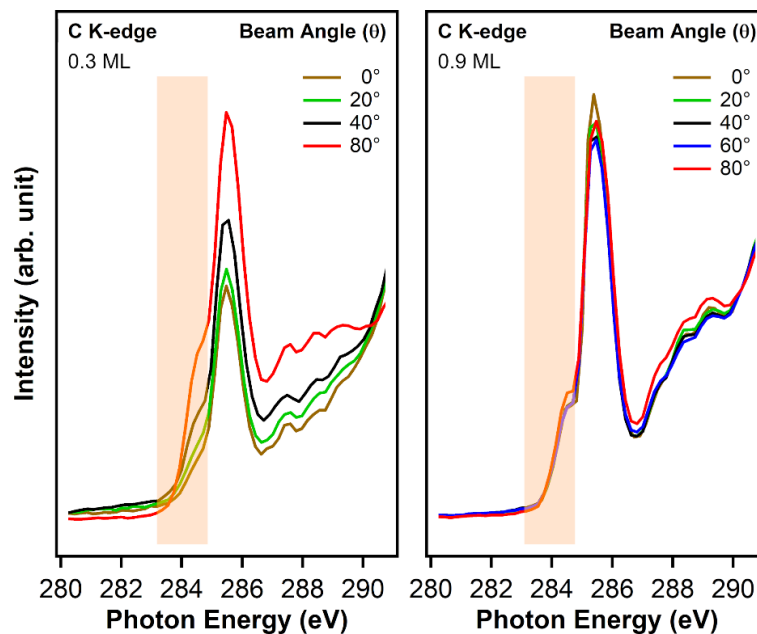


**Figure 21:**  $\pi^*$ -region of C K-edge NEXAFS measurements of 0.3 and 0.9 ML of MCTPP adsorbed on  $\text{TiO}_2(110)$ . The shoulder at around 284 eV (marked orange) is caused from transitions of electrons located at the macrocycle carbon atoms. The different incidence angle dependence of the two measurements shows that the adsorption geometry is different.

To prove that the adsorption geometry changes with coverage, NEXAFS measurements were performed. Figure 21 shows unpublished spectra recorded for 0.3 ML and 0.9 ML.  $\text{TiO}_2(110)$  is a two-fold symmetric surface and as described in Chapter 2.2.4 both the polar as well as the azimuthal dependency of the NEXAFS signal on the incident X-ray beam has to be measured to calculate adsorption angles. Unfortunately, we only measured at one azimuthal angle and therefore we cannot derive adsorption angles from the two measurements. However, the dependence on the incident X-ray beam is different: in the 0.7 ML measurement the macrocycle signal at around 284 eV shows highest intensities at gracing incidence ( $80^\circ$ ) whereas for higher coverages no polar dependency of the macrocycle is found. This means, that the adsorption geometry is between the two coverages is different, but we cannot tell if the porphyrin molecules inhibit a different tilt angle as expected or if only the azimuthal orientation of the molecules along the surface is different.

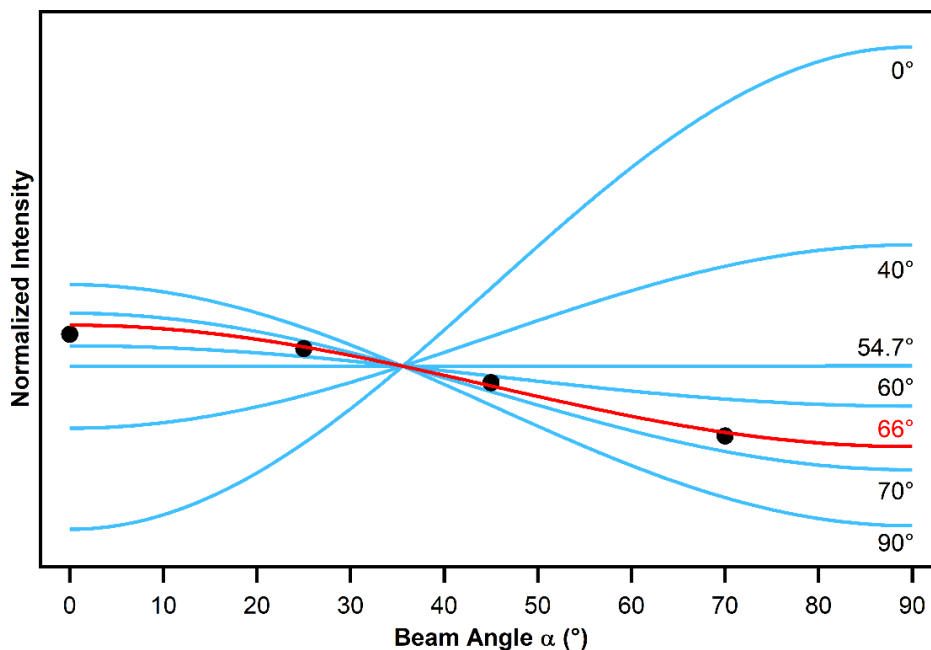


**Figure 22:** Angular dependence of the N K-edge NEXAFS measurements of 0.3 ML of wet-chemically deposited MCTPP on  $\text{TiO}_2(110)$ . The molecules adsorb tilted with an angle of  $66^\circ$  relative to the surface plane.

NEXAFS measurements were also performed on solution-deposited MCTPP layers. A detailed discussion of the wet-chemical preparation is given in Chapter 3.3. The data was recorded at the PGM-U11 beamline of the Brazilian Synchrotron Light Laboratory (LNLS) in Campinas, Brazil and published in article P3 together with Cynthia C. Fernández from Prof. Federico J. William's group. Figure 22 shows the plot of the N K-edge peak intensities against the incident angle of the X-ray beam. In this case, the data was measured at two azimuthal angles, but the measurements show no azimuthal dependence, which means either the azimuthal adsorption angle is  $45^\circ$  or a mixture of every azimuthal adsorption angle. The polar adsorption angle is  $66^\circ$  and this means that the molecules adsorb tilted, however, the coverage in this case is similar to the low coverage case shown previously and one would expect a flat-lying geometry. This could be caused by the preparational method: even though the porphyrin coverage is low, the remaining surface will not stay empty when put in solution. Solvent molecules and impurities from air and solution will coadsorb onto the surface and could induce the geometry change that we would expect only for higher coverages.

Coming back to the C K-edge NEXAFS measurements in Figure 21: when we assume the azimuthal adsorption angle is also  $45^\circ$  in the case of the evaporated porphyrin molecules we can calculate the respective polar adsorption angles. This yields  $55^\circ$  for the high-coverage preparation and  $32^\circ$  for the 0.3 ML coverage. Whereas the first angle is close to the angle observed for wet-chemically prepared MCTPP molecules and also near the range of other carboxylic acids on  $\text{TiO}_2$ <sup>96-98</sup> ( $60^\circ - 70^\circ$ ; see also Chapter 4.3), the latter is in the range of what a flat-adsorbed but

distorted tetraphenylporphyrin would yield: polar adsorption angles of  $30^\circ$  for CoTPP on Ag(111)<sup>27</sup>,  $31^\circ$  for CoTPP on Ag(100)<sup>51</sup> and  $20^\circ$  on Cu(111)<sup>90</sup> were reported based on C K-edge NEXAFS measurements. Due to the steric hindrance between the phenyl and pyrrole rings, porphyrins often adsorb in a distorted geometry and both, the well-known saddle shape structure<sup>49, 52, 53</sup> as well as the recently found inversed porphyrins<sup>50</sup> would appear as slightly tilted in NEXAFS because of the distorted macrocycle tilting the pyrrole rings relative to the surface.

In article P3, three more carboxylic acid functionalized molecules were studied: two tetraphenylporphyrins with acid groups at two phenyl rings in, respectively, cis and trans positions, and a molecule functionalized on all four phenyl rings. The cis-difunctionalized molecule shows the same adsorption geometry as MCTPP. The trans species on the other hand behaves different: it adsorbs with a tilt angle of  $45^\circ$ , which is also in range for a flat-adsorbed but distorted molecule. The carboxylic acid molecule with four groups shows no polar dependence. That means either that all molecules adsorb with an angle of  $54.7^\circ$  or they adsorb in different adsorption geometries with a mean angle of  $54.7^\circ$ . We think, that some TCPP molecules behave like cis-difunctionalized molecules and exhibit a tilted adsorption geometry, while others adsorb flat like the trans molecules.

## 4.2. Porphyrins at Solid/Liquid Interfaces

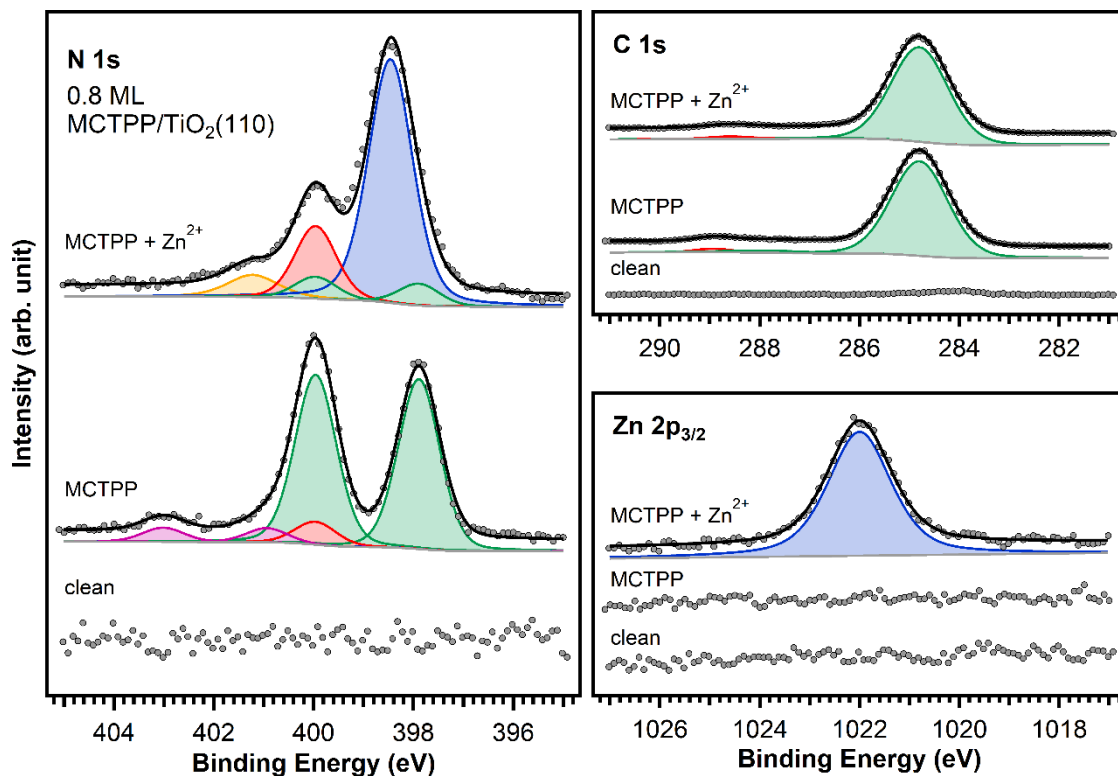
The second aim of this thesis is to study the influence of liquids on the different steps of porphyrin layer preparation. As discussed above, potential applications of large organic molecules, like porphyrins often need a metal oxide support, and important details were discussed in the previous part. But the previously shown measurements still do not resemble real every-day-systems. Preparing surfaces in UHV by sputtering and annealing, evaporating porphyrins and metalating them afterwards is a good way to get well-defined and impurity-free surfaces in a reproducible way that can be analyzed with surface-science techniques and can yield understanding of the processes on atomic level. However, for commercial applications, this preparation is in many cases too complex and too pricy. Wet-chemical preparation, on the other hand, is a very easy and cheap way to prepare surfaces. By immersing oxide crystals in porphyrin-containing solutions molecules can adsorb onto the surface but one risks the coadsorption of impurities which can lead to more complex XP spectra that are more difficult to interpret.

This chapter shows one potential way to bridge the gap: by using a step-by-step approach, the same system, MCTPP on  $\text{TiO}_2(110)$ , is prepared in several different ways, going from well-controllable pure UHV, as seen in the previous section, to a complete liquid approach in air, where ultrahigh vacuum was only involved in measuring XPS.

### 4.2.1. Reactions of Porphyrin Layers in Solution [P2]

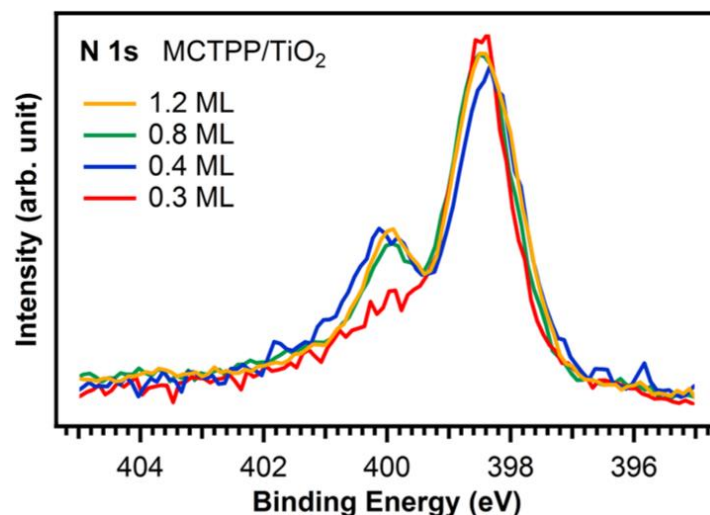
The data presented here was measured in the laboratory of Prof. Federico J. Williams in Argentina. It is the second part of Article P2 and discusses the effect of exposing UHV-prepared porphyrin layers on  $\text{TiO}_2(110)$  to aqueous zinc acetate solution in argon atmosphere.

Figure 23 shows the nitrogen, carbon and zinc XPS region of MCTPP on  $\text{TiO}_2(110)$  before and after  $\text{Zn}(\text{OAc})_2$  exposure. The change in shape of the N 1s spectrum shows that a metalloporphyrin is formed after the liquid treatment and a metalation degree of 69% is achieved. This fits well with the amount of zinc on the surface. In addition, at higher binding energies a new species is present after treatment. This comes from nitrogen-containing impurities and was also observed by Franke et al. in similar experiments with 2HTPP adsorbed on  $\text{Au}(111)$ .<sup>73, 74</sup> Franke et al. were able to desorb the impurities by annealing the surface to 523 K but in our case, with MCTPP adsorbed on  $\text{TiO}_2(110)$ , this was not possible. However, the total number of impurities, that are picked up during  $\text{Zn}(\text{OAc})_2$  exposure, is little: the nitrogen and carbon amounts increase only by less than 10%. We think that the almost full layer of porphyrins protects the surface from the adsorption of more impurities.



**Figure 23:** N 1s, C 1s, and Zn 2p<sub>3/2</sub> spectra of 0.8 ML MCTPP on TiO<sub>2</sub>(110) before and after exposure to a 1.0 mM aqueous solution of zinc acetate at pH 6 for 2 hours. The treatment with zinc ion-containing solution leads to partial metalation of the porphyrins. Modified from [P2] with permission from J. Phys. Chem. C.

As discussed in Chapter 4.1.2, the adsorption geometry of MCTPP on TiO<sub>2</sub>(110) is dependent on the coverage, resulting in molecules with their macrocycle close to the surface for lower amounts and tilted away for higher coverages. Therefore, different coverages were prepared, and it was found that lower coverages exhibit more metalation after the exposure to zinc acetate solution. One reason could be that the metal ions can easily reach the porphyrin center of the molecules with the macrocycle parallel to the surface, but in the high-coverage case, with the molecules forming densely packed upright-standing islands, the polar reaction solution cannot penetrate the non-polar layer of phenyl rings and it is more difficult for the metal ion to reach the porphyrin center.



**Figure 24:** Normalized N 1s spectra of MCTPP on TiO<sub>2</sub>(110) after exposure to an aqueous solution of 1.0 mM zinc acetate at pH 6 for 2 hours, indicating a coverage dependency of the metalation reaction. Coverages below 0.4 ML yield higher degrees of metalation and we think this is caused by a different adsorption geometry. Adapted from [P1] with permission from J. Phys. Chem. C.

From solution chemistry it is known that metalation of porphyrins is often favored under alkaline conditions.<sup>99</sup> This favors the abstraction of the protons from the two nitrogen atoms. Acidic conditions, on the other hand, can lead to an increased formation of protonated porphyrins, hinder the metalation reaction and even demetallate already metalated molecules.<sup>100</sup> We wanted to know how the pH value influences the metalation reaction of porphyrins adsorbed onto surfaces and therefore we prepared aqueous zinc acetate solutions with pH of 3, 6 (the previously shown spectra) and 14. Figure 25 shows that the highest degree of metalation is achieved at pH 6. As expected, for acidic pH values the degree of metalation is smaller, both for high and low coverages. However, for pH = 14 the amount of metalated porphyrins is even smaller. One explanation is that at this pH value the prominent zinc species is negatively charged zincate  $Zn(OH)_4^{2-}$ <sup>101, 102</sup> and to be able to get complexated by a porphyrin molecule it has to lose four hydroxyl groups, which is very difficult at these conditions. Another reason is that the TiO<sub>2</sub>(110) surface itself is negatively charged at these conditions and this might repel the zincate anions. Another observation is that in both cases, the high and the low pH preparation, the amount of impurities (yellow peaks) is much higher than for the pH 6 preparation. This is because to change the pH value additional chemicals had to be added and this increases the possibility of adding impurities to the solution. This is also why in no case buffer substances were used.

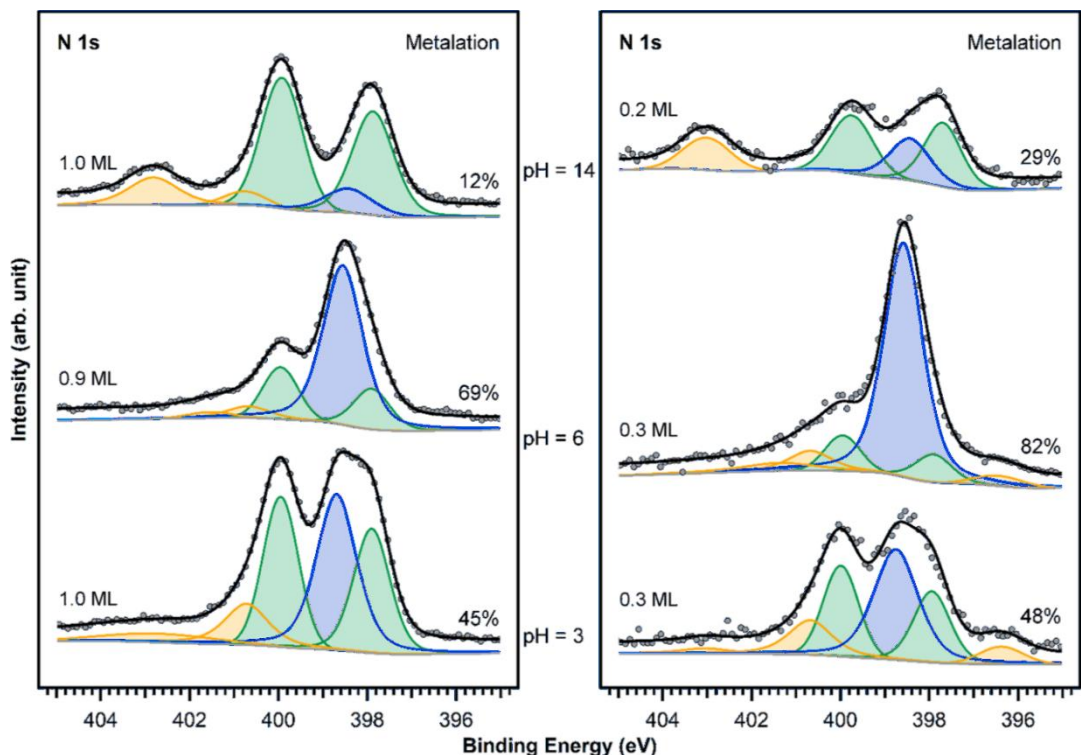


**Figure 25:** N 1s spectra of high- and low-coverage MCTPP on TiO<sub>2</sub>(110) after exposure to an aqueous solution of 1.0 mM zinc acetate at three pH values for 2 hours. The pH values were controlled with acetic acid (pH 3) and potassium hydroxide (pH 14), and the highest degree of metalation is obtained at a pH of 6. Modified from [P2] with permission from J. Phys. Chem. C.

#### 4.2.2. Deposition of Porphyrin Layers from Solution [Unpublished]

This part focuses on bringing the deposition of porphyrin molecules onto cleaned TiO<sub>2</sub>(110) crystals out of UHV into solution. As the measurements in the previous chapter, this work was done under argon atmosphere with the liquid cell setup of Prof. Federico J. Williams in Buenos Aires. The deposition step itself was kept simple: sputtered and annealed TiO<sub>2</sub>(110) crystals were dipped in ethanolic porphyrin solutions for 1 min, then rinsed with pure ethanol to remove excess porphyrins and the remaining solvent was blown off with an argon jet.

In Figure 26, the N 1s and C 1s spectra of solution deposited and evaporated MCTPP is compared. Both preparational techniques yield remarkably similar spectra and the amount of nitrogen and carbon is also in the same range. This proves that we were successfully depositing porphyrins from solution with the same coverage as a closed layer yielded by evaporation (which is around 3.2 ML of flat lying unfunctionalized 2HTPP; see Figure 19 in Chapter 4.1.2). There is an additional peak at 400.8 eV coming from impurities that were picked up during the deposition process. Another difference is the number of protonated porphyrins. At this coverage, between 5 – 6% of evaporated porphyrins are protonated, but in the solution deposited case it is twice the amount, 12%. We think this is caused by a higher amount of hydroxyl groups on the surface after the liquid treatment.

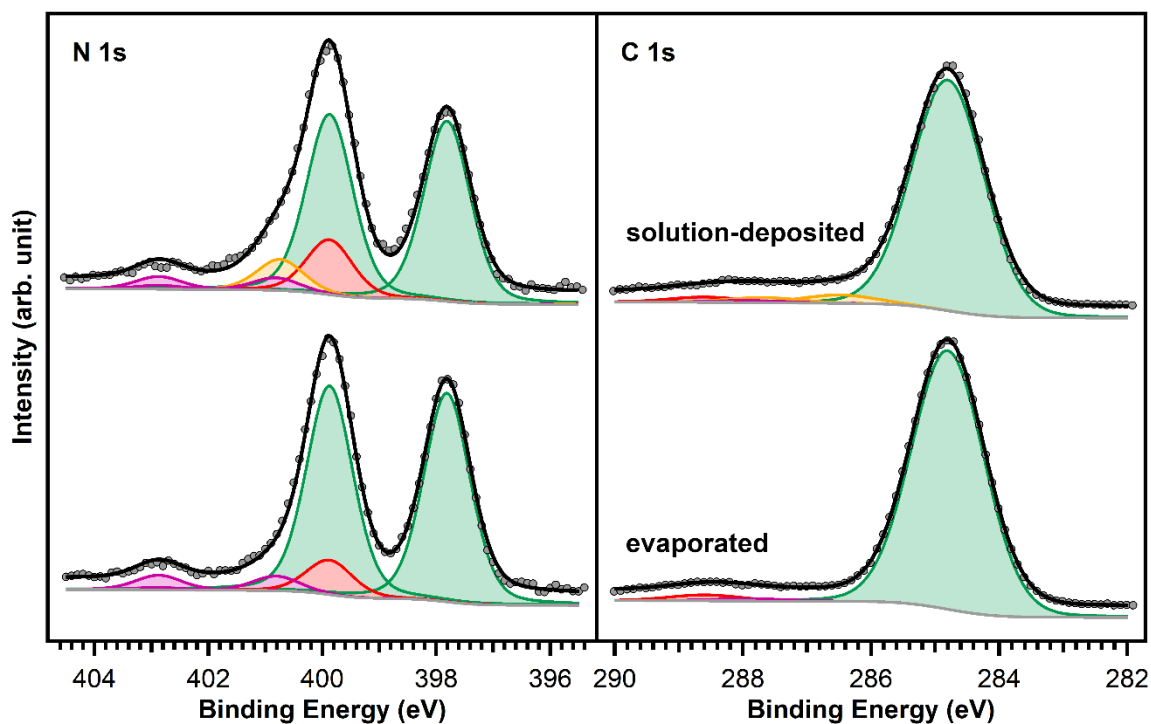


**Figure 26:** N 1s and C 1s spectra of MCTPP on TiO<sub>2</sub>(110) prepared from solution (top) and by evaporation in UHV (bottom). Green peaks belong to the free-base porphyrin, red peaks are assigned to protonated porphyrins (N 1s) or the carboxylic acid carbon (C 1s), violet peaks are shake-up satellites and yellow peaks are impurities.

Besides MCTPP we also deposited three other porphyrins from ethanolic solutions. Figure 27 shows N 1s and C 1s spectra of TCPP, a porphyrin molecule functionalized with four carboxylic acid groups, MPTPP, with one phosphonic acid group and TPPP functionalized with four phosphonic acid groups. These molecules were found to be almost impossible to evaporate (or not at all in the case of the phosphonic acid porphyrins) but it is possible to deposit porphyrin layers on TiO<sub>2</sub>(110) from ethanolic solution. However, the number of impurities was found to be higher in all three cases than with MCTPP.

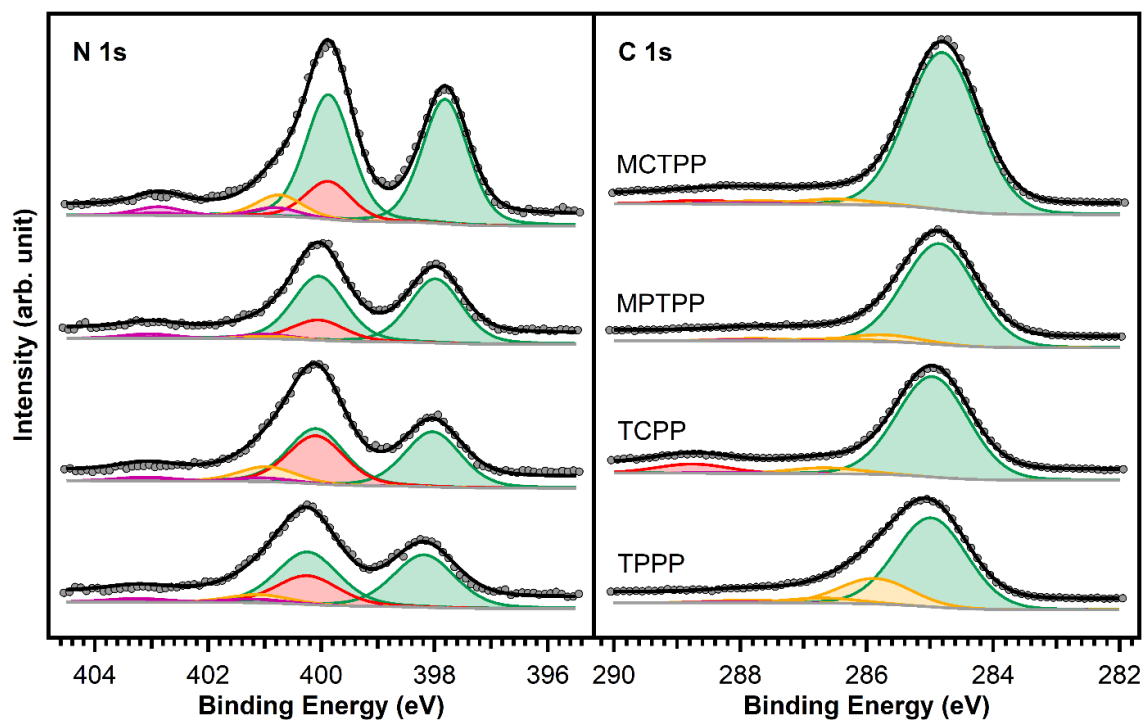


Figure 27: N 1s and C 1s spectra of MCTPP, MPTPP, TCPP and TPPP on TiO<sub>2</sub>(110) prepared from ethanolic solution. Green peaks belong to the free-base porphyrin, red peaks are assigned to protonated porphyrins (N 1s) or the carboxylic acid carbon (C 1s, only MCTPP and TCPP), violet peaks are shake-up satellites and yellow peaks are impurities.

#### 4.2.3. Full Ambient-condition Preparation of Porphyrin Monolayers [P4]

In the last part of this chapter the cleaning of the TiO<sub>2</sub>(110) crystals is brought out of UHV into solution. In addition, instead of working in argon atmosphere as in the previous steps, all experiments are performed in air. The aim of this chapter is to find an easy and reproducible method to prepare porphyrin layers on TiO<sub>2</sub>(110) outside of UHV, while keeping the amount of impurities as low as possible and then compare the results to pure ultrahigh vacuum-prepared surfaces and identify and analyze any potential differences between the different preparation methods. Big parts of the crystal preparation were performed in the laboratories of Prof. Jux from the Chair of Organic Chemistry II at our university. There, we had not only access to a well-equipped synthetic-chemistry lab, but we also benefited from the great expertise in the field of solution-based porphyrin chemistry. The measurements were performed with the Phi Quantera II XPS setup of Professor Karl Mayrhofer from the Helmholtz Institute Erlangen-Nürnberg. With this machine we were able to prepare several crystals at the same time (usually around ten), insert them all together and measure all of them over night; something that would have taken several days with our own XPS setup. The results are summarized in article P4, which is currently in preparation.

The cleaning procedure bases on a recipe described by the Diebold group<sup>103</sup> and is basically a variation of the SC-1 cleaning procedure to clean wafers<sup>104</sup>. The details are described in Chapter 3.2.2. The first step is to sonicate the crystals in soap solution to remove all grease and bigger

particles. After sonicating in clean ultrapure water, the crystal is placed in a 3:1 mixture of 25%  $\text{NH}_3$  and 30%  $\text{H}_2\text{O}_2$  that is heated to  $65^\circ\text{C}$  for 8 minutes. Afterwards the crystals are rinsed with ultrapure water and then sonicated with fresh water again. After cleaning, the crystals are either stored in ultrapure water or directly put into porphyrin solution for the next step.

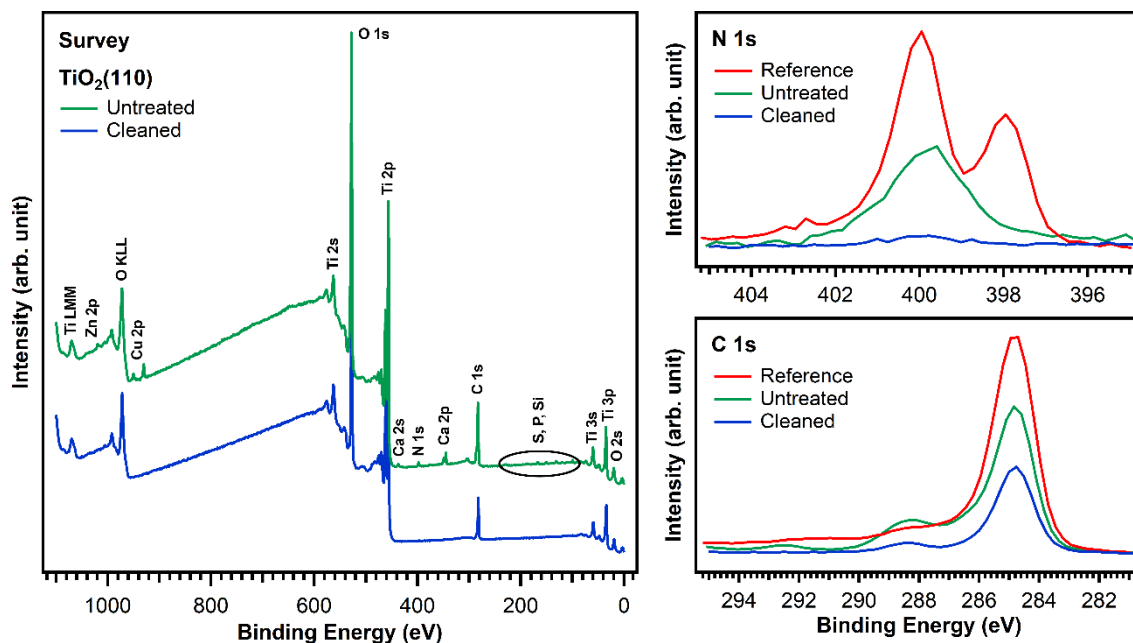


**Figure 28:** Comparison of XPS spectra of a fresh, as-bought  $\text{TiO}_2(110)$  crystal (green) and a cleaned one (blue). Besides carbon and nitrogen, traces of zinc, copper, calcium, sulfur, phosphorus, and silicon were found on the new crystal and removed by the wet-chemically cleaning procedure. The N 1s and C 1s spectra show an additional measurement of a  $\text{TiO}_2(110)$  crystal with wet-chemical deposited MCTPP as reference (red). Modified from [P4].

Figure 28 summarizes the XPS results of the cleaning procedure. The green trace shows a survey spectrum of a fresh crystal as bought and the blue one shows a crystal after the cleaning procedure. The liquid treatment removes all traces of impurities, like copper, zinc, silicon, calcium, nitrogen, phosphorus, and sulfur. Some nitrogen either remains after the cleaning procedure or readsorbs from air, but it is less than 5% of the N 1s signal from a densely packed porphyrin layer and therefore not enough to cause us problems. This is a notable result because the nitrogen region is the most important when studying metalation reactions with XPS. An impurity level as high as found on the untreated crystal would make the assignment and the subsequent analysis of the XPS signals more difficult or even impossible. The remaining number of carbon impurities on the other hand is still around 50% of the initial amount and 40% of the porphyrin reference. This is unavoidable when working in ultrahigh vacuum. Even if the cleaning procedure removes all carbon, organic impurities from air or in the solution will immediately form a carbon layer on the surface. Balajka et al. have shown that mainly short-chained carboxylic acids adsorb onto  $\text{TiO}_2(110)$  from water or air.<sup>105</sup>

The porphyrins we want to focus on have two different types of linker groups: carboxylic acid linker groups, just as the impurity molecules and phosphonic acid groups. The latter binds stronger to the surface than carboxylic acid<sup>106, 107</sup> and should therefore have an easier time displacing the impurities. By placing the impurity-covered crystals for a long-enough time in porphyrin solution, the carboxylic acid molecules should nevertheless be able to replace almost all impurity molecules because the concentration of porphyrins in solution is higher than of impurity molecules. At this point one must emphasize the meaning of the term “clean surface” in this chapter. When working under ambient conditions, clean does not mean that the surface only contains titanium and oxygen atoms, in contrast to the atomically clean crystals obtained by sputtering in ultrahigh vacuum, but it means a surface passivated by the reproducible organic layer we always observe after wet-chemical cleaning, see Figure 28.

For all our measurements we used one-side polished TiO<sub>2</sub>(110) single crystals, but the polished side is – on a microscopic level – still very rough. Figure 29 shows ambient condition AFM images, measured by Corinna Stumm from the group of Prof. Jörg Libuda, from such a polished but rough surface. In UHV studies the annealing steps after sputtering the single crystals create very flat surfaces with large terraces<sup>108</sup> and to achieve similar results outside of UHV, we annealed our crystals in pressurized air. Applying the same annealing temperature that we used in our UHV experiments, which is 970 K, for 90 minutes, does not yield flat surfaces as seen in the middle part of Figure 29. When increasing the annealing temperature to 1220 K for 22 hours, large terraces are formed, as shown in the right part of Figure 29. This temperature is in between 1100 and 1270 K; temperatures that were used by other groups to prepare flat surfaces on rutile TiO<sub>2</sub>(110) crystals.<sup>109-111</sup>

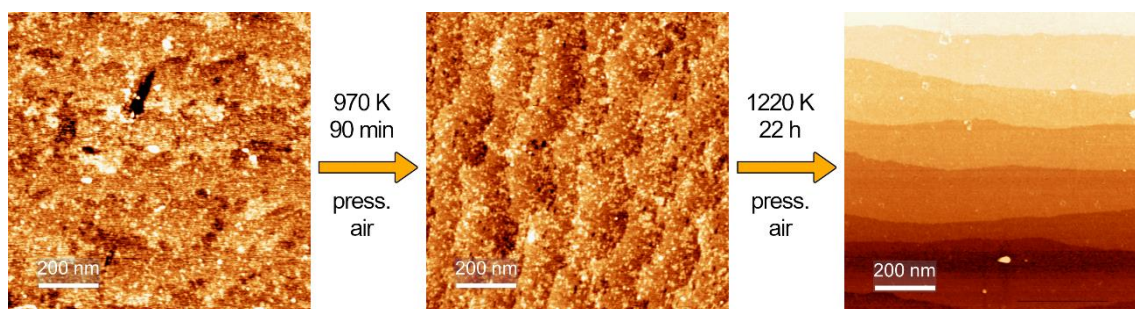


**Figure 29:** Ambient condition AFM images of an untreated TiO<sub>2</sub>(110) surface and after annealing in pressurized air. Annealing to 970 K, which is the annealing temperature for UHV-prepared crystals, does not yield flat surfaces. Increasing the annealing temperature to 1220 K for 22 hours results in large terraces. Modified from [P4].

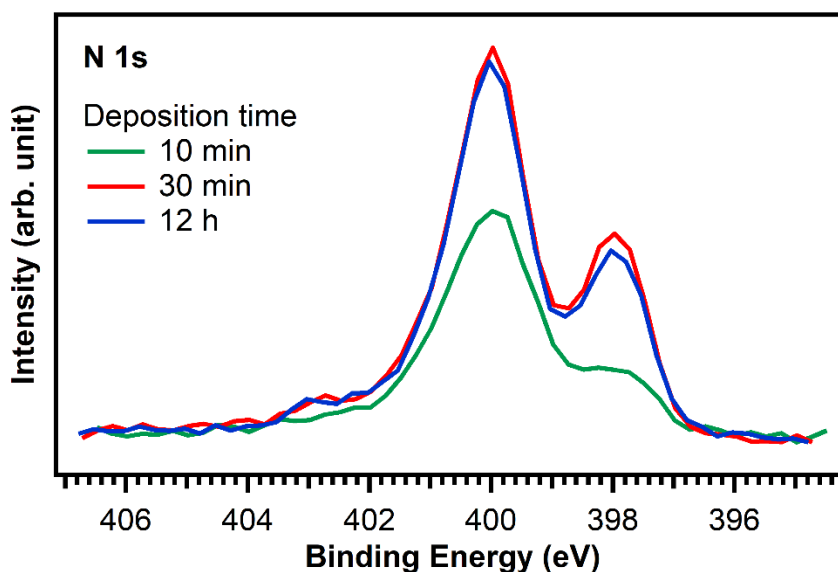


**Figure 30:** N 1s spectra of TiO<sub>2</sub>(110) crystals exposed to ethanolic 0.01 mM MCTPP solution for 10 and 30 minutes and 12 hours. After 30 minutes, the spectra do not change anymore, suggesting that saturation coverage is reached. The 10-minute preparation has less nitrogen and therefore also less porphyrins. Modified from [P4].

After cleaning, the crystals were placed in ethanolic porphyrin solution (0.01 mM). Figure 30 shows N 1s spectra of TiO<sub>2</sub>(110) crystals exposed to MCTPP solution for different amounts of time. After 30 minutes, the nitrogen region is not changing anymore, and we assume this means the saturation coverage, probably of upright-standing porphyrin molecules (see NEXAFS measurements in Chapter 4.1.2), is reached. When comparing the spectrum recorded after 30 minutes exposure to porphyrin solution with measurements of evaporated MCTPP in ultrahigh vacuum (Figure 31) one finds that both spectra look similar. All peaks are at the same binding energy position and no additional impurity signals are present. One difference is the amount of protonated porphyrin species, which is expressed by the ratio between the two nitrogen peaks. As discussed in previous chapters, we think that interactions of the iminic nitrogen atoms of the porphyrin molecules with hydroxyl groups on the surface lead to a protonation of the porphyrin. When comparing the N 1s shapes of the evaporated and the solution-deposited layer in Figure 31 it is clearly visible that the peak at around 400 eV is larger in the case of the solution-deposited molecules, indicating a higher degree of protonation. However, due to the liquid treatment, the crystal's surface is probably strongly hydroxylated, and this could lead to more protonation. This is also what we saw in the previous chapter, where we deposited porphyrins from solution onto a sputter-cleaned crystal. By comparing the carbon-to-nitrogen ratio one can calculate that impurities contribute only to 15% of the total carbon signal. Considering the full preparation was done outside of ultrahigh vacuum and the crystal was fully covered with carbon, this is a good result. Figure 30 also shows that for lower exposure times less nitrogen adsorbs onto the TiO<sub>2</sub>(110) crystal, leading to a lower porphyrin coverage. The amount of carbon (not shown) is also lower for the 10-minute preparation; however, the carbon-to-nitrogen ratio is higher, and this

means that the amount of carbon impurities is higher in the case of the 10-minute preparation. As discussed in Chapter 4.1.2, the MCTPP molecules adsorb probably not flat but tilted away from the surface and the remaining space on the surface is covered by impurities. To keep the number of impurities as low as possible we therefore did all subsequent experiments on crystals exposed to porphyrin solutions for at least 30 minutes.

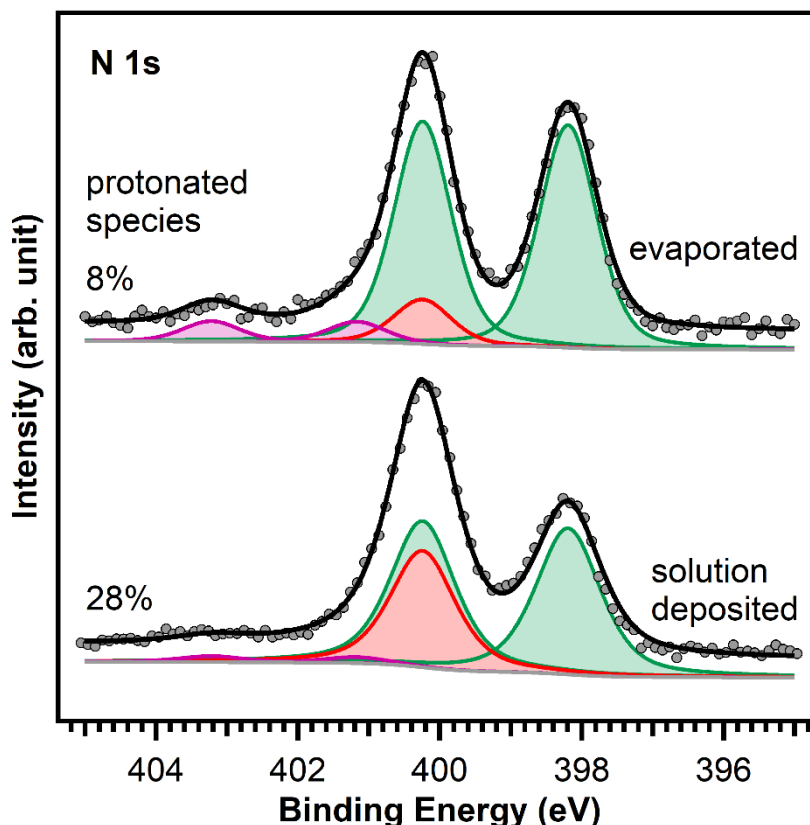


**Figure 31:** Comparison of the N 1s spectra of MCTPP evaporated (top) and wet-chemically deposited (bottom) onto  $\text{TiO}_2(110)$ . Modified from [P4].

In the next part, the reactivity of porphyrins deposited from solution onto wet-chemically cleaned  $\text{TiO}_2(110)$  crystals was compared to evaporated preparations. Therefore, the MCTPP-covered crystals were put in aqueous zinc acetate solution with a concentration of 0.01 M for one hour. This is the same treatment that was used to metalate crystals in the argon-filled liquid cell in Buenos Aires in Chapter 4.2.1. Figure 32 shows N 1s spectra for both preparations: the evaporated reference on the left side and the wet-chemically prepared crystals on the right side. The spectra on the top are the ones discussed in Figure 31 and in the middle the spectra after exposure to zinc solution are found. It is clearly visible that the result is very different. The spectral shape of the measurement before and after zinc exposure on the right side changes only slightly. Fitting the spectrum yields a degree of metalation of 17% in contrast to 51% on the left side. One reason for that unexpected behavior could be the higher degree of protonated porphyrins on the wet-chemical prepared crystal. Especially from ultrahigh vacuum studies of 2HTPP on  $\text{TiO}_2(110)$  it is known that the protonated porphyrin species is more resilient towards metalation and in this case higher

temperatures are necessary to metalate those porphyrins.<sup>37</sup> This is also known from metalation experiments of dissolved porphyrins: best yields are achieved for slightly basic pH values, because a deprotonated porphyrin easily reacts with a positively charged metal ion<sup>99</sup>, whereas the metal gets repelled by a protonated porphyrin<sup>100</sup>. In our case, with porphyrins adsorbed on a surface, positively charged molecules will most likely be less reactive towards metalation as well, however, we would not expect a difference between the two shown cases in Figure 32. The initial degree of protonation might be higher on the wet-chemical prepared sample but when put in the aqueous zinc acetate solution the degree of protonation should in both cases only be controlled by the acidity of the zinc acetate solution. Another reason could be how the porphyrin molecules adsorb onto the crystal: when evaporated at room temperature, the porphyrins have not enough energy to diffuse on the surface and this results in disordered adsorbate layer. Deposited from solution, the porphyrin layers could be highly ordered, because the molecules can detach and reattach as long as the crystal is placed in the ethanolic solution. A highly ordered porphyrin layer with molecules densely packed would probably yield less metalation because the metal ions have to diffuse through the non-polar adsorbate layer to reach the porphyrin center. Besides the small changes in between the free-base peaks, that is caused by the metalation peak, there are also changes at the high energy side where nitrogen impurity peaks are often found. As the solvent was the same that is used during the crystal cleaning, the source of those impurities is most likely the zinc acetate salt. In all cases, the amount of impurities from metalating with zinc acetate solution was below 10%.

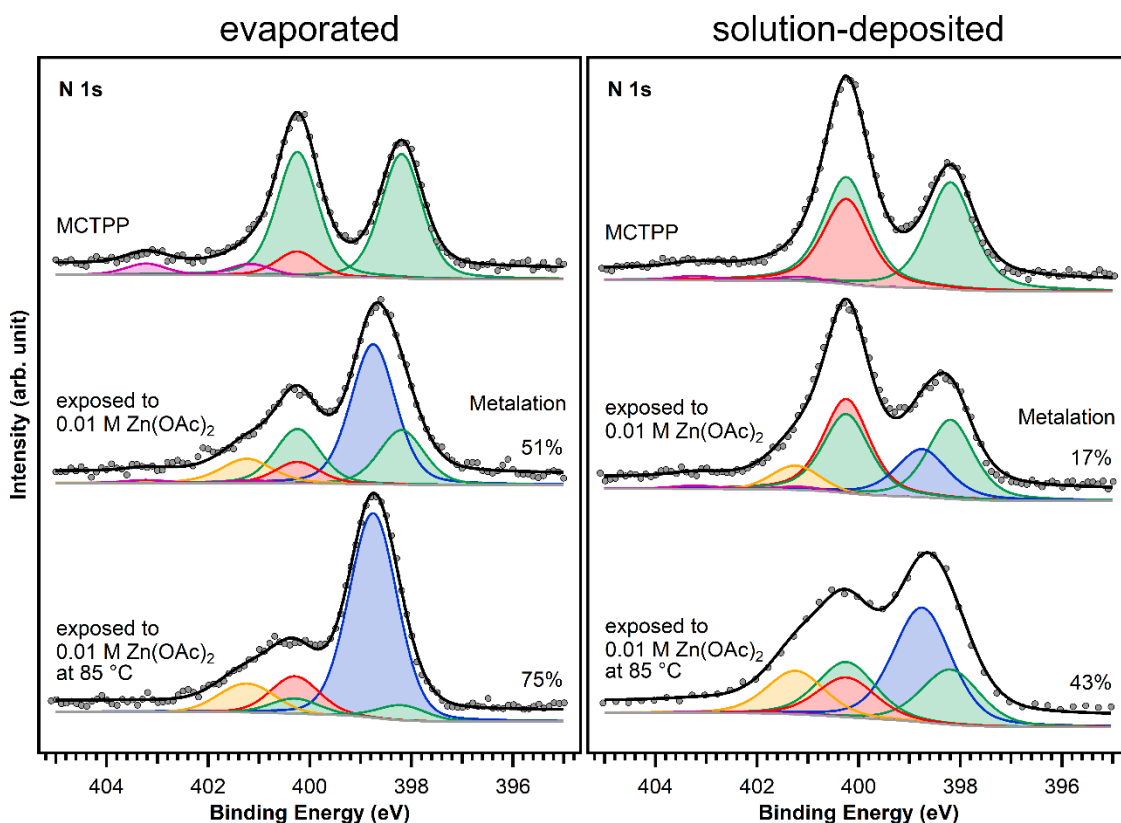
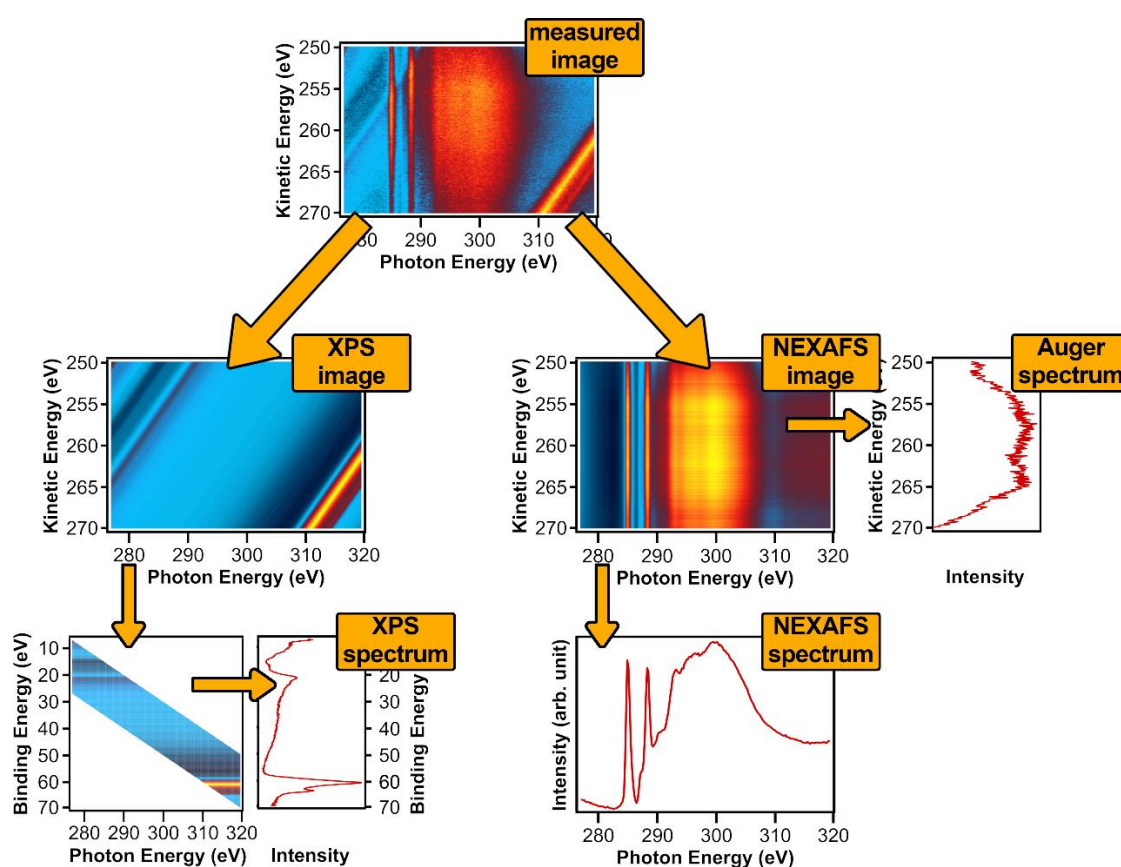


**Figure 32:** N 1s spectra of evaporated and solution-deposited layers of MCTPP onto TiO<sub>2</sub>(110) before and after metalation at room temperature and at 85°C with aqueous zinc acetate solution. Modified from [P4].

With the aim to increase the degree of metalation, freshly prepared crystals with MCTPP were put in zinc acetate solution for one hour while heated to 85°C. This leads to an increased degree of metalation of 75% on the evaporated-porphyrin sample and slightly more impurities than without heating. It is noteworthy that this treatment does still not yield full metalation while Franke et al. found for 2HTPP evaporated onto Au(111) complete metalation with zinc acetate solution already at room temperature<sup>73</sup> and we do not know if this is due to the different porphyrin and the resulting different adsorption geometry or the higher reactivity of the TiO<sub>2</sub>(110) surface: after exposure to zinc acetate solution, the amount of zinc on the surface is high enough to yield full metalation. In the case of the wet-chemically prepared porphyrins, the heated solution increases the degree of metalation as well, but only to 43%, which is still less than for the evaporated-porphyrin sample at room temperature. This is also the highest degree of metalation we were able to prepare. Neither increasing the reaction time, changing the metal salts, increasing the concentrations, using other solvents nor changing the pH value yielded more metalation. This shows that there is a considerable difference between the two preparations. Even though we can deposit porphyrins with both methods, their reactivity is not the same and therefore, the influence of solutions and air on the preparation of porphyrin layers on oxide surfaces is worth to be studied more intense. The methods described in this chapter might be a viable way to study those influences that occur during ambient condition preparations.

### 4.3. Removing Photoemission Features from Auger-yield NEXAFS Spectra [P5]

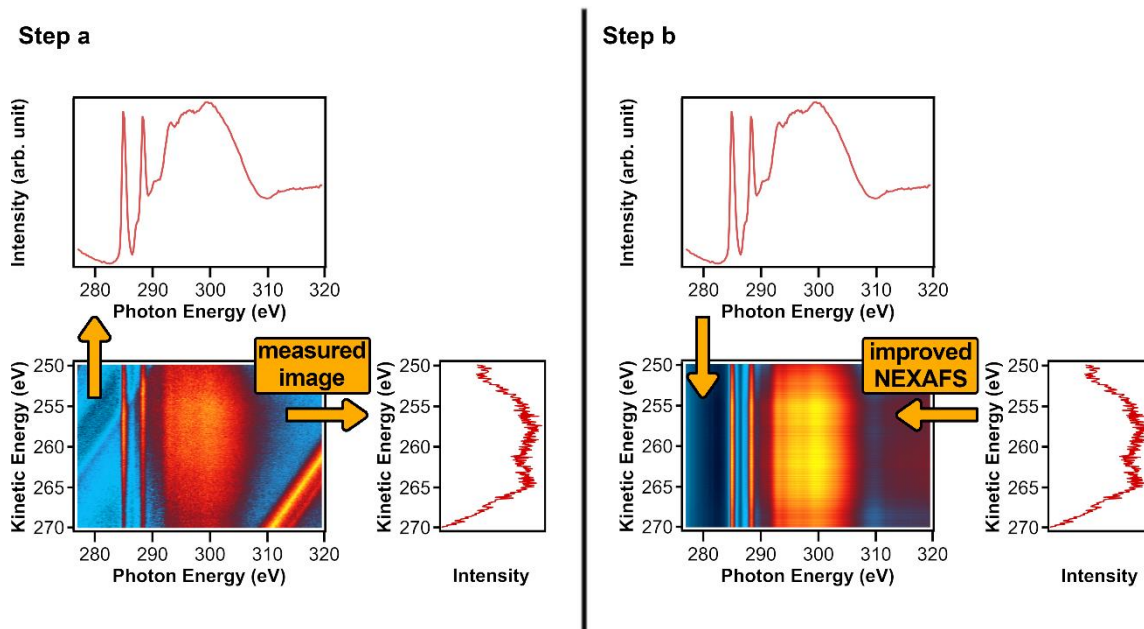
The last part of the thesis is about how to deal with photoemission features in two-dimensional Auger-yield NEXAFS measurements. In Chapter 2.2.3 it was already shown how photoelectron signals can interfere with NEXAFS measurements and it was discussed that there is no established way to remove those interferences. To be able to analyze spectra measured at several beamtimes at the Material Science Beamline at the Elettra Sincrotrone in Trieste, Italy we developed a new approach that is published in article P5. This also includes a detailed description of the method. Here, the single steps will be described with an unpublished set of data: phthalic acid on  $\text{Co}_3\text{O}_4(111)$ .



**Figure 33:** A measured two-dimensional NEXAFS image with photoelectron features can be split into two two-dimensional images with one containing only XPS features and one containing only NEXAFS features. From the XPS image, a one-dimensional XPS spectrum can be obtained and the NEXAFS image can be divided into a NEXAFS spectrum and a Auger spectrum.

The basic assumption behind the idea is that the measured two-dimensional images are described by a superimposition of a two-dimensional image containing only NEXAFS features and one containing only the diagonal XPS lines, see Figure 33. The NEXAFS image itself can be deconstructed into a one-dimensional NEXAFS spectrum, which is what one is usually interested in, and a one-dimensional Auger spectrum, which gives the intensity of the Auger peaks as a function of kinetic energy. From the XPS image a one-dimensional XPS spectrum can be obtained

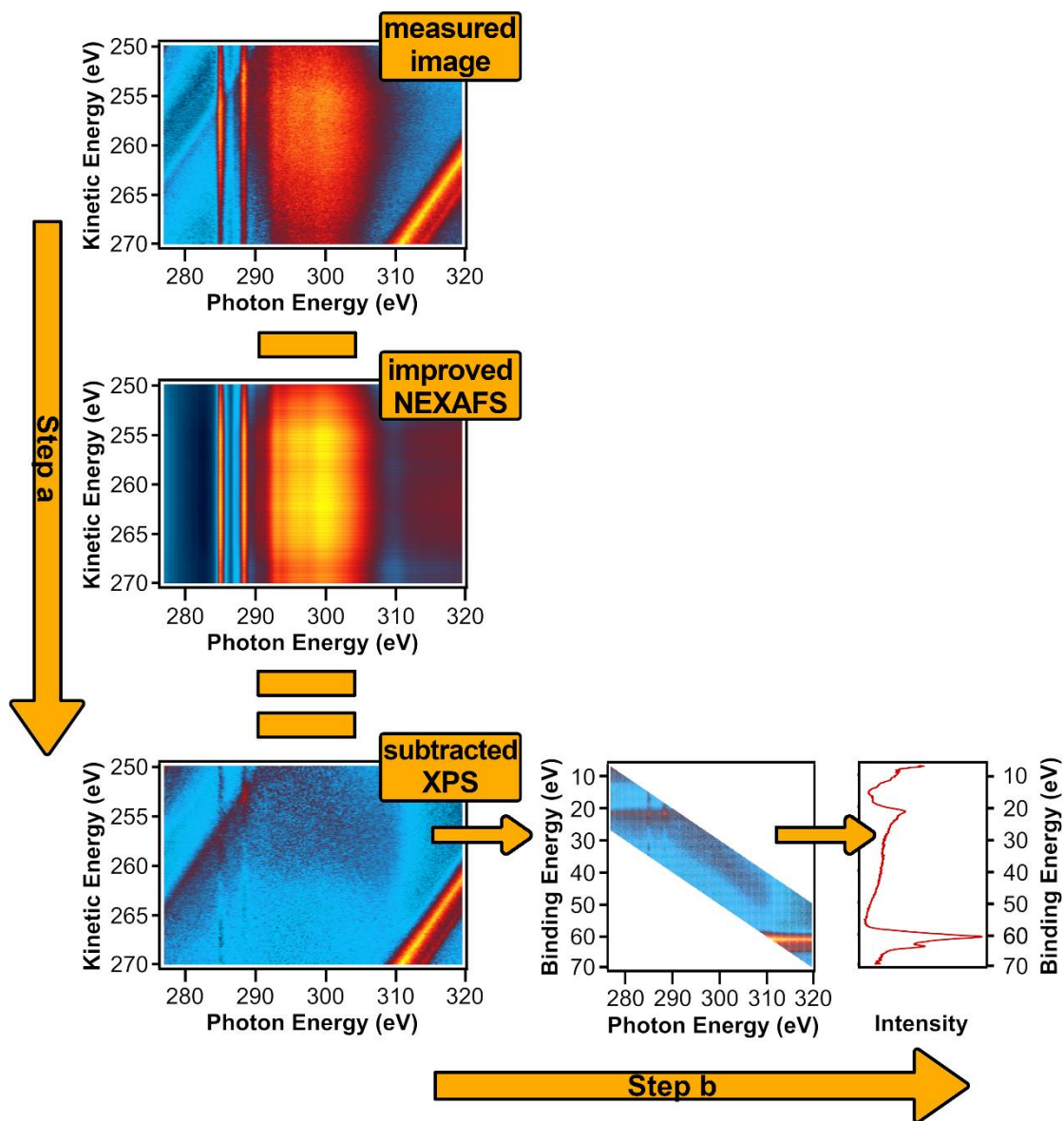
by converting the kinetic energy axis to binding energies. The two-dimensional NEXAFS image can be obtained by subtracting the XPS image from the measured image and vice versa, but we neither have the NEXAFS nor the XPS image. The idea of our procedure is to create those images in an iterative loop and to do so only the measured two-dimensional image is needed.



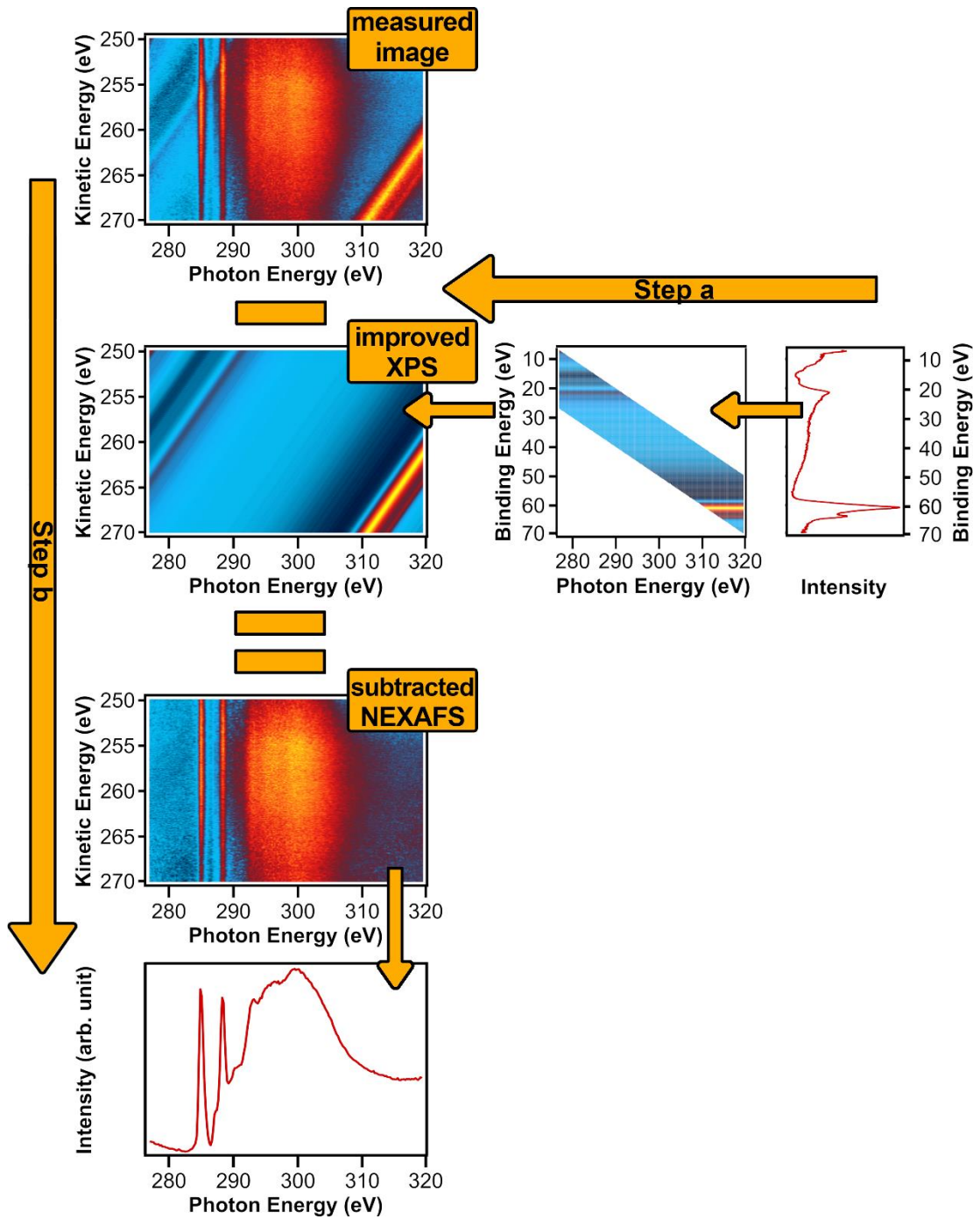
**Figure 34:** Step a (left): by summing up and averaging the datapoints along the kinetic energy axis a one-dimensional NEXAFS spectrum is obtained. The diagonal XPS lines lead to an increased background (in this example especially between 310 and 320 eV photon energy). Averaging along the photon energy axis yields the Auger spectrum. Step b (right): by combining the two spectra obtained in Step 1 a two-dimensional image is created. The XPS lines are not sharp anymore but smeared out.

Figure 34 shows on the left side the measured two-dimensional image of the carbon K-edge after photon flux correction at  $80^\circ$  with respect to the surface normal of phthalic acid on  $\text{Co}_3\text{O}_4(111)$  which was grown on Ir(100). The main photoelectron features, which are represented as diagonal lines (see also Chapter 2.2.3) are at photon energies of 310 eV and higher, well above the Auger peaks, but also at low photon energies diagonal lines cross the image. They lead to an increased background in the beginning and at the end of the spectrum and it is important to remove them correctly to be able to normalize the spectra to the edge jump and compare them with ones measured at different incident beam angles. To start with, the measured image is split into initial guesses for the NEXAFS and Auger spectra. In both spectra, the photoelectron features are smeared out and contribute only to the background not to intense peaks. By combining both spectra, a two-dimensional image is obtained that only shows Auger peaks. In Figure 35, this newly created image is subtracted from the originally measured and the result shows almost only photoelectron peaks and only some faint residuals of the Auger peaks. Now the kinetic energy axis is converted to binding energies, graphically this means the image is shear-distorted, and then the XPS spectrum is created by summing up along the photon energy axis. This time the Auger peaks are smeared out and contribute only to the background. In the first step of Figure 36 a two-

dimensional image is again created out of the photoelectron spectrum. This image is again subtracted from the originally measured image and the result shows only Auger features. In this example this is already enough to remove the photoelectron features completely. Otherwise, one would take this image and start from Figure 34 again and repeat all steps until the result is satisfying. This takes usually not more than ten to twenty loops.



**Figure 35:** The image obtained in the second Step in Figure 34 is subtracted from the originally measured image. The result shows mainly XPS features and only some artifacts of the vertical Auger lines. The kinetic energy axis is converted into binding energy and the datapoints are averaged along the photon energy axis to yield an photoelectron spectrum.



**Figure 36:** In Step a the photoelectron spectrum obtained in Figure 35 is converted back into a two-dimensional image. The Auger artifacts are now smeared out and almost only XPS features are visible. After changing the axis back to kinetic energy, the image is subtracted from the originally measured image. The resulting two-dimensional spectrum does not contain any XPS features anymore. After averaging along the kinetic energy axis, a NEXAFS spectrum is obtained.

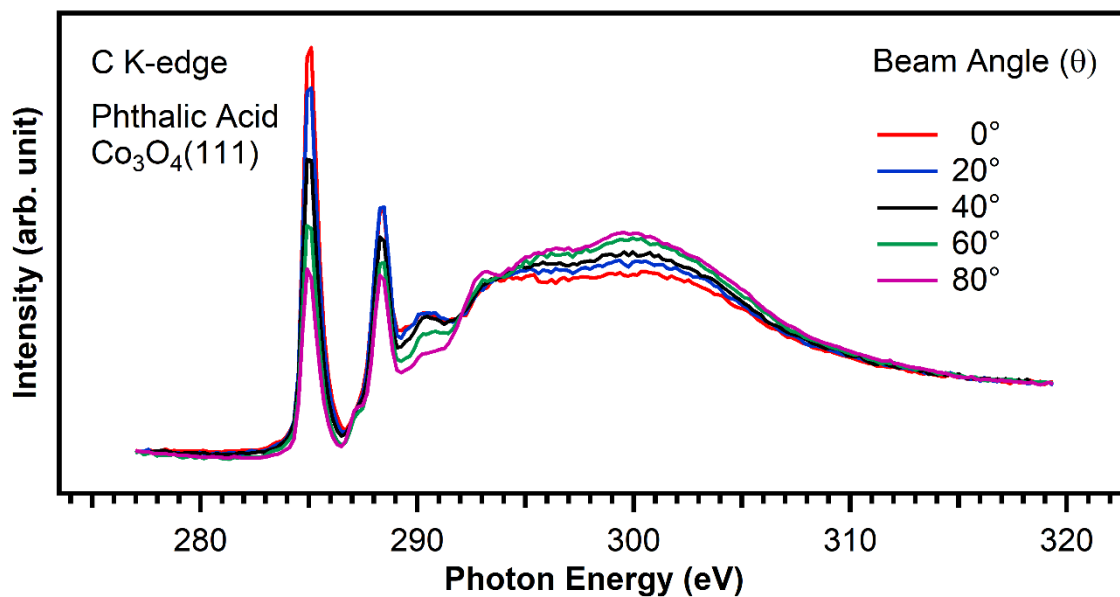


**Figure 37:** NEXAFS measurements of phthalic acid on Co<sub>3</sub>O<sub>4</sub>(111) after removing photoemission features.

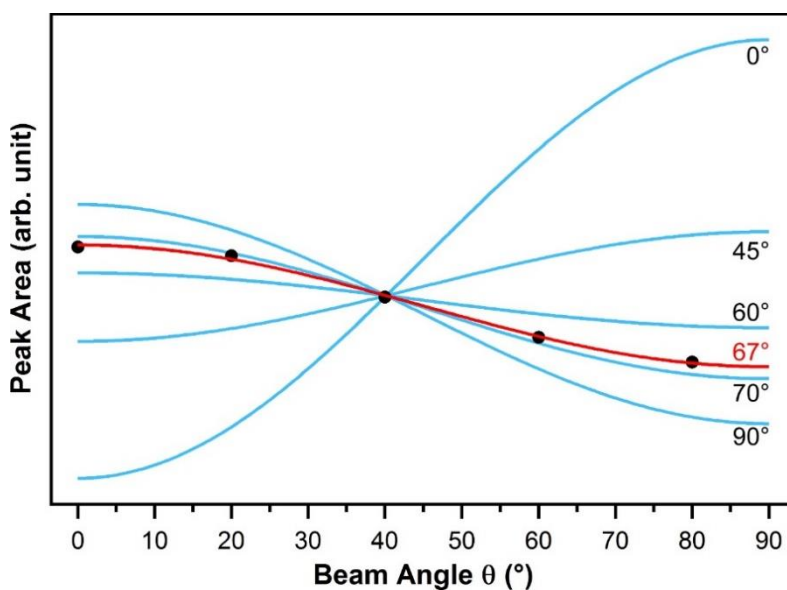


**Figure 38:** Angular dependence of the first  $\pi^*$  peak of the NEXAFS measurements of phthalic acid on Co<sub>3</sub>O<sub>4</sub>(111). The molecules adsorb tilted with an angle of 67° relative to the surface.

Figure 37 shows the NEXAFS spectra of all incidence beam angles after correction and normalization and Figure 38 shows the resulting angular dependencies. The adsorption angle of 67° agrees very well with adsorption angles of other carboxylic acids.<sup>96-98</sup>

This example shows that it is possible to remove photoelectron features from Auger-yield NEXAFS spectra without the need to measure any additional reference spectra of the clean surface. This is especially beneficial in cases, where it is not possible to measure a clean reference

sample, or where the photoelectron peaks are caused by the adsorbate itself. More examples with severe photoelectron features can be found in article P5.



## 5. Conclusion and Outlook

In this thesis XPS and NEXAFS spectroscopy were used to study the adsorption and reactivity of porphyrins on different oxide surfaces prepared under ultra-high vacuum but also ambient conditions.

To gain a better understanding about the influence of the substrate structure 2HTPP was investigated on two cobalt oxides with different surface structure. At room temperature, no differences were observed and even more, the behavior is very similar to that of the same porphyrin on MgO(100): already at 300 K, a substantial number of porphyrins are metalated and thus we conclude that this might be a general trend for +2-metal oxides. On the other hand, 2HTPP does not metalate at room temperature on TiO<sub>2</sub>(110), a +4-metal oxide probably because a (Ti=O)<sup>2+</sup> unit instead of a Ti<sup>4+</sup>-ion has to be complexated by the porphyrin to match the stoichiometry.

The influence of anchoring groups on the adsorption and reactivity of porphyrins was studied with the carboxylic-acid functionalized MCTPP. It was shown that the molecule metalates with the substrate when annealed on TiO<sub>2</sub>(110), but the degree of metalation is dependent on the coverage. We conclude, and this is also supported by NEXAFS measurements, that there is a coverage-dependent change in adsorption geometry: at low coverages, the molecules adsorb with the macrocycle closer to the surface making it easier to pick up substrate atoms while they adsorb with a more tilted geometry at higher coverages.

Studying porphyrin adsorption and metalation under ambient conditions and compare it with UHV was the aim of the second part. In a step-by-step approach, the same system was studied with different preparative approaches. To start with, MCTPP was evaporated on TiO<sub>2</sub>(110) in ultrahigh vacuum and exposed to zinc acetate solution. It was found that a metalloporphyrin species is formed already at room temperature and that the degree of metalation depends on the molecular coverage, probably again caused by the coverage-dependent change in adsorption geometry. In the next step, techniques were developed to grow porphyrin layers from solution on UHV-cleaned TiO<sub>2</sub>(110) and in the end, methods were found to reproducibly clean TiO<sub>2</sub>(110) wet-chemically and prepare layers of MCTPP with a cleanliness comparable to samples prepared in ultrahigh vacuum. However, when these wet-chemically prepared samples were exposed to zinc acetate solution, the degree of metalation was substantially lower than for the UHV-prepared crystals. We think the reason is that wet-chemically prepared porphyrin layers are more densely packed which decreases the probability that metal ions can reach the porphyrin metal center because they have to diffuse through the non-polar adsorbate layer.

The third and last part has presented a novel way to remove photoemission features from two-dimensional Auger-yield NEXAFS images. This is a fast and easy method which needs no

additional reference measurement, and thus works also in cases, where the photoemission features change upon adsorption of molecules.

By the end of this thesis, the adsorption of porphyrins on oxide surfaces and their reactivity is better understood than in the beginning. This work, but also many more publications, helped to shed some more light onto this topic. However, there are still many things unknown. The details of metalation on +2 oxides are still under research. One theory, and this fits with the presented finding on cobalt oxide, suggests that metalation happens at defect sites, but the exact mechanism is still unclear. Even less is known about metalation on  $\text{TiO}_2(110)$ . To date we only assume that free-base porphyrins coordinate a  $(\text{Ti}=\text{O})^{2+}$  unit and form a titanylporphyrin (TiOTPP) instead of a titanium porphyrin (TiTPP). Especially for metalation reactions, the origin of the protonated porphyrin species has to be found. We assume that it is caused by an interaction of the free-base porphyrin with hydroxyl groups on the surface. Last, but not least, the wet-chemical experiments have shown that the adsorption and reaction behavior of porphyrins is different when they are prepared under ambient conditions. For future applications, it is crucial to understand the reason for those differences and therefore, more studies should be performed which combine preparations outside of the ultrahigh vacuum environment with surface science techniques.

## 6. Zusammenfassung

In dieser Arbeit wurde das Adsorptionsverhalten und die Reaktivität von Porphyrinen auf verschiedenen Oxidoberflächen mit XPS und NEXAFS-Spektroskopie untersucht. Die Oberflächen wurden dabei sowohl im Ultrahochvakuum als auch unter Umgebungsbedingungen präpariert.

Um ein tieferes Verständnis über den Einfluss der Oberflächenstruktur zu erlangen, wurde 2HTPP auf zwei Cobaltoxiden mit unterschiedlicher Oberflächenstruktur adsorbiert und untersucht. Es hat sich gezeigt, dass trotz der unterschiedlichen Oberfläche das Verhalten bei Raumtemperatur das gleiche ist und darüber hinaus auch dem auf Magnesiumoxid gleicht: Bereits bei 300 K ist eine erhebliche Anzahl an Porphyrinmolekülen metalliert. Wir schließen daraus, dass es sich hierbei um ein generelles Phänomen bei +2-Metalloxiden handeln könnte. Auf  $\text{TiO}_2(110)$ , einem +4-Metalloxid, wurde keine Metallierung bei Raumtemperatur beobachtet. Das könnte daran liegen, dass anstatt eines  $\text{Ti}^{4+}$ -Ions eine  $(\text{Ti}=\text{O})^{2+}$ -Einheit aus der Oxidoberfläche herausgelöst werden muss, um die Stöchiometrie zu erfüllen.

Der Einfluss von Linkergruppen auf das Adsorptions- und Reaktionsverhalten von Porphyrinen wurde anhand des Moleküls MCTPP erforscht. Beim Heizen der Moleküle auf  $\text{TiO}_2(110)$  wird ein Metalloporphyrin geformt, aber der Grad an Metallierung ist abhängig von der Bedeckung. Wir schließen daraus, und das wird durch NEXAFS-Messungen bestätigt, dass die Adsorptiongeometrie von der Anzahl der Moleküle auf der Oberfläche abhängt. Bei niedrigen Bedeckungen liegen die Porphyrinmoleküle annähernd flach auf dem Substrat und können einfacher Substratome komplexieren. Bei höheren Bedeckungen adsorbieren die Porphyrinmoleküle hingegen gewinkelt.

Im zweiten Teil wurde die Adsorption und Metallierung von Porphyrinen außerhalb des Ultrahochvakuums untersucht und mit UHV-Studien verglichen. Schritt für Schritt wurde das gleiche System auf verschiedene Weisen präpariert und untersucht. Zu Beginn wurde MCTPP auf  $\text{TiO}_2(110)$  im Ultrahochvakuum aufgedampft und in Zinkacetatlösung getaucht. Dies führte bereits bei Raumtemperatur zur Bildung einer Metalloporphyrinspezies. Der Grad der Metallierung ist dabei abhängig von der Bedeckung. Wir vermuten, dass auch hier der Grund in der bedeckungsabhängigen Adsorptionsgeometrie liegt. Im nächsten Schritt wurden Methoden entwickelt, um Porphyrine aus Lösungen auf Kristalle abzuscheiden, die im Ultrahochvakuum gereinigt wurden. Und schließlich wurde ein Verfahren gefunden um  $\text{TiO}_2(110)$ -Kristalle reproduzierbar in Lösung zu Reinigen und Porphyrinlagen aufzubringen, deren Reinheit der von UHV-präparierten Kristallen sehr nahekommt. Werden die nasschemisch präparierten Kristalle in Zinkacetat-Lösung gegeben unterscheidet sich der Grad an Metallierung allerdings erheblich von dem von im UHV präparierten Kristallen. Wir denken, dass nasschemisch-präparierte

Porphyrinlagen dichter gepackt adsorbieren und die Wahrscheinlichkeit deswegen geringer ist, dass ein Metallion durch die unpolare Adsorbatschicht zum Porphyrincenter dringen kann.

Im dritten und letzten Teil wurde ein neues Verfahren zur Entfernung von Photoemissionslinien aus zweidimensionalen Auger-yield NEXAFS-Daten vorgestellt. Es handelt sich hierbei um eine schnelle und einfache Methode, die keine zusätzlichen Referenzmessungen benötigt. Sie funktioniert deshalb auch, wenn sich die Photoemissionslinien während der Adsorption von Molekülen verändern.

Zum Ende dieser Arbeit hat sich unser Verständnis über das Adsorptions- und Reaktionsverhalten von Porphyrinen auf Oxidoberflächen verbessert. Diese Arbeit, aber auch viele weitere Veröffentlichungen in den letzten Jahren, haben geholfen etwas Licht ins Dunkel zu bringen. Es gibt allerdings immer noch einige Dinge, die unklar geblieben sind. Die Details der Metallierung auf +2-Oxidoberflächen ist immer noch nicht abschließend geklärt. Ein Erklärungsvorschlag, der auch zu den hier vorgestellten Daten auf Cobaltoxid passt, besagt, dass die Defektstellen die reaktiven Seiten sind, aber der genaue Reaktionsmechanismus ist noch nicht bekannt. Über die Metallierung auf  $\text{TiO}_2(110)$  ist sogar noch weniger bekannt. Zum jetzigen Zeitpunkt können wir nur vermuten, dass das Reaktionsprodukt der Selbstmetallierung ein Titanylporphyrin ist und eine  $(\text{Ti}=\text{O})^{2+}$ -Einheit komplexiert wird. Vor allem für die Metallierungsreaktionen ist es außerdem wichtig, dass mehr über den Ursprung der protonierten Porphyrinspezies herausgefunden wird. Wir vermuten bisher, dass freie-Basen Porphyrine mit Hydroxylgruppen auf der Oberfläche reagieren und diese Spezies formen. Als letzter Punkt haben die nasschemischen Experimente gezeigt, dass das Adsorptions- und Reaktionsverhalten von Porphyrinen anders ist, wenn sie außerhalb des Ultrahochvakuums präpariert werden. Für zukünftige porphyrinbezogene Anwendungen ist es wichtig zu verstehen, woher diese Unterschiede kommen und deswegen sollte dieser Ansatz, Präparationen außerhalb des Ultrahochvakuums gepaart mit Oberflächenanalysemethoden, auch in Zukunft weiterverfolgt werden.

## 7. Acknowledgement

Now, in the end of my thesis, it is a pleasure for me to thank all the people that contributed to the results and supported me in the last years:

Prof. Hans-Peter Steinrück for giving me the opportunity to work at his chair and for providing this great working environment throughout my early years as a bachelor student until the end of my Ph.D. thesis.

Dr. Ole Lytken for providing me guidance but giving me also the freedom to make my own experiences, for the discussions and all his unconventional ideas, and of course also for his fantastic data analysis procedure.

Prof. Dr. Federico Williams and Cynthia Fernández for the fruitful collaboration and the fantastic time in Buenos Aires and in Erlangen.

My former and current colleagues, Dr. Matthias Franke, Dr. Michael Röckert, Quratulain Tariq, Julia Köbl, Dr. Elmar Kataev, and Alexander Wolfram for the good working atmosphere. It was a pleasure to work with you.

The beamline staff from the Material Science Beamline at Elettra, especially Nataliya Tsud for her valuable help day and night, and from the I09 Beamline at Diamond, Tien-Lin Lee and Pardeep Kumar Thakur.

Prof. Norbert Jux and his group members, especially David Reger, Michael Ruppel and Helen Hölzel, for providing me space for my wet-chemical experiments and answering all my questions about synthetic chemistry.

The group of Prof. Jörg Libuda, especially Corinna Stumm and Dominik Blaumeiser, for providing me with AFM and infrared measurements.

Prof. Karl Mayrhofer from the Helmholtz Institute Erlangen-Nürnberg for letting me use the XPS machine.

Hans-Peter Bäumler, Bernd Kreß, Friedhold Wölfel, and all members of the mechanical workshop, for the quick and competent help whenever something had to be repaired.

All the members of PC II for the good time.

My parents and my brother for their never-ending support through all my life.

Finally, I want to thank my wife Ramona for her patience, her support and for remembering me that science is not everything in life.



## 8. References

1. Zeller, M. V.; Hayes, R. G., X-ray photoelectron spectroscopic studies on the electronic structures of porphyrin and phthalocyanine compounds. *J. Am. Chem. Soc.* **1973**, *95* (12), 3855-3860.
2. Cady, S. S.; Pinnavaia, T. J., Porphyrin intercalation in mica-type silicates. *Inorg. Chem.* **1977**, *17* (6), 1501-1507.
3. Davis, D. G.; Murray, R. W., Surface electrochemistry of iron porphyrins and iron on tin oxide electrodes. *Anal. Chem.* **1977**, *49* (2), 194-198.
4. Lavalleye, D. K.; Brace, J.; Winograd, N., X-Ray Photoelectron-Spectra of N-Methyltetraphenylporphyrins - Evidence for a Correlation of Binding-Energies with Metal-Nitrogen Bond Distances. *Inorg. Chem.* **1979**, *18* (7), 1776-1780.
5. Macquet, J. P.; Millard, M. M.; Theophanides, T., X-ray photoelectron spectroscopy of porphyrins. *J. Am. Chem. Soc.* **1978**, *100* (15), 4741-4746.
6. Muralidharan, S.; Hayes, R. G., Satellite in the x-ray photoelectron spectra of metalloporphyrins. *J. Chem. Phys.* **1979**, *71* (7), 2970-2974.
7. Fleischer, E. B., Structure of porphyrins and metalloporphyrins. *Acc. Chem. Res.* **1970**, *3* (3), 105-112.
8. Milgrom, L. R., *The Colours of Life: An Introduction to the Chemistry of Porphyrins and Related Compounds*. Oxford University Press: **1997**.
9. Kadish, K.; Smith, K. M.; Guillard, R., *Chlorophylls and Bilins: Biosynthesis, Synthesis and Degradation*. Academic Press: San Diego, **2002**.
10. Kadish, K.; Smith, K. M.; Guillard, R., *Biochemistry and Binding: Activation of Small Molecules*. Academic Press: San Diego, **1999**.
11. Pfaltz, A.; Jaun, B.; Fassler, A.; Eschenmoser, A.; Jaenchen, R.; Gilles, H. H.; Diekert, G.; Thauer, R. K., Zur Kenntnis des Faktors F430 aus methanogenen Bakterien: Struktur des porphinoïden Ligandensystems. *Helv. Chim. Acta* **1982**, *65* (3), 828-865.
12. Hodgkin, D. C.; Kamper, J.; Mackay, M.; Pickworth, J.; Trueblood, K. N.; White, J. G., Structure of vitamin B12. *Nature* **1956**, *178* (4524), 64-66.
13. Guillard, R.; Kadish, K. M., Some aspects of organometallic chemistry in metalloporphyrin chemistry: synthesis, chemical reactivity, and electrochemical behavior of porphyrins with metal-carbon bonds. *Chem. Rev.* **1988**, *88* (7), 1121-1146.
14. Král, V.; Králova, J.; Kaplánek, R.; Bríza, T.; Martásek, P., Quo vadis porphyrin chemistry? *Physiol. Res.* **2006**, *55*, 3-26.
15. Suijkerbuijk, B. M.; Klein Gebbink, R. J., Merging porphyrins with organometallics: synthesis and applications. *Angew. Chem. Int. Ed.* **2008**, *47* (39), 7396-7421.
16. Smith, P. D.; James, B. R.; Dolphin, D. H., Structural aspects and coordination chemistry of metal porphyrin complexes with emphasis on axial ligand binding to carbon donors and mono- and diatomic nitrogen and oxygen donors. *Coord. Chem. Rev.* **1981**, *39* (1-2), 31-75.
17. da G.H. Vicente, M.; M. Smith, K., Syntheses and Functionalizations of Porphyrin Macrocycles. *Curr. Org. Synth.* **2014**, *11* (1), 3-28.
18. Hiroto, S.; Miyake, Y.; Shinokubo, H., Synthesis and Functionalization of Porphyrins through Organometallic Methodologies. *Chem. Rev.* **2017**, *117* (4), 2910-3043.

19. Mochida, I.; Suetsugu, K.; Fujitsu, H.; Takeshita, K.; Tsuji, K.; Sagara, Y.; Ohyoshi, A., A Kinetic-Study on Reduction of Nitric-Oxide over Cobalt Tetraphenylporphyrin Supported on Titanium-Dioxide. *J. Catal.* **1982**, *77* (2), 519-526.
20. Paddock, R. L.; Hiyama, Y.; McKay, J. M.; Nguyen, S. T., Co(III) porphyrin/DMAP: an efficient catalyst system for the synthesis of cyclic carbonates from CO<sub>2</sub> and epoxides. *Tetrahedron Lett.* **2004**, *45* (9), 2023-2026.
21. Berg, K.; Selbo, P. K.; Weyergang, A.; Dietze, A.; Prasmickaite, L.; Bonsted, A.; Engesaeter, B. O.; Angell-Petersen, E.; Warloe, T.; Frandsen, N.; Høgset, A., Porphyrin-related photosensitizers for cancer imaging and therapeutic applications. *J. Microsc.* **2005**, *218* (Pt 2), 133-147.
22. Sharman, W. M.; Allen, C. M.; van Lier, J. E., Photodynamic therapeutics: basic principles and clinical applications. *Drug Discov. Today* **1999**, *4* (11), 507-517.
23. Filippini, D.; Alimelli, A.; Di Natale, C.; Paolesse, R.; D'Amico, A.; Lundstrom, I., Chemical sensing with familiar devices. *Angew. Chem. Int. Ed.* **2006**, *45* (23), 3800-3803.
24. Rakow, N. A.; Suslick, K. S., A colorimetric sensor array for odour visualization. *Nature* **2000**, *406* (6797), 710-713.
25. Vilmercati, P.; Cudia, C. C.; Larciprete, R.; Cepek, C.; Zampieri, G.; Sangaletti, L.; Pagliara, S.; Verdini, A.; Cossaro, A.; Floreano, L.; Morgante, A.; Petaccia, L.; Lizzit, S.; Battocchio, C.; Polzonetti, G.; Goldoni, A., Molecular Orientations, Electronic Properties and Charge Transfer Timescale in a Zn-Porphyrin/C<sub>70</sub> Donor-Acceptor Complex for Solar Cells. *Surf. Sci.* **2006**, *600* (18), 4018-4023.
26. Campbell, W. M.; Burrell, A. K.; Officer, D. L.; Jolley, K. W., Porphyrins as light harvesters in the dye-sensitised TiO<sub>2</sub> solar cell. *Coord. Chem. Rev.* **2004**, *248* (13-14), 1363-1379.
27. Auwärter, W.; Seufert, K.; Klappenberger, F.; Reichert, J.; Weber-Bargioni, A.; Verdini, A.; Cvetko, D.; Dell'Angela, M.; Floreano, L.; Cossaro, A.; Bavdek, G.; Morgante, A.; Seitsonen, A. P.; Barth, J. V., Site-Specific Electronic and Geometric Interface Structure of Co-Tetraphenyl-Porphyrin Layers on Ag(111). *Phys. Rev. B* **2010**, *81* (24), 245403/1-245403/14.
28. Beggan, J. P.; Krasnikov, S. A.; Sergeeva, N. N.; Senge, M. O.; Cafolla, A. A., Control of the axial coordination of a surface-confined manganese (III) porphyrin complex. *Nanotechnology* **2012**, *23* (23), 235606/1-235606/10.
29. Gottfried, J. M.; Flechtner, K.; Kretschmann, A.; Lukasczyk, T.; Steinrück, H.-P., Direct synthesis of a metalloporphyrin complex on a surface. *J. Am. Chem. Soc.* **2006**, *128* (17), 5644-5645.
30. Diller, K.; Klappenberger, F.; Marschall, M.; Hermann, K.; Nefedov, A.; Woll, C.; Barth, J. V., Self-metalation of 2H-tetraphenylporphyrin on Cu(111): an x-ray spectroscopy study. *J. Chem. Phys.* **2012**, *136* (1), 014705/1-014705/13.
31. Ditze, S.; Röckert, M.; Buchner, F.; Zillner, E.; Stark, M.; Steinrück, H.-P.; Marbach, H., Towards the engineering of molecular nanostructures: local anchoring and functionalization of porphyrins on model-templates. *Nanotechnology* **2013**, *24* (11), 115305/1-115305/11.
32. Werner, K.; Mohr, S.; Schwarz, M.; Xu, T.; Amende, M.; Döpfer, T.; Görling, A.; Libuda, J., Functionalized Porphyrins on an Atomically Defined Oxide Surface: Anchoring and Coverage-Dependent Reorientation of MCTPP on Co<sub>3</sub>O<sub>4</sub>(111). *J. Phys. Chem. Lett.* **2016**, *7* (3), 555-560.
33. Bürker, C.; Franco-Cañellas, A.; Broch, K.; Lee, T. L.; Gerlach, A.; Schreiber, F., Self-Metalation of 2H-Tetraphenylporphyrin on Cu(111) Studied with XSW: Influence of the

- Central Metal Atom on the Adsorption Distance. *J. Phys. Chem. C* **2014**, *118* (25), 13659-13666.
34. Classen, A.; Pöschel, R.; Di Filippo, G.; Fauster, T.; Malcıoğlu, O. B.; Bockstedte, M., Electronic structure of tetraphenylporphyrin layers on Ag(100). *Phys. Rev. B* **2017**, *95* (11), 115414/1-115414/7.
  35. Röckert, M.; Franke, M.; Tariq, Q.; Ditze, S.; Stark, M.; Uffinger, P.; Wechsler, D.; Singh, U.; Xiao, J.; Marbach, H.; Steinrück, H.-P.; Lytken, O., Coverage- and temperature-dependent metalation and dehydrogenation of tetraphenylporphyrin on Cu(111). *Chem. Eur. J.* **2014**, *20* (29), 8948-8953.
  36. Kollhoff, F.; Schneider, J.; Li, G.; Barkaoui, S.; Shen, W.; Berger, T.; Diwald, O.; Libuda, J., Anchoring of Carboxyl-Functionalized Porphyrins on MgO, TiO<sub>2</sub>, and Co<sub>3</sub>O<sub>4</sub> Nanoparticles. *Phys. Chem. Chem. Phys.* **2018**, *20* (38), 24858-24868.
  37. Köbl, J.; Wang, T.; Wang, C.; Drost, M.; Tu, F.; Xu, Q.; Ju, H.; Wechsler, D.; Franke, M.; Pan, H.; Marbach, H.; Steinrück, H.-P.; Zhu, J.; Lytken, O., Hungry Porphyrins: Protonation and Self-Metalation of Tetraphenylporphyrin on TiO<sub>2</sub>(110)-1×1. *ChemistrySelect* **2016**, *1* (19), 6103-6105.
  38. Schneider, J.; Franke, M.; Gurrath, M.; Röckert, M.; Berger, T.; Bernardi, J.; Meyer, B.; Steinrück, H.-P.; Lytken, O.; Diwald, O., Porphyrin Metalation at MgO Surfaces: A Spectroscopic and Quantum Mechanical Study on Complementary Model Systems. *Chem. Eur. J.* **2016**, *22* (5), 1744-1749.
  39. Lovat, G.; Forrer, D.; Abadia, M.; Dominguez, M.; Casarin, M.; Rogero, C.; Vittadini, A.; Floreano, L., On-Surface Synthesis of a Pure and Long-Range-Ordered Titanium(IV)-Porphyrin Contact Layer on Titanium Dioxide. *J. Phys. Chem. C* **2017**, *121* (25), 13738-13746.
  40. Olszowski, P.; Zając, Ł.; Godlewski, S.; Such, B.; Jöhr, R.; Glatzel, T.; Meyer, E.; Szymonski, M., Role of a Carboxyl Group in the Adsorption of Zn Porphyrins on TiO<sub>2</sub>(011)-2×1 Surface. *J. Phys. Chem. C* **2015**, *119* (37), 21561-21566.
  41. Nayak, A.; Knauf, R. R.; Hanson, K.; Alibabaei, L.; Concepcion, J. J.; Ashford, D. L.; Dempsey, J. L.; Meyer, T. J., Synthesis and photophysical characterization of porphyrin and porphyrin–Ru(II) polypyridyl chromophore–catalyst assemblies on mesoporous metal oxides. *Chem. Sci.* **2014**, *5* (8), 3115-3119.
  42. Mallakpour, S.; Madani, M., A review of current coupling agents for modification of metal oxide nanoparticles. *Prog. Org. Coat.* **2015**, *86*, 194-207.
  43. Li, J.; He, Y.; Sun, W.; Luo, Y.; Cai, H.; Pan, Y.; Shen, M.; Xia, J.; Shi, X., Hyaluronic acid-modified hydrothermally synthesized iron oxide nanoparticles for targeted tumor MR imaging. *Biomaterials* **2014**, *35* (11), 3666-3677.
  44. Wilson, D.; Langell, M. A., XPS analysis of oleylamine/oleic acid capped Fe<sub>3</sub>O<sub>4</sub> nanoparticles as a function of temperature. *Appl. Surf. Sci.* **2014**, *303*, 6-13.
  45. Gottfried, J. M., Surface chemistry of porphyrins and phthalocyanines. *Surf. Sci. Rep.* **2015**, *70* (3), 259-379.
  46. Barlow, D. E.; Scudiero, L.; Hipps, K. W., Scanning Tunneling Microscopy Study of the Structure and Orbital-Mediated Tunneling Spectra of Cobalt(II) Phthalocyanine and Cobalt(II) Tetraphenylporphyrin on Au(111): Mixed Composition Films. *Langmuir* **2004**, *20* (11), 4413-4421.
  47. Brede, J.; Linares, M.; Lensen, R.; Rowan, A. E.; Funk, M.; Bröring, M.; Hoffmann, G.; Wiesendanger, R., Adsorption and conformation of porphyrins on metallic surfaces. *J. Vac. Sci. Technol. B* **2009**, *27* (2), 799-804.

48. Chen, M.; Feng, X.; Zhang, L.; Ju, H.; Xu, Q.; Zhu, J.; Gottfried, J. M.; Ibrahim, K.; Qian, H.; Wang, J., Direct Synthesis of Nickel(II) Tetraphenylporphyrin and Its Interaction with a Au(111) Surface: A Comprehensive Study. *J. Phys. Chem. C* **2010**, *114* (21), 9908-9916.
49. Stark, M.; Ditze, S.; Drost, M.; Buchner, F.; Steinrück, H.-P.; Marbach, H., Coverage dependent disorder-order transition of 2H-tetraphenylporphyrin on Cu(111). *Langmuir* **2013**, *29* (12), 4104-4110.
50. Lepper, M.; Köbl, J.; Schmitt, T.; Gurrath, M.; de Siervo, A.; Schneider, M. A.; Steinrück, H.-P.; Meyer, B.; Marbach, H.; Hieringer, W., "Inverted" porphyrins: a distorted adsorption geometry of free-base porphyrins on Cu(111). *Chem. Commun.* **2017**, *53* (58), 8207-8210.
51. Wechsler, D.; Franke, M.; Tariq, Q.; Zhang, L.; Lee, T.-L.; Thakur, P. K.; Tsud, N.; Bercha, S.; Prince, K. C.; Steinrück, H.-P.; Lytken, O., Adsorption Structure of Cobalt Tetraphenylporphyrin on Ag(100). *J. Phys. Chem. C* **2017**, *121* (10), 5667-5674.
52. Seufert, K.; Bocquet, M. L.; Auwarter, W.; Weber-Bargioni, A.; Reichert, J.; Lorente, N.; Barth, J. V., Cis-dicarbonyl binding at cobalt and iron porphyrins with saddle-shape conformation. *Nat. Chem.* **2011**, *3* (2), 114-119.
53. Mielke, J.; Hanke, F.; Peters, M. V.; Hecht, S.; Persson, M.; Grill, L., Adatoms underneath single porphyrin molecules on Au(111). *J. Am. Chem. Soc.* **2015**, *137* (5), 1844-1849.
54. González-Moreno, R.; Sánchez-Sánchez, C.; Trelka, M.; Otero, R.; Cossaro, A.; Verdini, A.; Floreano, L.; Ruiz-Bermejo, M.; García-Lekue, A.; Martín-Gago, J. Á.; Rogero, C., Following the Metalation Process of Protoporphyrin IX with Metal Substrate Atoms at Room Temperature. *J. Phys. Chem. C* **2011**, *115* (14), 6849-6854.
55. Li, Y.; Xiao, J.; Shubina, T. E.; Chen, M.; Shi, Z.; Schmid, M.; Steinrück, H.-P.; Gottfried, J. M.; Lin, N., Coordination and metalation bifunctionality of Cu with 5,10,15,20-tetra(4-pyridyl)porphyrin: toward a mixed-valence two-dimensional coordination network. *J. Am. Chem. Soc.* **2012**, *134* (14), 6401-6408.
56. Shubina, T. E.; Marbach, H.; Flechtner, K.; Kretschmann, A.; Jux, N.; Buchner, F.; Steinrück, H.-P.; Clark, T.; Gottfried, J. M., Principle and mechanism of direct porphyrin metalation: joint experimental and theoretical investigation. *J. Am. Chem. Soc.* **2007**, *129* (30), 9476-9483.
57. Röckert, M.; Franke, M.; Tariq, Q.; Lungerich, D.; Jux, N.; Stark, M.; Kaftan, A.; Ditze, S.; Marbach, H.; Laurin, M.; Libuda, J.; Steinrück, H.-P.; Lytken, O., Insights in Reaction Mechanistics: Isotopic Exchange during the Metalation of Deuterated Tetraphenyl-21,23D-porphyrin on Cu(111). *J. Phys. Chem. C* **2014**, *118* (46), 26729-26736.
58. Haq, S.; Hanke, F.; Dyer, M. S.; Persson, M.; Iavicoli, P.; Amabilino, D. B.; Raval, R., Clean coupling of unfunctionalized porphyrins at surfaces to give highly oriented organometallic oligomers. *J. Am. Chem. Soc.* **2011**, *133* (31), 12031-12039.
59. Kretschmann, A.; Walz, M. M.; Flechtner, K.; Steinrück, H.-P.; Gottfried, J. M., Tetraphenylporphyrin picks up zinc atoms from a silver surface. *Chem. Commun.* **2007**, (6), 568-570.
60. Goldoni, A.; Pignedoli, C. A.; Di Santo, G.; Castellarin-Cudia, C.; Magnano, E.; Bondino, F.; Verdini, A.; Passerone, D., Room Temperature Metalation of 2H-TPP Monolayer on Iron and Nickel Surfaces by Picking up Substrate Metal Atoms. *ACS Nano* **2012**, *6* (12), 10800-10807.
61. Wang, C.; Fan, Q.; Han, Y.; Martinez, J. I.; Martín-Gago, J. A.; Wang, W.; Ju, H.; Gottfried, J. M.; Zhu, J., Metalation of tetraphenylporphyrin with nickel on a TiO<sub>2</sub>(110)-1x2 surface. *Nanoscale* **2016**, *8* (2), 1123-1132.

62. Schneider, J.; Kollhoff, F.; Schindler, T.; Bichlmaier, S.; Bernardi, J.; Unruh, T.; Libuda, J.; Berger, T.; Diwald, O., Adsorption, Ordering, and Metalation of Porphyrins on MgO Nanocube Surfaces: The Directional Role of Carboxylic Anchoring Groups. *J. Phys. Chem. C* **2016**, *120* (47), 26879-26888.
63. Guo, Q.; Cocks, I.; Williams, E. M., The adsorption of benzoic acid on a TiO<sub>2</sub>(110) surface studied using STM, ESDIAD and LEED. *Surf. Sci.* **1997**, *393* (1-3), 1-11.
64. Xu, T.; Schwarz, M.; Werner, K.; Mohr, S.; Amende, M.; Libuda, J., Structure-Dependent Anchoring of Organic Molecules to Atomically Defined Oxide Surfaces: Phthalic Acid on Co<sub>3</sub>O<sub>4</sub> (111), CoO(100), and CoO(111). *Chem. Eur. J.* **2016**, *22* (15), 5384-5396.
65. Gutiérrez-Sosa, A.; Martínez-Escolano, P.; Raza, H.; Lindsay, R.; Wincott, P. L.; Thornton, G., Orientation of carboxylates on TiO<sub>2</sub>(110). *Surf. Sci.* **2001**, *471* (1-3), 163-169.
66. Lovat, G.; Forrer, D.; Abadia, M.; Dominguez, M.; Casarin, M.; Rogero, C.; Vittadini, A.; Floreano, L., Hydrogen capture by porphyrins at the TiO<sub>2</sub>(110) surface. *Phys. Chem. Chem. Phys.* **2015**, *17* (44), 30119-30124.
67. Lavalley, D. K., Complexation and Demetalation Reactions of Porphyrins. *Comments Inorganic Chem.* **1986**, *5* (3), 155-174.
68. Burnham, B. F.; Zuckerman, J. J., Complex formation between porphyrins and metal ions. *J. Am. Chem. Soc.* **1970**, *92* (6), 1547-1550.
69. Murakami, K.; Yamamoto, Y.; Yorimitsu, H.; Osuka, A., Demetalation of Metal Porphyrins via Magnesium Porphyrins by Reaction with Grignard Reagents. *Chem. Eur. J.* **2013**, *19* (28), 9123-9126.
70. Orzeł, Ł.; van Eldik, R.; Fiedor, L.; Stochel, G. y., Mechanistic Information on Cu<sup>II</sup> Metalation and Transmetalation of Chlorophylls. *Eur. J. Inorg. Chem.* **2009**, *2009* (16), 2393-2406.
71. Shamim, A.; Hambright, P., Exchange reactions of transition metal ions and labile cadmium porphyrins. *J. Inorg. Nucl. Chem.* **1980**, *42* (11), 1645-1647.
72. Kumar, M.; Neta, P.; Sutter, T. P. G.; Hambright, P., One-electron reduction and demetallation of copper porphyrins. *J. Phys. Chem.* **1992**, *96* (23), 9571-9575.
73. Franke, M.; Marchini, F.; Steinrück, H.-P.; Lytken, O.; Williams, F. J., Surface Porphyrins Metalate with Zn Ions from Solution. *J. Phys. Chem. Lett.* **2015**, *6* (23), 4845-4849.
74. Franke, M.; Marchini, F.; Jux, N.; Steinrück, H.-P.; Lytken, O.; Williams, F. J., Zinc Porphyrin Metal-Center Exchange at the Solid-Liquid Interface. *Chem. Eur. J.* **2016**, *22* (25), 8520-8524.
75. Fernández, C. C.; Spedalieri, C.; Murgida, D. H.; Williams, F. J., Surface Influence on the Metalation of Porphyrins at the Solid-Liquid Interface. *J. Phys. Chem. C* **2017**, *121* (39), 21324-21332.
76. Watts, J. F.; Wolstenholme, J., *An Introduction to Surface Analysis by XPS and AES*. John Wiley & Sons Inc: New York, **2003**.
77. Briggs, D.; Seah, M. P., *Auger and X-ray Photoelectron Spectroscopy*. 2 ed.; John Wiley & Sons: Chichester, **1990**.
78. Stöhr, J., *NEXAFS Spectroscopy*. Springer-Verlag Berlin Heidelberg: **1992**.
79. The Nobel Prize in Physics 1921.  
<http://www.nobelprize.org/prizes/physics/1921/summary/> (accessed 23.07.2020).

80. Wagner, C. D.; Davis, L. E.; Zeller, M. V.; Taylor, J. A.; Raymond, R. H.; Gale, L. H., Empirical atomic sensitivity factors for quantitative analysis by electron spectroscopy for chemical analysis. *Surf. Interface Anal.* **1981**, 3 (5), 211-225.
81. Wagner, C. D., Sensitivity factors for XPS analysis of surface atoms. *J. Elec. Spec. Rel. Phenom.* **1983**, 32 (2), 99-102.
82. Graber, T.; Forster, F.; Schöll, A.; Reinert, F., Experimental determination of the attenuation length of electrons in organic molecular solids: The example of PTCDA. *Surf. Sci.* **2011**, 605 (9-10), 878-882.
83. Lukasczyk, T.; Flechtner, K.; Merte, L. R.; Jux, N.; Maier, F.; Gottfried, J. M.; Steinrück, H.-P., Interaction of Cobalt(II) Tetraarylporphyrins with a Ag(111) Surface Studied with Photoelectron Spectroscopy. *J. Phys. Chem. C* **2007**, 111 (7), 3090-3098.
84. Larson, P. E.; Kelly, M. A., Surface charge neutralization of insulating samples in x-ray photoemission spectroscopy. *J. Vac. Sci. Technol. A* **1998**, 16 (6), 3483-3489.
85. Green, G. K., Spectra and optics of synchrotron radiation; BNL-50522 **1976**.
86. Kim, K. J., Polarization characteristics of synchrotron radiation sources and a new two undulator system. *Nucl. Instrum. Methods Phys. Res.* **1984**, 222 (1-2), 11-13.
87. Atrei, A.; Bardi, U.; Rovida, G., Structure and composition of the titanium oxide layers formed by low-pressure oxidation of the Ni<sub>94</sub>Ti<sub>6</sub>(110) surface. *Surf. Sci.* **1997**, 391 (1-3), 216-225.
88. Chang, Z.; Thornton, G., Reactivity of thin-film TiO<sub>2</sub>(110). *Surf. Sci.* **2000**, 462 (1-3), 68-76.
89. Suzuki, Y.; Nagata, T.; Yamashita, Y.; Nabatame, T.; Ogura, A.; Chikyow, T., Thin-film growth of (110) rutile TiO<sub>2</sub> on (100) Ge substrate by pulsed laser deposition. *Jpn. J. Appl. Phys.* **2016**, 55 (6S1), 06GG06/1-06GG06/5.
90. Giovanardi, C.; Hammer, L.; Heinz, K., Ultrathin cobalt oxide films on Ir(100)-(1×1). *Phys. Rev. B* **2006**, 74 (12), 125429/1-125429/9.
91. Heinz, K.; Hammer, L., Epitaxial cobalt oxide films on Ir(100)-the importance of crystallographic analyses. *J. Phys. Condens. Matter* **2013**, 25 (17), 173001/1-173001/20.
92. Xiao, J.; Ditze, S.; Chen, M.; Buchner, F.; Stark, M.; Drost, M.; Steinrück, H.-P.; Gottfried, J. M.; Marbach, H., Temperature-Dependent Chemical and Structural Transformations from 2H-tetraphenylporphyrin to Copper(II)-Tetraphenylporphyrin on Cu(111). *J. Phys. Chem. C* **2012**, 116 (22), 12275-12282.
93. Di Santo, G.; Blankenburg, S.; Castellarin-Cudia, C.; Fanetti, M.; Borghetti, P.; Sangaletti, L.; Floreano, L.; Verdini, A.; Magnano, E.; Bondino, F.; Pignedoli, C. A.; Nguyen, M. T.; Gaspari, R.; Passerone, D.; Goldoni, A., Supramolecular engineering through temperature-induced chemical modification of 2H-tetraphenylporphyrin on Ag(111): flat phenyl conformation and possible dehydrogenation reactions. *Chem. Eur. J.* **2011**, 17 (51), 14354-14359.
94. Schwarz, M.; Mohr, S.; Hohner, C.; Werner, K.; Xu, T.; Libuda, J., Water on Atomically-Defined Cobalt Oxide Surfaces Studied by Temperature-Programmed IR Reflection Absorption Spectroscopy and Steady State Isotopic Exchange. *J. Phys. Chem. C* **2018**, 7673-7681.
95. Chen, Z. Structure-Activity Correlations and Interfacial Chemistry of Cobalt Oxides and Oxyhydroxides for Oxygen Evolution. Princeton University, Princeton, NJ, 2017.

96. Patthey, L.; Rensmo, H.; Persson, P.; Westermark, K.; Vayssieres, L.; Stashans, A.; Petersson, Å.; Brühwiler, P. A.; Siegbahn, H.; Lunell, S.; Mårtensson, N., Adsorption of bisisonicotinic acid on rutile TiO<sub>2</sub>(110). *J. Chem. Phys.* **1999**, *110* (12), 5913-5918.
97. Rahe, P.; Nimmrich, M.; Nefedov, A.; Naboka, M.; Wöll, C.; Kühnle, A., Transition of Molecule Orientation during Adsorption of Terephthalic Acid on Rutile TiO<sub>2</sub>(110). *J. Phys. Chem. C* **2009**, *113* (40), 17471-17478.
98. Li, S. C.; Wang, J. G.; Jacobson, P.; Gong, X. Q.; Selloni, A.; Diebold, U., Correlation between bonding geometry and band gap states at organic-inorganic interfaces: catechol on rutile TiO<sub>2</sub>(110). *J. Am. Chem. Soc.* **2009**, *131* (3), 980-984.
99. Sheinin, V. B.; Simonova, O. R.; Ratkova, E. L., Effect of pH on Formation of Metalloporphyrins. *Macroheterocycles* **2008**, *1* (1), 72-78.
100. Cheung, S. K.; Dixon, F. L.; Fleischer, E. B.; Jeter, D. Y.; Krishnamurthy, M., Kinetic studies of the formation, acid-catalyzed solvolysis, and cupric ion displacement of a zinc porphyrin in aqueous solutions. *Bioinorg. Chem.* **1973**, *2* (4), 281-294.
101. Pandya, K. I.; Russell, A. E.; McBreen, J.; O'Grady, W. E., EXAFS Investigations of Zn(II) in Concentrated Aqueous Hydroxide Solutions. *J. Phys. Chem.* **1995**, *99* (31), 11967-11973.
102. Dirkse, T. P., The Nature of the Zinc-Containing Ion in Strongly Alkaline Solutions. *J. Electrochem. Soc.* **1954**, *101* (6), 328-331.
103. Müllner, M.; Balajka, J.; Schmid, M.; Diebold, U.; Mertens, S. F. L., Self-Limiting Adsorption of WO<sub>3</sub> Oligomers on Oxide Substrates in Solution. *J. Phys. Chem. C* **2017**, *121* (36), 19743-19750.
104. Kern, W.; Puotinen, D. A., Cleaning solutions based on hydrogen peroxide for use in silicon semiconductor technology. *RCA Review* **1970**, *31*, 187-206.
105. Balajka, J.; Hines, M. A.; DeBenedetti, W. J. I.; Komora, M.; Pavelec, J.; Schmid, M.; Diebold, U., High-affinity adsorption leads to molecularly ordered interfaces on TiO<sub>2</sub> in air and solution. *Science* **2018**, *361* (6404), 786-789.
106. Nilsing, M.; Persson, P.; Ojamäe, L., Anchor group influence on molecule-metal oxide interfaces: Periodic hybrid DFT study of pyridine bound to TiO<sub>2</sub> via carboxylic and phosphonic acid. *Chem. Phys. Lett.* **2005**, *415* (4-6), 375-380.
107. Pujari, S. P.; Scheres, L.; Marcelis, A. T.; Zuilhof, H., Covalent surface modification of oxide surfaces. *Angew. Chem. Int. Ed.* **2014**, *53* (25), 6322-6356.
108. Dulub, O.; Valentin, C. D.; Selloni, A.; Diebold, U., Structure, defects, and impurities at the rutile TiO<sub>2</sub>(011)-(2×1) surface: A scanning tunneling microscopy study. *Surf. Sci.* **2006**, *600* (19), 4407-4417.
109. Sanz, M.; Walczak, M.; Oujja, M.; Cuesta, A.; Castillejo, M., Nanosecond pulsed laser deposition of TiO<sub>2</sub>: nanostructure and morphology of deposits and plasma diagnosis. *Thin Solid Films* **2009**, *517* (24), 6546-6552.
110. Mostéfa-Sba, H.; Domenichini, B.; Bourgeois, S., Iron deposition on TiO<sub>2</sub>(110): effect of the surface stoichiometry and roughness. *Surf. Sci.* **1999**, *437* (1-2), 107-115.
111. Xue, S.; Sasahara, A.; Onishi, H., Atomic-scale topography of rutile TiO<sub>2</sub>(110) in aqueous solutions: A study involving frequency-modulation atomic force microscopy. *J. Chem. Phys.* **2020**, *152* (5), 054703/1-054703/7.



## 9. Appendix: Articles P1 – P6

### [P1] Interfacial Reactions of Tetraphenylporphyrin with Cobalt-Oxide Thin Films

Daniel Wechsler, Cynthia C. Fernández, Quratulain Tariq, Nataliya Tsud, Kevin C. Prince, Federico J. Williams, Hans-Peter Steinrück, and Ole Lytken *Chem. Eur. J.* **2019**, 25, 13197 – 13201.

The author's contribution is the sample preparation, measurement, data analysis, data interpretation and manuscript preparation.

### [P2] Covalent Anchoring and Interfacial Reactions of Adsorbed Porphyrins on Rutile TiO<sub>2</sub>(110)

Daniel Wechsler, Cynthia C. Fernández, Hans-Peter Steinrück, Ole Lytken, and Federico J. Williams *J. Phys. Chem. C* **2018**, 122, 4480 – 4487.

The author's contribution is the sample preparation, measurement, data analysis, data interpretation and manuscript preparation.

### [P3] Adsorption geometry of carboxylic acid functionalized porphyrin molecules on TiO<sub>2</sub>(110)

Cynthia C. Fernández, Daniel Wechsler, Tulio C. R. Rocha, Hans-Peter Steinrück, Ole Lytken, Federico J. Williams *Surf. Sci.* **2019**, 689, 121462.

The author's contribution is the performance of preliminary measurements and detailed discussion during data analysis, data interpretation and manuscript preparation.

### [P4] Wet-chemically Prepared Porphyrin-layers on Rutile TiO<sub>2</sub>(110)

Daniel Wechsler, Cynthia C. Fernández, Julia Köbl, List-Marie Augustin, Corinna Stumm, Norbert Jux, Hans-Peter Steinrück, Federico J. Williams, and Ole Lytken Submitted

The author's contribution is the sample preparation, XPS measurement, data analysis, data interpretation and manuscript preparation.

### [P5] Removing photoemission features from Auger-yield NEXAFS spectra

Ole Lytken, Daniel Wechsler, Hans-Peter Steinrück *J. Elec. Spec. Rel. Phenom.* **2017**, 218, 35 – 39.

The author's contribution is the detailed discussion during development, test analysis and manuscript reading.

### [P6] Adsorption Structure of Cobalt Tetraphenylporphyrin on Ag(100)

Daniel Wechsler, Matthias Franke, Quratulain Tariq, Liang Zhang, Tien-Lin Lee, Pardeep K. Thakur, Nataliya Tsud, Sofiia Bercha, Kevin C. Prince, Hans-Peter Steinrück, and Ole Lytken *J. Phys. Chem. C* **2017**, 121, 5667 – 5674.

The author's contribution is the sample preparation, measurement, data analysis, data interpretation and manuscript preparation.